PhD degree in Molecular Medicine (curriculum in Molecular Oncology)

European School of Molecular Medicine (SEMM),

University of Milan and University of Naples “Federico II”

Settore disciplinare: BIO/10

Functional and structural characterization of myosin VI isoforms

Biancospino Matteo

Fondazione IFOM, Milan

Matricola n. 823497

Supervisor: *Dr. Simona Polo*

Fondazione IFOM, Milan

Anno accademico 2014/2015

TABLE OF CONTENTS

LIST OF ABBREVIATIONS

ANTH	AP180 N-terminal homology
AP2	Adaptor protein 2
CBD	Cargo binding domain
CC	Coiled-Coil
CCV	Clathrin coated vesicle
CFTR	Cystic fibrosis transmembrane conductance regulator
CLTC	Clathrin heavy chain
CME	Clathrin-mediated endocytosis
Dab2	Disabled homolog 2
ECM	Extracellular Matrix
EGF	Epidermal growth factor
EGFR	Epidermal growth factor receptor
EM	Electron-Microscopy
EPS15	Epidermal growth factor receptor substrate 15
EPSIN	Eps15-interacting protein
ER	Endoplasmic reticulum
GPCR	G protein-coupled receptor
GST	Glutathione S-transferase
HSC70	Heat Shock Cognate 70
KD	Knock down
LC	Clathrin light chain

LCa	Clathrin light chain a
LCb	Clathrin light chain b
LDLR	Low-density lipoprotein receptor
LIR	LC3-interaction motif
MIU	Inverted Ubiquitin Interacting Motif
PCR	Polymerase Chain Reaction
PI3K	Phosphoinositide 3-kinase
PIP2	Phosphatidylinositol-4,5-bisphosphate
PTB	Phosphotyrosine-binding
RTK	Receptor tyrosine kinase
SEAP	Secreted alkaline phosphatase
SH3	Src homology 3
shRNA	Short hairpin RNA
siRNA	Small interfering RNA
sv	Snell's Waltzer
SV40	Simian virus 40
TCL	Total cell lysate
TfR	Transferrin receptor
VEGF	Vascular Endothelial Growth Factor
VSV-G	Vesicular Stomatitis Virus-Glycoprotein
WT	Wild type
ZF	Zinc-Finger domain

FIGURES INDEX

TABLE INDEX

ABSTRACT

Myosin VI is unique among the many members of the myosin superfamily. The peculiarities of this motor protein reside on its ability to travel along actin microfilaments towards their pointed-end, as well as its capacity to act either as anchor or as processive motor. As a consequence, myosin VI has been implicated in clathrin-mediated endocytosis, vesicle trafficking, autophagy, cell migration and tumorigenesis. The current understanding of the myosin VI protein does not explain how it carries out these diverse processes, as functional mechanistic studies are lacking. Alternative splicing in the tail region generates myosin VI molecules with different features (myosin VI_{short} and myosin VI_{long}) but little is known about the impact of the variable region on physiological and pathological functions of myosin VI.

In this study, we have analysed the myosin VI isoforms from a molecular and a functional perspective. Using quantitative mass spectrometry approach and modern NMR we identified and structurally characterized clathrin light chain as novel and isoform-specific interactor. Within the novel clathrin-binding domain that is unique to myosin VI_{long}, an isoform-specific regulatory helix, named α2-linker, defines a specific myosin VI_{long} conformation. Its presence or absence determines the target selectivity of myosin VI_{short} and myosin VI_{long} isoforms, acting like a molecular switch that regulates their functional involvement in migratory or endocytic pathways, respectively. The adaptor-binding RRL motif is embedded in the clathrin-binding domain and is masked in the structural configuration adopted by the myosin VI_{long}. Consequently, the previously identified RRL interactors show selective binding to myosin VI_{short}. Thus, we can provide for the first time a mechanistic explanation of why the various isoforms show different localization and function (i.e. myosin VI_{long} selectively involved in clathrin-mediated endocytosis).

We also found that alternative myosin VI splicing is aberrantly regulated in ovarian cancers, where exon skipping dictates myosin VI_{short}-only expression. Importantly, cancer cell lines selectively expressing the myosin VI_{short} isoform exhibit severe migration defects when myosin VI is knocked down.

1. INTRODUCTION

1.1 Actin and myosins in cell motility

1.1.1 How the cell move: an overview

Different type of protein filaments, known as microtubules, intermediate filaments, and microfilaments, form the cytoskeleton. The cytoskeleton supports and actively participates in various processes such as internalization of molecules and vesicles from the plasma membrane [Smythe *et al.*, 2006], exocytosis [Porat-Shliom *et al.*, 2013], and last, but not least cells movement. This dynamic system is indeed essential in order to generate the force necessary to move cells. Movement is the results of different stimuli transmitted from grow factors receptors such as receptor tyrosine kinases (RTKs) or G protein–coupled receptors (GPCRs) to the cytoplasmic environment through adhesion molecules such as integrins and cadherins. Such molecules can elicit and control signal cascades, causing major cytoskeleton rearrangements, which ultimately lead to cell movement.

Physiological processes such as embryonic development, wound healing, and immune responses exploit single- and/or multiple-cell migration and both processes are highly regulated [Ridley, 2011]. In normal condition the movement ceases when the cell reaches its final destination, terminal differentiates, or ends its functions. Lack of movement, or uncontrolled motility leads to diverse pathological conditions such as cancer-cell dissemination (metastasis), developmental defects, immunosuppression of autoimmune reactions [Yamaguchi *et al.*, 2007] [Ridley, 2011].

To achieve cell movement, several processes occur in a coordinate fashion. The first step begins with the extension of the protrusions mediated by actin-structures at the leading edge [Nurnberg *et al.*, 2011]. These structures contain actin filaments and

are called lamellipodia and filopodia (**Figure 1**). Then, adhesions at the rear of the cell must be disassembled and internalized, while new adhesions should be formed at the front through exocytosis processes [Ridley *et al.*, 2003].

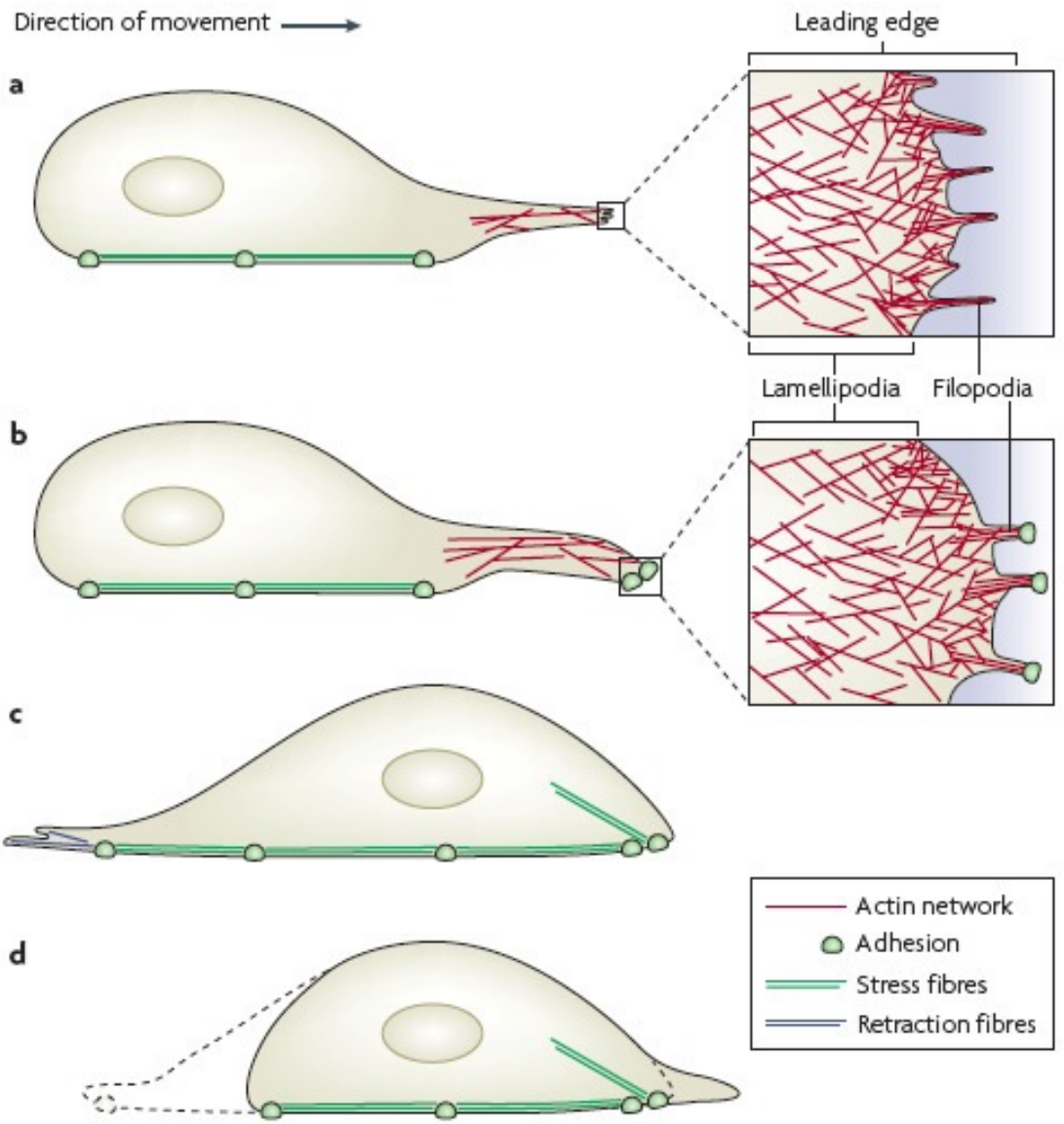

Figure 1 Steps in cell migration. a) Formation of actin protrusions at the leading edge drives the process. **b)** Establishment of new adhesive sites stabilizes the protrusions **c)** The tensile forces between adhesions and actin- cytoskeleton lead the nucleus and the cell body to translocate forward in the direction of migration **d)** At the cell rear, old adhesions disassemble, and the trailing edge retracts Adapted from [Mattila *et al.*, 2008].

1.1.2 Actin and the microfilament system

Actin together with different motor proteins (myosins), and actin regulatory proteins form the microfilament system, the most dynamic component of the cytoskeleton and the major responsible for cell motility.

Actin polymers (filamentous, F-actin) are formed by single 42 kDa monomers (globular G-actin) that posses the ability to bind ATP and ADP. Polymerization of molecules to form F-actin is the major driving responsible for formation of protrusions. This was demonstrated to be an autocatalytic process *in vitro*. When assembled, actin filaments resemble a twisted string of approximately 7 nm with a structural and functional polarization. A fast polymerizing or *barbed end* (plus or "+" end) represents one terminus, while a slow polymerizing or *pointed end* (minus or "–" end) forms the other terminus of the filament. Most of the large-scale rearrangements of actin cytoskeleton, during protrusions formation are due to actin polymerization, and take place just beneath the plasma membrane where the vast majority of barbed-ends are positioned [Carlier *et al.*, 2015]. Spatial and temporal regulation of actin polymerization are obtained through the action of a plethora of actin binding proteins (ABPs) such as profilin, which maintain a pool of ready-to-polymerize actin, or capping proteins that can bind and block both barbed- and pointed-end of filaments. Other ABPs affect F-actin formation through their severing, bundling or nucleating factors, thus resulting in filaments disruption, reinforcement or *de novo* polymerization, respectively (**Figure 2**). The combined activity of all these proteins generates cell movement, thanks to constant actin polymerization and filaments-network assembly at the cell front while depolymerization of filaments, together with disassembly of cell/surface adhesions occurs at the cell rear.

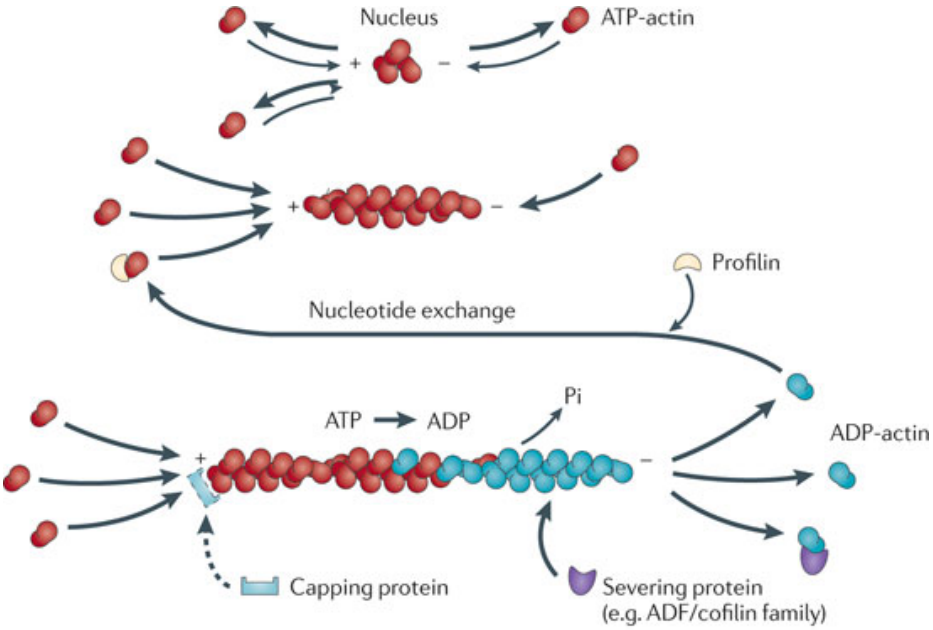

Figure 2 Actin nucleation and polymerization. Simplified representation of actin polymerization dynamics. Spontaneous, ATP-bound actin oligomers (or nuclei) formation is kinetically unfavourable, and this slows down the whole actin filaments formation. Once this stage is overcome, actin polymerization is fast, especially at the plus-end. ATP is quickly hydrolysed by F-actin forming ADP-actin, which favours depolymerization of filaments. Both polymer formation and dissociation are influenced by several actin-binding proteins such as ADF/cofilin (favouring dissociation), or capping proteins (stabilizing and thus blocking one of the two ends of the filament). ADP to ATP exchange on actin is catalysed by profilin, which maintain a pool of ready-to-polymerize actin. From [Nurnberg *et al.*, 2011].

1.1.3 The myosin superfamily of motor proteins

Several molecular motors exploit microfilaments and microtubules to travel within the cell. In the case of actin filaments, diverse ATPases known as myosins have evolved in all eukaryotes [Foth *et al.*, 2006]. This large family of motor-proteins participates in every aspect of the motility of living beings, being involved in macroscopic processes such as muscle contraction [Geeves, 1991], as well as in microscopic phenomena such as vesicle internalization [Chandrasekar *et al.*, 2014]. Muscle class II myosin has been the first identified and the most studied one among the actin-based molecular motors [Geeves, 1991]. It forms macromolecular, rod-

shaped complexes, which are tightly interconnected with actin filaments. By reciprocal sliding, actin filaments and myosin class II complexes cause muscle shortening, and thus contraction. We refer to these class II molecules as the conventional myosins. The later discovery of class I myosin [Pollard *et al.*, 1973] opened the route to the identification of novel myosin classes, which, with the advance in genome sequencing raised the number of known classes to 37 [Richards *et al.*, 2005] (**Figure 3**). All myosins, a part from muscle myosin II, are known as unconventional myosins [Woolner *et al.*, 2009].

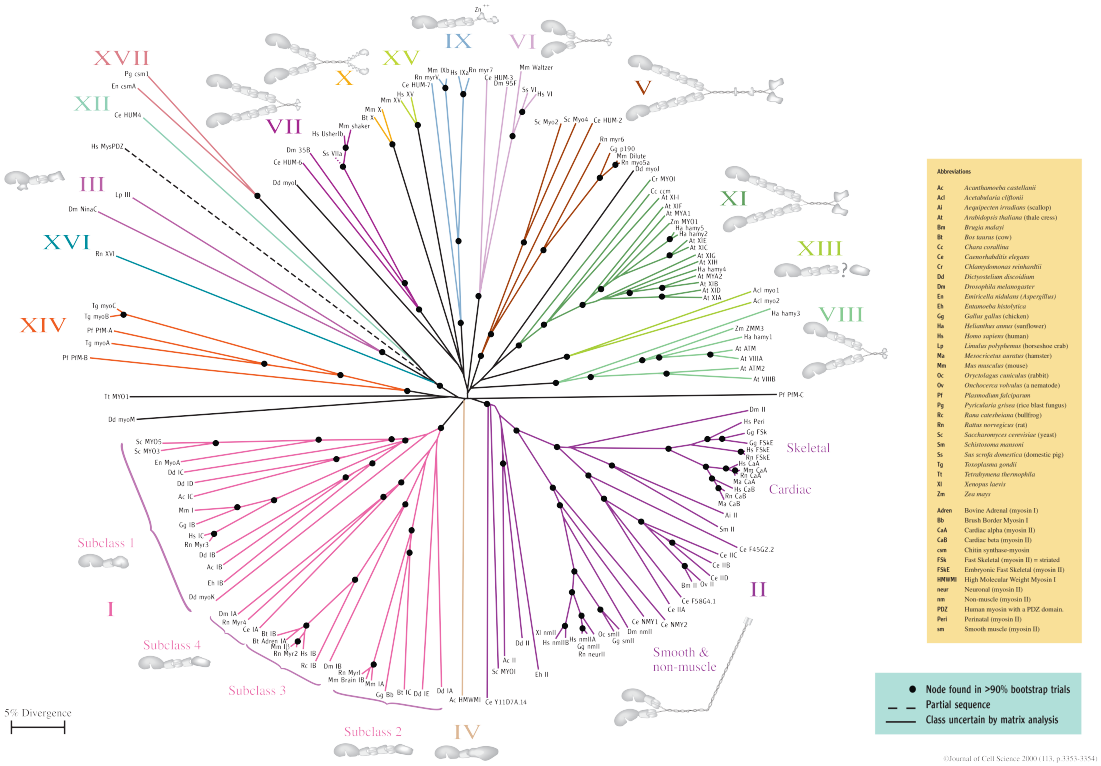

Figure 3 Myosins differentiation tree. Unrooted phylogenetic tree of the myosin superfamily is derived from an alignment of 139 members of the myosin superfamily. The alignment compared the core motor domains (equivalent to residues 88-780 of chicken skeletal myosin II) of each myosin, using distance matrix analysis performed with the Clustal-W package [Hodge *et al.*, 2000]

The overall domain organization of all actin-based molecular motors is quite conserved. At the N-terminal region is the ATP- and actin-binding region, known as motor domain, which spans 700 to 800 amino acids. This part of the protein allows myosins to travel along the microfilament system to exert their functions (further described below). The motor domain is the most conserved region of the protein and allows the classification of the myosins' classes.

Towards the C-terminus a converter and neck (or lever) domains are found in all known myosins. The filament-bound motor head cause the rotation of the converter region; the lever then amplifies such rearrangements and allows the reciprocal movement of the motor heads. The neck encompasses from one to six basic- and hydrophobic-rich (IQXXXRGXXXR) IQ motifs, which confer to the myosin molecule the ability to interact with proteins such as troponin or myosin light chains that regulate myosin activity [Tyska *et al.*, 2002].

The C-terminal part of the myosin molecules is known as the tail domain and is responsible for the specific functions of the different myosin. Indeed sequence analysis of myosins tails point to low levels of conservation through evolution. In general, myosin tails are composed of various interaction surfaces that allow them to dimerize, to bind lipids (i.e. myosin I and VI) and/or specific binding partners. Because of these interactions this region is also acknowledged as cargo-binding domain (CBD). Binding surfaces on myosins might include FERM (4.1 protein, Ezrin, Radixin and Moesin containing) domain, MyTH4 (Myosin Tail Homology), SH3 (Src Homology 3 domain), PH (Pleckstrin Homology) domain [Krendel. *et al.*, 2005], and MIU (inverted Ubiquitin Interacting Motif) [Penengo *et al.*, 2006], (**Figure 4**).

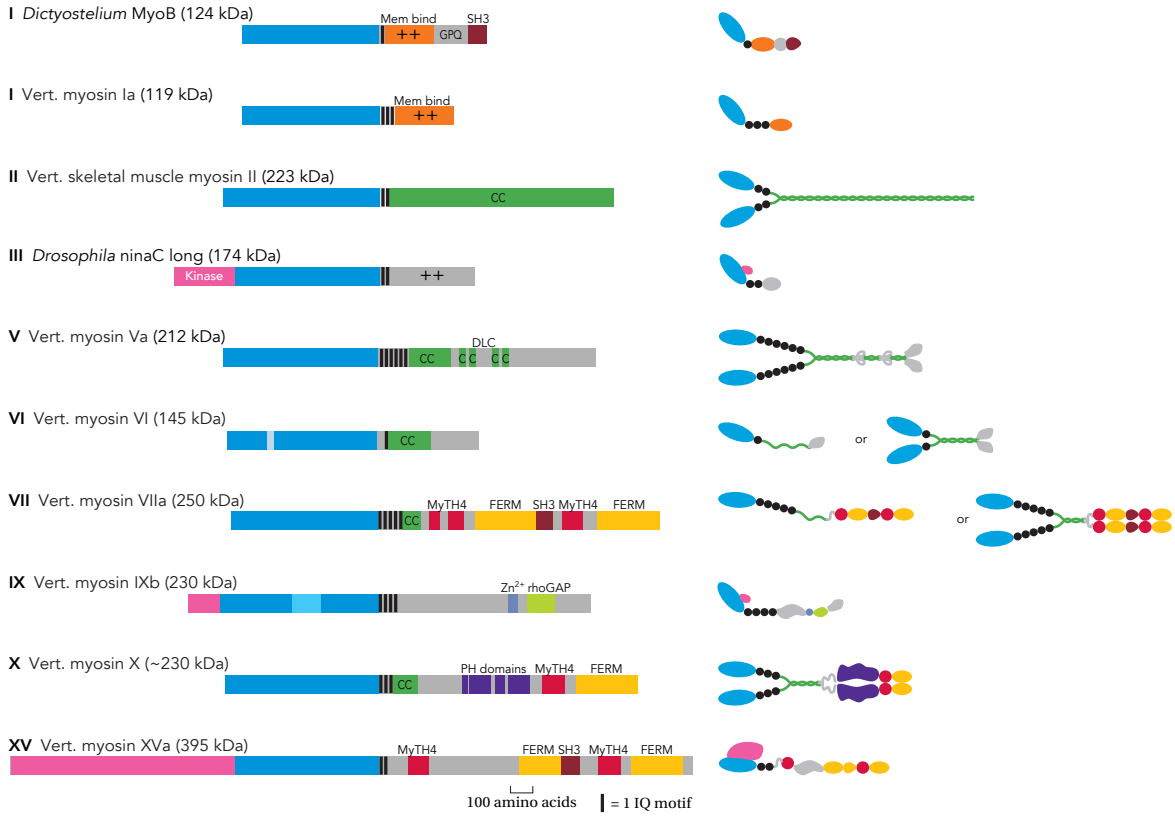

Figure 4 Myosins domains organization. Schematic representation of the diverse myosin structures. The blue region highlight the motor domain, inserts are shown as diagonally hatched boxes. Coloured boxes in the tail domains represent different regions predicted by sequence homology: GPQ identifies a glycine-, proline-, and glutamine-rich region; + + , positively charged regions; SH3, SRC homology 3 domains; CC, coiled-coil domains; MyTH4, myosin tail homology 4 domains; DLC, presumptive dynein light chain binding domain; talin, talin homology domain; Zn^{2+}, zinc binding domain; rhoGAP, rho GTPase-activating protein domain; and PH, pleckstrin homology domain. From [Krendel. *et al.*, 2005].

Myosin translocation along actin filaments depends on structural rearrangements of the motor domain caused by ATP hydrolysis. The classical myosin cycle starts with the detachment of the motor protein from actin upon ATP-binding. Successive formation of the intermediate myosin-ADP-P_i allows reattachment to actin, which is followed by the release of ADP and P_i, the final step that causes conformational changes and thus force generation, as well as the clearance of the ATP-binding cleft, ready for a new cycle. Such conformational changes are then amplified by the converter and lever arm domains, which direct the motion (swing lever arm hypothesis).

1.1.4 Myosins functions

Intracellular transport of molecules, vesicles, and organelles are the most intuitive purpose of myosins within a cell, however diverse other functions have emerged with time. A role in mRNA movement was demonstrated for class V myosin in yeast, transporting mRNA toward the bud tip [Graydon B. Gonsalvez *et al.*, 2005]. Mitochondria transport has been instead ascribed to depend on myosin XIX in human [Quintero *et al.*, 2009] as well as on myosin V and VI in flies [Pathak *et al.*, 2010]. On top of the transport functions, myosins can also tether cargoes to actin, such as in the case of myosin V and VI that can anchor melanosomes and Golgi membranes, respectively. Myosins not only exploit microfilaments for their motor or anchor activities, but also can influence actin dynamics itself. This is the case of yeast myosin I that, through the interaction with WASp and the Arp2/3 complex, promotes actin polymerization [Sirotkin *et al.*, 2005].

In the complex process of cell migration myosins acquire more disparate roles. Albeit cell protrusion are primarily fuelled by actin polymerization at the leading edge, contraction forces generated by myosin II on microfilament bundles coordinate the retraction of the rear of the moving cell. While migrating, cells exploit also myosin X to form new integrin-based adhesions with the ECM at the leading edge [Zhang *et al.*, 2004], and contemporarily recycle older integrin through the action of myosin VI [Valdembri *et al.*, 2009]

1.1.4.1 Myosins and cancer

Uncontrolled proliferation, ability to prevent growth suppression, maintenance of replicative immortality, disruption of the programmed cell death mechanisms, evasion of immune surveillance, induction of angiogenesis, and the ability to migrate and form metastasis are acknowledged hallmarks of cancer [Hanahan *et al.*, 2011].

We previously stated the involvement of myosins in the latter two processes (see above). Nevertheless actin-based motors, through their functions, can lead to the appearance of many other cancer hallmarks in cells. Of outstanding interest, p53 posttranslational stability has been recently linked to the function of non-muscle myosin IIa. Knockdown of such motor protein stimulates squamous cell carcinoma formation in tumour-susceptible background [Schramek *et al.*, 2014]. Similarly, myosin VI was previously shown to participate in the p53-mediated survival pathway [Enari *et al.*, 2006]. Programmed cell death, which allows cells to kill themselves before becoming tumoural, was instead demonstrated to be influenced class V myosin, through its sequestering action of Bmf, a pro-apoptotic factor [Puthalakath *et al.*, 2001]. Moreover myosins are often involved in the maintenance of apical-basolateral polarity, which is lost in tumour cells undergoing epithelial-mesenchymal transition. On top of this, myosins play in processes such as angiogenesis, inflammation, and immune response, often hijacked from cancer cells [Ouderkirk *et al.*, 2014].

1.2 Myosin VI

Among all the myosin classes, myosin VI has the unique property to travel along actin filaments toward their minus-end. This protein is ubiquitously expressed in all multicellular eukaryotes. Myosin VI was first characterized in *Drosophila* [Kellerman *et al.*, 1992] and successively identified in *G. gallus*, *S. scrofa* [Hasson *et al.*, 1994], *M. musculus* [Avraham. *et al.*, 1995], in *C. elegans [Baker et al., 1997]* and *H. sapiens* [Avraham *et al.*, 1997].

1.2.1 Myosin VI mechanical properties and structural organization

At a molecular scale, myosin VI consists of a ≈1250-1300 amino acids-long polypeptide with two main functional domains (**Figure 5**), a motor–IQ domain sufficient for pointed-end (minus-end) directed movement, and a tail region. The N-terminus motor domain can interact with actin and ATP and possess ATPase activity, which is regulated by the unique insert 1 [Pylypenko *et al.*, 2011]. Release of ADP and P_i, the final step of the myosin motor cycle, causes conformational changes and thus force generation that are then transmitted to the rest of the molecule through the converter region to the insert 2, a stretch of ≈30 amino acids that can bind calmodulin and bestow myosin VI its unique reverse directionality through repositioning of the lever arm [Bryant *et al.*, 2007]; [Park *et al.*, 2007]. Downstream insert 2 a canonical IQ motif forms the lever-arm and allows interaction with a second calmodulin molecule. Some peculiarities of the motor property of myosin VI, such as its large (30-36 nm steps on actin [Nishikawa *et al.*, 2002]) were found to depend on the tail region. The proximal part is arranged in an extensible three alpha-helix bundle [Mukherjea *et al.*, 2009], while the distal part forms an elongated single alpha helix (or SAH) [Spink *et al.*, 2008] and terminates into a cargo-binding region of about 250 amino acids. Both these subdomains are unique to myosin VI and might explain the long pace of myosin VI. Two alternative hypotheses on the stepping mechanism of myosin VI have been put forward. In the first scenario, myosin VI SAH act as the lever-arm extension and dimerization occur between the cargo-binding domains and/or within the adaptor protein bound to the cargo-binding domain [Spink *et al.*, 2008]; [Yu *et al.*, 2009]. In the second hypothesis the unfolded three-helix bundle works as lever arm extension and dimerization takes place between this region and the SAH domain [Mukherjea *et al.*, 2009]; [Mukherjea *et al.*, 2014]. For certain functions dimerization of myosin VI seemed dispensable, as in the case of spermatid individualization, where

dimerization-defective mutants were shown to function as the wild-type molecule [Noguchi *et al.*, 2009; Noguchi *et al.*, 2006].

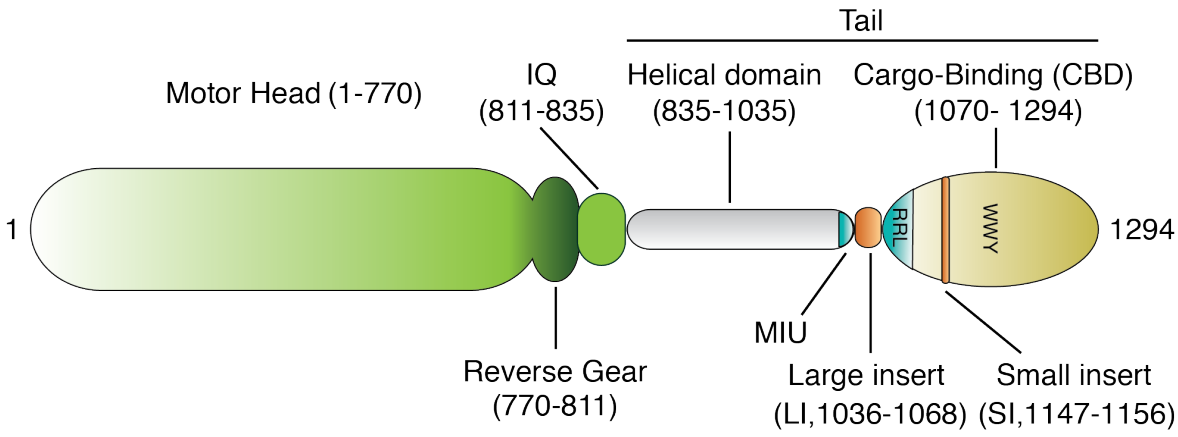

Figure 5: Myosin VI domains organization. Scheme of the different subdomains of myosin VI reported with their boundaries.

In the cargo-binding domain of myosin VI three main interaction surfaces are found. Among them a MIU (Motif Interacting with Ubiquitin) has been identified in myosin VI to bind ubiquitin [Penengo *et al.*, 2006]. On top of this the CBD contains also two acknowledged myosin VI ligand interaction surfaces, the "RRL" and "WWY" motifs (reviewed in [Tumbarello *et al.*, 2013]). The RRL triplet is reported to bind endocytic adaptors, including GAIP-interacting protein C-terminus (GIPC) [Bunn *et al.*, 1999; Spudich *et al.*, 2007], and autophagy receptors, such as optineurin [Sahlender *et al.*, 2005], Nuclear Dot Protein 52 (NDP52) and Traf6-binding protein (T6BP) [Morriswood *et al.*, 2007]. In the CBD of myosin VI, between the MIU and the RRL domains (**Figure 5**), an alternative splicing region has been identified [Buss *et al.*, 2001]. This has been defined as large insert (LI) and encompasses the sequence between residues 1036 and 1068 (numbering from the longest isoform), a region codified by three exons (**Figure 13**). A second alternatively spliced region is coded by

a single exon and encompass 9 amino acids, known as short insert (SI). This latter region is positioned downstream the RRL motif [Buss *et al.*, 2001].

An intrinsic level of complexity in deciphering myosin VI functions comes from the presence of different isoforms. Although myosin VI is widely expressed in most tissues, isoforms containing the LI are specifically found in polarized epithelial cells with well-developed apical microvilli [Au *et al.*, 2007; Buss *et al.*, 2001]. How the presence of LI in the tail influences the functions and intracellular targeting of myosin VI is not known. Up to now, isoforms lacking the LI present no specific expression/localization but they are required for polarized transport of tyrosine motif containing basolateral membrane proteins [Au *et al.*, 2007] and for maintaining an active pool of secretory granules near the plasma membrane of neurosecretory cells [Tomatis *et al.*, 2013].

1.2.2 Myosin VI functions

In the past years, different animal and cellular models have been exploited to investigate the functions of myosin VI. These studies have revealed that this motor protein potentially influences a large number of processes including asymmetric cell division, organelles architectures, autophagy, endocytosis, exocytosis, and cell migration.

In *Drosophila melanogaster* Jaguar (myosin VI) deletion was recently demonstrated to partially impact on flies viability since fly's progeny lacking Jaguar are viable but at non-Mendelian frequency [Morrison *et al.*, 2008]. Possible explanations for this effect might come from earlier studies where myosin VI was shown to be involved in oogenesis. During this process, knockdown of myosin VI revealed its importance in follicle cell morphology and migration [Deng *et al.*, 1999]. Myosin VI is also required to form and maintain the actin-cone that drives

cytoplasmic expulsion in spermatid individualization. In such process the individualization complex traverses the length of each spermatid resulting in the shared membrane of 64 spermatids. Jaguar allows membrane rearrangements that resolves the syncytium into individual spermatid [Rogat *et al.*, 2002];[Noguchi *et al.*, 2006]; [Noguchi *et al.*, 2009]. Myosin VI plays a critical role also in *C.* elegans spermatogenesis, being required for asymmetric segregation of cellular components [Kelleher *et al.*, 2000].

During embryonic development, in the process of syncytial blastoderm cleavage, Jaguar was shown to participate in furrow formation before cytokinesis [Mermall *et al.*, 1995]. In later stages of embryogenesis of *Drosophila*, myosin VI is involved in asymmetric cell division of neuroblasts progenitors. In these cells mitotic spindles align with the apical-basal axis and the subsequent asymmetric division generates a Ganglion Mother Cell (GMC) and a neuroblast. Accumulation of some cell-fate determinants, such as Miranda, at the basal membrane, depends on Jaguar activity during metaphase [Erben *et al.*, 2008].

The intracellular transport ability of myosin VI was also shown in *Drosophila* primary neurons, where it regulates the transport of mitochondria [Pathak *et al.*, 2010]. In this process, Jaguar establishes a tug-of-war with microtubules based motor proteins. Its depletion increases retrograde transport of mitochondria along the axon [Pathak *et al.*, 2010]. In the mature *Drosophila* nervous system, myosin VI is critical for the correct localization of recycling vesicles at the synapsis. This activity possibly depends on the tethering ability of the protein. Notably, in neuromuscular junctions myosin VI depletion causes an increase vesicles motility [Kisiel *et al.*, 2014].

The first direct evidences of a role for myosin VI in cell migration were obtained in *Drosophila*. In the process of oogenesis, a group of follicle cells (border cells) migrate towards the oocyte in a process that requires a functional Jaguar, DE-

cadherins and armadillo, the *Drosophila* homologue of β-catenin [Geisbrecht *et al.*, 2002]. Myosin VI knockdown was later found to inhibit ovarian cancer dissemination in nude mice [Yoshida *et al.*, 2004], a process that shows similarities with border cells migration.

In mammals, perturbations of myosin VI activity have been linked to several phenotypes. Studies on genetic-linked deafness highlighted the importance of several myosins, among which myosin VI. The *Snell's waltzer* (*sv*) mouse strain displays loss of hearing and balance in an autosomal and recessive way. Investigation on this mouse led to the identification of a truncation in the gene encoding for myosin VI as the primary cause of the phenotype [Avraham. *et al.*, 1995]. In normal mice, myosin VI is expressed at the level of the sensory hair cells of the inner ear. These cells develop short microvilli at the apical membrane, and some of them can further mature into elongated structure, known as stereocilia. Myosin VI is required to maintain the shape and integrity of these cellular protrusions. In the *Snell's waltzer* (*sv*) mouse the first steps of development of the stereocilia are normal but then they often fuse together [Self *et al.*, 1999]. Myosin VI localizes at the level of the cuticolar plate and the pericuticolar necklace of sensory hair cells. Absence of myosin VI lead to a rise of the apical membrane, which detach from the cuticolar plate, possibily indicate an anchoring function of this motor protein [Hasson *et al.*, 1997]. These findings were successively reproduced and corroborated in *Danio rerio* and *Homo sapiens*. In the first case, one of the two myosin VI-coding genes, *myo6b*, is predominantly expressed and localized at the level of the sensory epithelium of the ear [Seiler *et al.*, 2004]. In human, genetic and sequence analysis of myosin VI gene in deaf patients linked myosin VI mutations to a non-syndromic autosomal dominant form of deafness and cardiomyopathies [Melchionda *et al.*, 2001]; [Mohiddin *et al.*,

2004], therefore proving for a conserved role of myosin VI in the development of auditory system.

1.2.3 Myosin VI at the Golgi

One of the first observation on the intracellular localization of endogenous myosin VI in cultured cells was its enrichment at the level of the Golgi complex and at the leading edge of migrating cells in NRK and A431 [Buss *et al.*, 1998]. The Golgi complex is composed of a system of packed membranous cisternae that are divided into *cis*-, *medial*-, and *trans*-Golgi compartments (along the nucleus/periphery-axis). From the two sides of the complex an intricate net of tubules and vesicles emerge, forming the *cis*- and *trans*-Golgi networks [Gurel *et al.*, 2014]. Being a central node of vesicle trafficking in the cell, the Golgi complex receives and modifies proteins from the endoplasmic reticulum and those proteins are later engulfed into vesicles that might undergo exocytosis and/or fusion with other membranes. Clathrin cages coat vesicles emerging from the Golgi complex in a process similar to the one occurring at the plasma membrane during endocytosis [Liu *et al.*, 2001]. Early-, late-, and recycling endosomal compartments constantly exchange components with the Golgi [Lu *et al.*, 2014a]. Not surprisingly, this intricate system maintains its plasticity thanks to interaction with the cytoskeleton (both actin- and microtubule components), which act as a scaffold and directly affect vesicle budding and fission processes [Gurel *et al.*, 2014]. Myosin VI localization at the Golgi was shown to influence the morphology of the cisternae as well as the secretion of proteins. In particular, primary fibroblast from *Snell's waltzer* mouse showed reduced (~40%) size and altered morphology of the Golgi [Warner *et al.*, 2003]. Secretion of a soluble and secreted form of alkaline phosphatase (SEAP) was also reduced up to ~80% compared to controls [Warner *et al.*, 2003]. Overexpression of full-length myosin VI was able to rescue both

phenotypes [Warner *et al.*, 2003]. These functional observations were later confirmed in primary human prostate cancer cells, where myosin VI and GOLPH2 (a Golgi-resident protein) colocalize and were proposed as possible prostate cancer markers [Wei *et al.*, 2008]. Another link between myosin VI and the Golgi complex was found by Sahlender and colleagues who showed that depletion of optineurin results in Golgi complex fragmentation and myosin VI de-localization from the *trans*-Golgi network. Optineurin was identified as myosin VI interactor via an yeast two-hybrid assay [Sahlender *et al.*, 2005]. The authors could identify the region between amino acids 412 and 520 of optineurin as critical for myosin VI binding. By structure-function analysis and subsequent mutagenesis, the interaction surface on myosin VI was mapped on the ^{1116}RRL^{1118} sequence [Sahlender *et al.*, 2005]. SEAP secretion in fibroblast derived from *Snell's waltzer* mice was rescued by the overexpression of WT myosin VI, but not by the one of an optineurin binding-impaired mutant. Two threonine phosphorylation sites (^{1097}TINT^{1100}) on myosin VI were also found to be critical for optineurin binding [Sahlender *et al.*, 2005]. Trafficking of Vesicular Stomatitis Virus Glycoprotein (VSV-G) from the Golgi to the plasma membrane, as well as co-localization of myosin VI and Rab8 in vesicles underneath the plasma membrane was reduced in optineurin-depleted cells [Sahlender *et al.*, 2005]. Thus, in the Golgi optineurin appears to bridge myosin VI to Rab8, forming a tether that counteracts microtubule-mediated transport events [Sahlender *et al.*, 2005] (**Figure 6**). The deficiency in exocytosis described upon perturbation of myosin VI:optineurin complex was then more precisely ascribed to defects in the ER-to-Golgi transport and to diminished vesicle fusion events at the plasma membrane [Bond *et al.*, 2011].

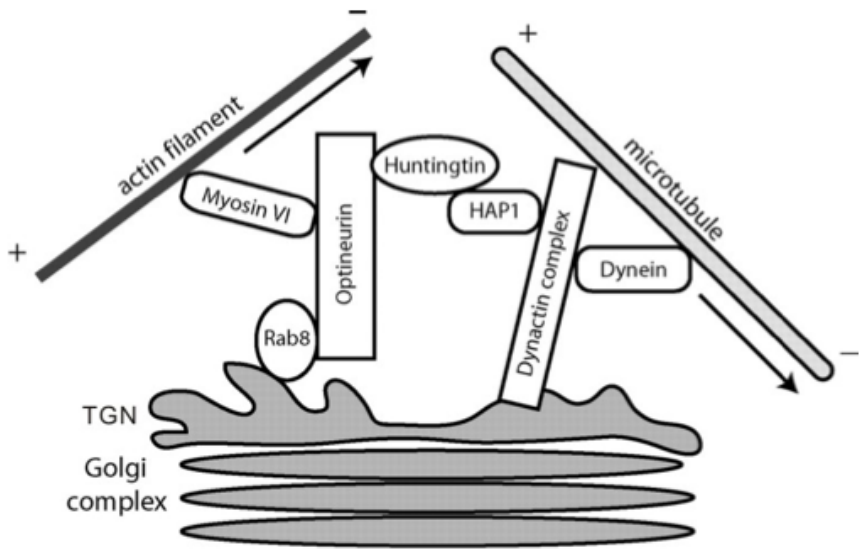

Figure 6: Optineurin bridges myosin VI to the Golgi system. Schematic representation proposed for the myosin VI:optineurin:Rab8 interaction at the level of the TGN. The complex stabilizes the Golgi architecture in a tug-of-war with microtubules and microtubule-based motor proteins. From [Sahlender *et al.*, 2005].

The ^{1116}RRL^{1118} motif in myosin VI has been shown to be critical for the interaction with proteins other than optineurin, namely TRAF6-binding protein (T6BP, also called TAXBP1), and its homologue nuclear dot protein 52 (NDP52) [Morriswood *et al.*, 2007]. These three proteins share common structural features [Birgisdottir *et al.*, 2013] and contain an LC3-interacting region (or LIR). As a consequence, they have been recently implicated in autophagy [Birgisdottir *et al.*, 2013] and mitophagy [Heo *et al.*, 2015]. LC3 is a ubiquitin-like modifier which, once lipidated (LC3-II), is incorporated into autophagosomes membrane and drives the process of fusion with endosomes and lysosomes. LC3-receptors that bind the surface of LC3-II-positive vesicles influence their fate [Birgisdottir *et al.*, 2013]. Indeed, optineurin, T6BP, and NDP52 [Birgisdottir *et al.*, 2013], participate to this process (**Figure 7a)**. Recently, also myosin VI has been involved in autophagy. Tumbarello and colleagues discovered that this motor protein acts as a bridge between the

endosomal marker Tom1 and the autophagosomal markers optineurin, T6BP, and NDP52 [Tumbarello *et al.*, 2012]. The authors demonstrated that autophagosomes accumulate in cells depleted for myosin VI, due to a defect in autophagosomes maturation and fusion with lysosomes. Taken together these results led to three hypotheses about of role of myosin VI in autophagosomes-lysosome fusion [Tumbarello *et al.*, 2012] that are reported in **Figure 7b**.

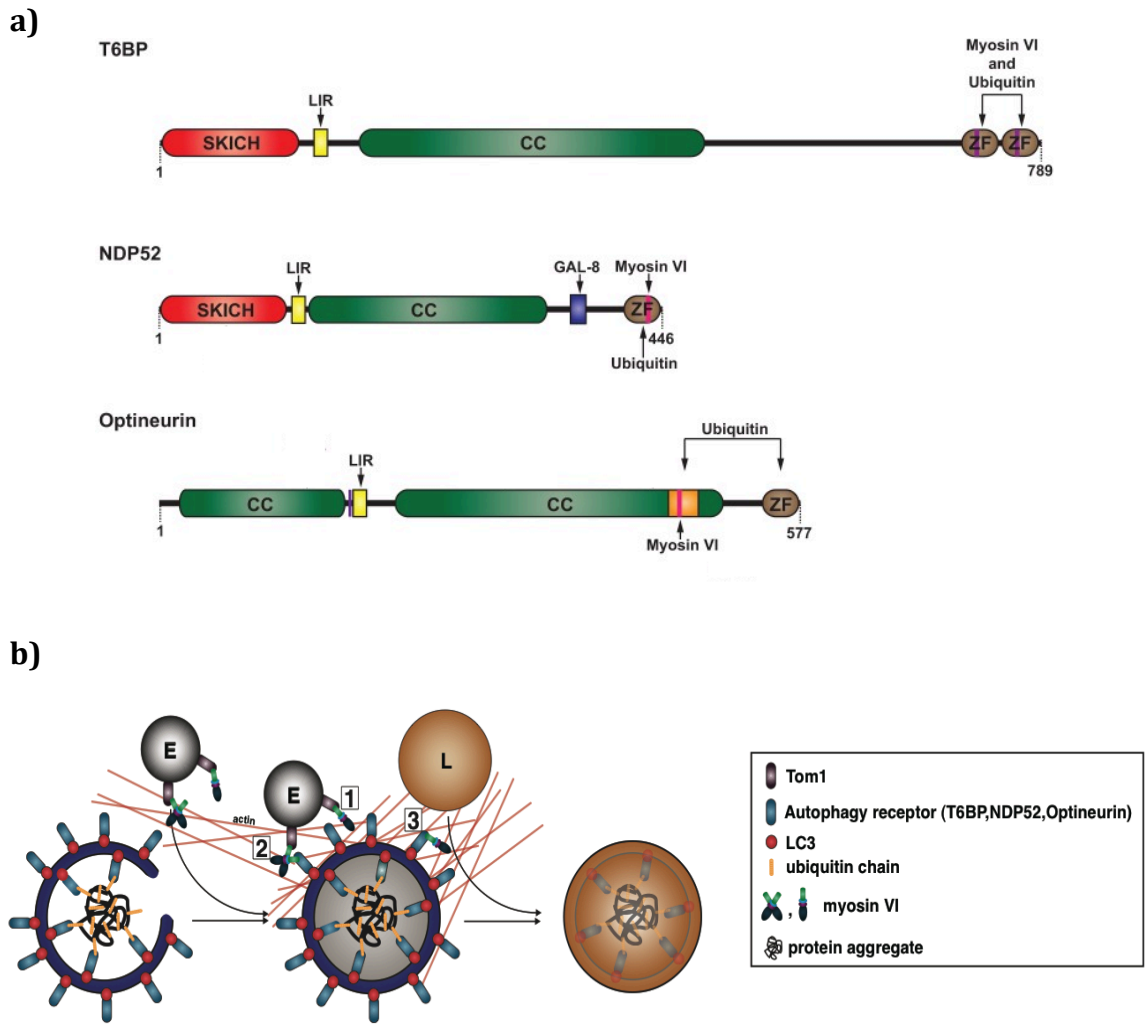

Figure 7 Possible functions of myosin VI and its interactors in autophagy. a) Domain structure and interacting partners of T6BP, NDP52 and optineurin. LIR, LC3-interaction motif; SKICH, SKIP–carboxyl homology domain; CC, coiled-coil domain; ZF, zinc-finger domain; GAL-8, galectin-8. Adapted from [Tumbarello *et al.*, 2012]. **b)** In the process of autophagy myosin VI might extert its function at three different levels: **1)** Monomeric myosin VI tethers Tom1-positive endosomes with

autophagosomes, a process required for autophagosome maturation. **2)** Dimeric myosin VI might bridge endosomal and autophagic compartments (presenting LC3II) through the simultaneous interactions with Tom1 and autophagy adaptors such as optineurin, NDP52, and T6BP. **3)** Tom1 localizes myosin VI to autophagosomes where it interacts with the autophagy adaptors and tethers autophagosomes to the actin cytoskeleton required for fusion with the lysosomal compartment. E = endosome, L = lysosome. [Tumbarello *et al.*, 2012].

1.2.4 Myosin VI at the Clathrin Coated Pits (CCPs)

As previously stated the tail of myosin VI can undergo alternative splicing in two different sites (LI and SI) [Buss *et al.*, 2001]; [Tomatis *et al.*, 2013]. Increasing evidences show that highly polarized tissues such as the intestine predominantly express the full LI sequence (myosin VI+LI) [Buss *et al.*, 2001]). Immunofluorescence studies localized myosin VI+LI containing at the apical region of polarized Caco-2 cells, a cell line that recapitulates most of the intestinal cells features [Buss *et al.*, 2001]). This isoform of myosin VI was shown to co-localize with clathrin-coated pits and to co-fractionate with clathrin-coated vesicles [Buss *et al.*, 2001]. Moreover overexpression of a dominant negative myosin VI tail bearing the LI impaired transferrin internalization at the plasma membrane.

Mechanistically, Disabled-2 (Dab2) was found to be the bridge between myosin VI and clathrin by yeast- and mammalian-two hybrid screens [Morris *et al.*, 2002]. Dab2 is an adaptor protein able to recognize specific cargoes or receptors at the plasma membrane [K.Mishra *et al.*, 2002]. This adaptor protein contains αAP-2- and clathrin-binding sites, as well as an N-terminal PTB (Phosphotyrosine interaction domain) [K.Mishra *et al.*, 2002] and a PtdIns(4,5)P_2 recognition domain [Alajlouni *et al.*, 2011] that anchors the molecule to the plasma membrane (**Figure 8**). Through its multiple interaction surfaces, Dab2 is able to recruit the endocytic machinery at the sites of internalization and to link clathrin-mediated endocytosis to the actin microfilament system via the myosin VI protein [K.Mishra *et al.*, 2002; Morris *et al.*,

2001]. The Dab2 interaction surface in myosin VI was mapped on the relatively conserved ^{1191}WWY^{1193} sequence [Spudich *et al.*, 2007].

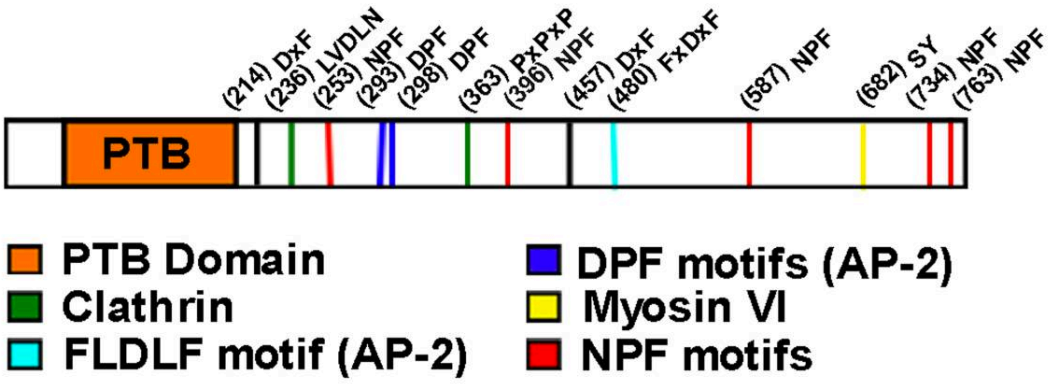

Figure 8: Disabled-2 domains organization. Schematic representation of the binding domains in mouse Dab-2. PTB: phospho-tyrosine binding; NPF: asparagine-proline-phenylalanine bound by EH domains (Eps15 Homology); DPF: aspartic-proline-phenylalanine bound by EH domains. From [Collaco *et al.*, 2010].

Later structural studies led to the identification on myosin VI of two additional interaction surfaces for Dab2, centered on R1160 and L1227. On the Dab2 molecule, the interaction myosin VI was mapped on the ^{682}SYF^{684} motif [Yu *et al.*, 2009]. The same study gave strong molecular evidences supporting the hypothesis that cargo binding induces dimerization of myosin VI, thus regulating the processive movement of the motor protein along actin filaments. Nevertheless additional studies showed that binding of molecules other than Dab2 trigger myosin VI dimerization. Among them PtdIns(4,5)P_2 that, upon binding to the motor protein, cause it to form dimers and contribute to myosin VI localization on clathrin vesicles [Spudich *et al.*, 2007].

The functional role of myosin VI in clathrin mediated endocytosis was demonstrated in highly polarized cells such as small intestine cells, polarized human airway epithelial cells, and renal proximal tubular cells. In the first two models endocytosis of the cystic fibrosis transmembrane conductance regulator (CFTR) was

used as substrate for the analysis. CFTR is a cyclic AMP-regulated Cl^- channel expressed in fluid transporting epithelia, and localized at the apical membrane of the cells forming the tissue. In polarized Calu-3 cells myosin VI was shown to co-immunoprecipitate with CFTR, Dab2, and clathrin in endogenous condition. Knockdown of the motor protein was also shown to increase the amount of CFTR at the apical membrane of the cells, due to defects in endocytosis, however the authors claimed that the myosin VI+LI splice variant was not necessarily the one involved in the process. Furthermore they postulated the role of αAP-2 in the CFTR endocytosis [Swiatecka-Urban *et al.*, 2004], which was later confirmed in following studies that proved a direct role of αAP-2 in directing myosin VI to CFTR, since αAP-2 but not Dab2 were found to interact directly with the ion channel [Collaco *et al.*, 2010]. In the same way myosin VI-knockout mice (*sv*) showed that renal proximal tubular cells have defects in morphology of the microvilli and in clathrin-mediated endocytosis [Gotoh *et al.*, 2010].

Non-canonical clathrin-mediated endocytosis processes were also shown to depend on myosin VI. In the case of big cargoes such as the intracellular parasite *Listeria monocytogenes* there is an active recruitment, induced by the bacteria, at the sites of internalization. In particular, Dab2, clathrin heavy chain, clathrin light chain, Huntingtin-interacting protein 1-related (Hip1R, which can promote actin polymerization at endocytic sites [Boulant *et al.*, 2011]), and finally myosin VI are recruited following a highly regulated cascade of events [Bonazzi *et al.*, 2012]. Myosin VI was shown to be necessary for the successful internalization of the cargo (**Figure 9**) [Bonazzi *et al.*, 2011]. In this context, this motor protein possibly provides the pulling force needed for the unusual membrane-deformation event at the basis of the clathrin-mediated endocytosis. Interestingly, the same molecular mechanism that mediate bacteria internalization, is responsible for reorganization of E-cadherin

mediated cell-cell junctions in cultured monolayers [Bonazzi *et al.*, 2012]. This might suits with previous evidences of the function of myosin VI in E-cadherin junction formation and stabilization [Maddugoda *et al.*, 2007].

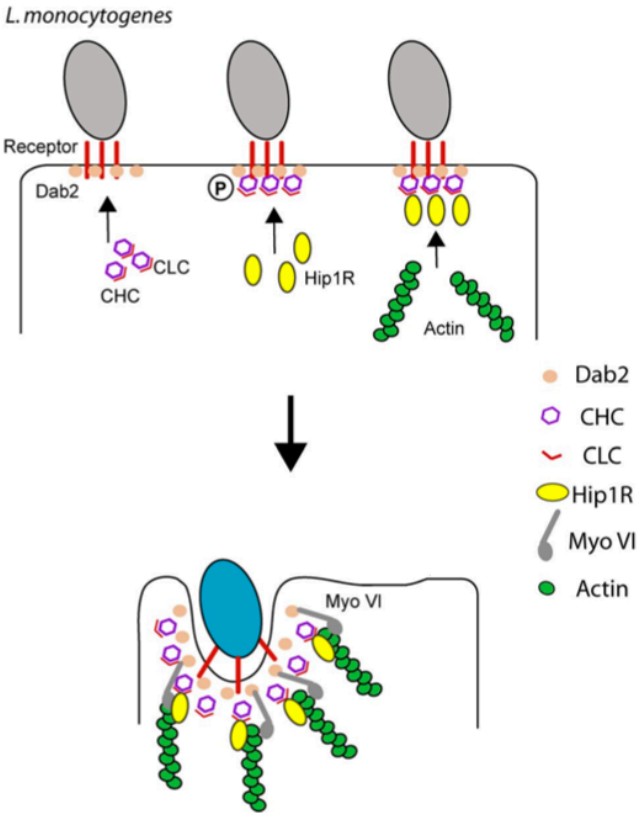

Figure 9: Model for myosin VI-dependent bacteria internalization. Receptors, activated by bacteria, recruit Dab2, clathrin heavy and light chains, followed by Hip1R, actin and myosin VI. The motor protein provides the pulling forces necessary for internalization. Adapted from [Bonazzi *et al.*, 2011].

1.2.5 Myosin VI at the cell-cell and cell-matrix adhesion sites

The active involvement of myosin VI in cell-cell adhesion (E-cadherin mediated) was demonstrated in several experimental setups. During the formation of mature adherens-junctions, Myosin VI bridges the intracellular region of E-cadherin with vinculin [Maddugoda *et al.*, 2007]. Again, functional studies performed in *Drosophila* pioneered the mammalian ones. In the fruit fly it was shown that the expression level

of E-cadherin, myosin VI, and armadillo (β-catenin) is mutually dependent, and that the motor protein interacts with armadillo by reciprocal pulldown experiments [Geisbrecht *et al.*, 2002]. In mammals, myosin VI knockdown resulted in altered junctions formation, both at the lateral and apical part of the cell [Maddugoda *et al.*, 2007]. The interaction of E-cadherin with myosin VI was later shown to be direct by *in vitro* pull-down experiments [Mangold *et al.*, 2012].

Migrating cells need to attach to substrates (usually extracellular matrix proteins, or ECM) in order to move and highly regulated balance of force of adhesion is of paramount importance in this context. Integrin are transmembrane dimeric proteins that are capable of signal across the membrane in both directions. They can sense the interaction with ECM components and transmit the signal to the cytoskeleton, or they can transduce an intracellular signal to the ECM [Harburger *et al.*, 2009]. In endothelial cells, myosin VI was shown to regulate, together with neuropilin1 (Nrp1) and GAIP-interacting protein C terminus (GIPC1), integrin traffic and therefore adhesion. The knockdown of myosin VI led to a reduced number of active (bound to the ECM) number of integrin molecules [Valdembri *et al.*, 2009]. The investigators showed that Nrp1, a receptor for vascular endothelial growth factor (VEGF) and semaphorin (SEMA) interact with GIPC at the site of cell-ECM adhesion. GIPC-dependent myosin VI recruitment on integrin regulates integrin activation in a positive manner [Valdembri *et al.*, 2009].

1.2.6 Myosin VI in cell migration and cancer

Increasing evidence showed that myosin VI contributes to the migrating/metastatic potential of cancer cells [Chibalina *et al.*, 2009]. Microarray expression data as well as immunohistochemistry analysis of tumour tissues from independent research groups revealed a strong overexpression of myosin VI in ovarian and prostate cancer tissues

[Dunn *et al.*, 2006; Yoshida *et al.*, 2004] that positively correlates with a clinically aggressive behavior. Notably, silencing of myosin VI expression in ovarian and prostate cancer cell lines decreases the migratory potential of these cells [Dunn *et al.*, 2006; Yoshida *et al.*, 2004]. Moreover, in prostate cancer cells, a reduction in clonogenic potential in soft-agar was also observed upon myosin VI depletion, suggesting an involvement of this protein in anchorage-independent growth [Dunn *et al.*, 2006]. Finally, myosin VI was identified as modulator of androgen receptor (AR)-dependent gene expression in prostate cancer [Loikkanen *et al.*, 2009].

Chibalina and colleagues have showed direct mechanistic evidences of the role of myosin VI in cell migration [Chibalina *et al.*, 2010]. The motor protein was described to confer directionality to cells moving towards an epidermal growth factor (EGF) gradient. This phenotype is due to the concerted role of myosin VI and optineurin that allow the delivery of the EGF-receptor (EGFR) directly on the leading edge, thus sustaining signalling and ultimately migration. In unstimulated condition myosin VI knockdown was also described to reduce the overall number and dimension of lamellipodia. However, in such condition, no reduction in the final speed of cells was scored [Chibalina *et al.*, 2010].

1.3 Clathrin and clathrin-mediated endocytosis

Cells exploit different routes of endocytosis to internalize plasma membrane receptors and small molecules from the external milieu. Among them, the clathrin-mediated endocytosis or CME, is the most extensively studied [McMahon *et al.*, 2011].

Clathrin is present in all eukaryotic cells and covers vesicles (CCV) that internalize from the plasma membrane. The Golgi complex also generates vesicles that present a clathrin-based coat [Liu *et al.*, 2001], but the term CME and CCV refers only to events occurring at the plasma membrane.

Clathrin not only acts in the endocytosis of a wide variety of molecules including nutrient, transporters, adhesion molecules, and receptors, but it also functions in mitosis [Royle *et al.*, 2005] and transcription regulation [Enari *et al.*, 2006]. Furthermore, bacteria and viruses can hijack clathrin-mediated endocytosis to enter the cytoplasm and accomplish their life cycle [Humphries *et al.*, 2013].

1.3.1 Clathrin-coated vescicles

Observed for the first time in 1964 by EM, clathrin-coated vesicles were isolated about a decade later when Barbara Pearse fractionated pig brain lysate and was able to obtain pure CCVs. The major component of these vesicles resulted to be a protein of about 180 kDa that was named clathrin [Pearse, 1976]. After 40 years of intense studies we know that clathrin-coated vesicles are composed of three layers: an internal membrane bilayer, a medial layer of adaptor proteins, and the most external and scaffolding clathrin cage. The scaffold is a supramolecular protein complex formed by subunits of three copies of clathrin heavy chain and three clathrin light chain that, together, form a three-legged curled and pinwheel-like triskelion [Brodsky, 2012].

Vesicles usually form and are filled of cargos in a tightly regulated way, but some receptors, such as the transferrin receptor or the low-density lipoprotein receptor, are internalized constitutively even without any bound ligand. For receptor tyrosine kinases (RTKs) or G-protein coupled receptors the ligand-induced clathrin-mediated endocytosis starts after a conformational changed induced by the ligand activation. This could be due to an unmasking of structural signal/s already present in the tail of the receptors or by post-translational modifications occurring at the receptor (phosphorylation and ubiquitination are the most common one, see [Sigismund *et al.*, 2012] for a review). Adaptor proteins recognize these signals on the

cytoplasmic side of the receptors and allow for an increase of local concentration of receptors at the site where clathrin-coat start to assemble. Clathrin is able to self-assemble into lattice at the plasma membrane [Ybe *et al.*, 1999]. While some CCPs might undergo spontaneous dissolution, cargo accumulation into pits is a crucial step that allows the further recruitment of clathrin and formation of a productive vesicle [Loerke *et al.*, 2009]. The successive clathrin polymerization drives further membrane curvature and the final step, the vesicle scission, is due to dynamin GTPases [Mettlen *et al.*, 2009]. A schematic representation of a pit formation, maturation and vesicle scission is reported in **Figure 10**.

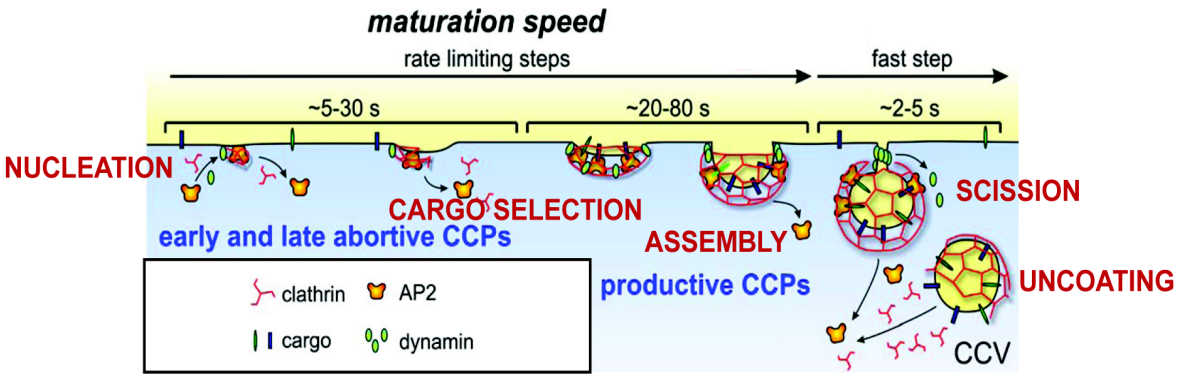

Figure 10: **Clathrin-coated vesicle formation**. Clathrin-coated vesicles (CCVs) forms from productive clathrin-coated pits (CCPs) that have undergone the maturation process. The maturation process foresees nucleation, cargo selection, coat assembly, vesicle scission, and uncoating. An endocytosis checkpoint, dependent on the concentration of cargo, AP2 adaptors, and likely other factors, controls progress through the maturation process. CCPs that do not progress beyond this restriction point abort by sequential disassembly of AP2 and clathrin. From [Loerke *et al.*, 2009].

1.3.2 The clathrin-coat: clathrin heavy chain

Clathrin lattices are polyhedral assembly of clathrin heavy and light chains. These protein are quite conserved among eukaryotes and underwent gene-duplication during evolution in conjunction with the appearance of vertebrates [Wakeham *et al.*,

2005]. In humans, the two clathrin heavy chain genes are CLTC and CLTCL1 (also known as CHC17 and CHC22), positioned at chromosome 17 and 22, respectively. The two proteins show 85% of sequence identity. Most of the biochemical, functional, and structural data in literature refer to CLTC that is responsible of the ubiquitous clathrin coated vesicles that mediate membrane traffic [Brodsky, 2012]. CLTCL1 is implicated in specialized membrane organization in skeletal muscle [Vassilopoulos *et al.*, 2014], is involved in retrograde transport from endosomes to the *trans*-Golgi network [Liu *et al.*, 2001], and in regulation of the glucose transporter GLUT4 in muscle and fat cells [Vassilopoulos *et al.*, 2009].

Clathrin heavy chains molecules are quite big proteins (different isoforms comprise from 1640 to 1679 amino acids) and no high-resolution full-length structures are up to now available. Nonetheless, efforts from different groups led to the knowledge of the overall conformation of the protein (see **Figure 11** for a schematic view). The N-terminus of CLTC, (1-330 amino acids), is known as the terminal domain (or TD) and assume a β-propeller conformation [Haar *et al.*, 1998], which allows the interaction with several adaptor proteins. Binding with proteins containing the clathrin box (generalized as $L\Phi X\Phi$[DE]) usually takes place at four different spots on the propeller. A short linker separate the TD from the following regions named ankle, distal leg, knee, and proximal leg. All these parts are organized into eight CHC repeats element (CHCR), α-solenoids composed of 10 helices of 10-12 residues. The vast majority of the interactions that allow the trimerization of CHC are mapped in the C-terminal region of the molecule, in the trimerization domain (or TxD). This comprises a helical tripod, starting from CHCR7 that gives the triskelion its classical orientation in respect to the plasma membrane [Wilbur *et al.*, 2010]. The proximal leg region of clathrin heavy chain, as well as its TxD domain, are involved in

the interaction with clathrin light chains.

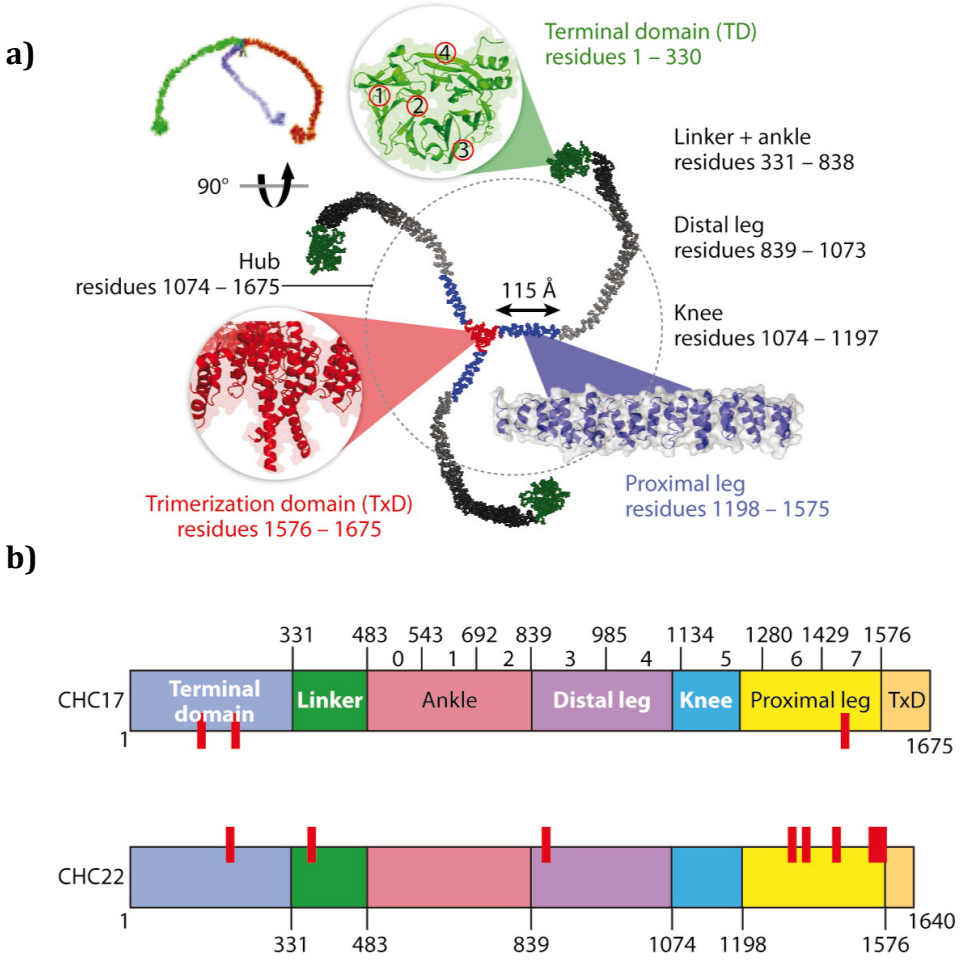

Figure 11: **Clathrin heavy chains**. **a)** structure of CHC17, derived from PDBs (triskelion-accession number 3IYV; trimerization domain-accession number 3LVH; terminal domain-accession number 2XZG; proximal leg-accession number 1B89). The four numbered sites on the TD structure represent the binding sites for interacting proteins. **b)** aligned domain organization of CHC17 and CHC22. The eight CHCRs (0 to7) in CHC17 are reported with their boundaries. The red marks highlight differences between the CHC17 and CHC22 proteins. From [Brodsky, 2012]

1.3.3 The clathrin-coat: clathrin light chain

In contrast to the two heavy chains, the two vertebrate clathrin light chains (LCa or CLCa and LCb or CLCb) have more divergent sequences (60% identity), but their functions are more similar. Within the cell, LCa/b binds selectively to CLTC, whereas CLTCL1 does not functionally interact with either light chain.

Clathrin light chains are polypeptides of around 25 kDa. In human the two genes LCa and LCb are positioned at chromosome 9 and chromosome 5, respectively. The two proteins show similar domain organization (see **Figure 12** for a schematic view).. Already in 1991, Brodsky and colleagues described LCs as linear array of interaction surfaces [Brodsky *et al.*, 1991], and indeed, several proteins were found to interact with them. As reported in **Figure 12**, from the N- to the C-terminal LCs present: a conserved region of 23 aa with 100% identity, the Hip1/Hip1R binding region [Ybe *et al.*, 2007a], a calcium (Ca^{2+}) binding region, the heavy chain binding region, a neuronal-specific insert, and a calmodulin-binding domain. Interestingly, some features are exclusively present in one of the two genes, such as the phosphorylation site on LCb and the Hsc70 interacting surface on LCa (reviewed in [Brodsky, 2012]).

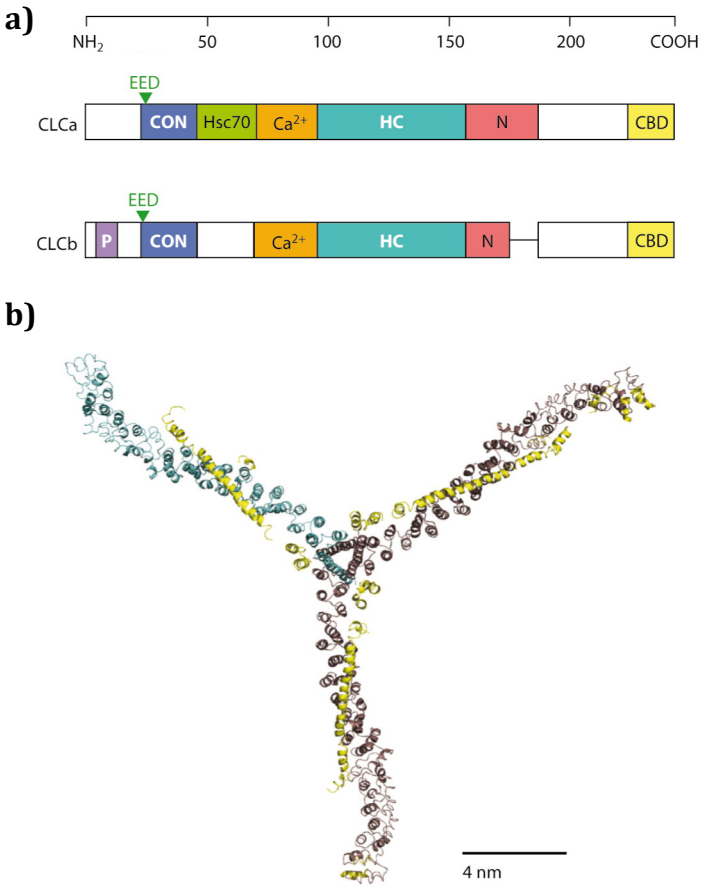

Figure 12: **Clathrin light chains**. **a)** Domain organization and alignment of LCa and LCb. EED are the three acid charged residues that regulate clathrin assembly within the 22-residue conserved region (CON). This sequence includes the binding site for Hip proteins. Other features shared by the two LCs include an EF-hand that binds calcium (Ca2+), the heavy-chain-binding region (HC), neuronal-expressed intron (N), and a calmodulin-binding domain (CBD) at the C-terminal. LCa has a unique region (Hsc70) that stimulates Hsc70 activity in vitro, and LCb has a unique serine phosphorylation site (P). **b)** Low-resolution structure (7.9 Å) of LCb (in yellow) bound to the CLTC Hub region (residues 1074–1675). Modified from [Brodsky, 2012]

Even though the presence of LCs on clathrin coats has been known for long now, their functions are partly unclear or under debate. The non-rigid structure of LCs allows the molecules to establish wide interaction surfaces on CLTC that goes from the TxD domain to the knee region and LC is thought to stabilize trimerization [Ybe *et al.*, 2007b]. On another study, LCs appear to fine-tune the conformation of triskelia by assuming a more extended or retracted conformation on the knee region [Wilbur *et al.*, 2010]. While this interaction impacts directly on cages formation, LC can also

influence the life of a vesicle through the interaction with the uncoating factor heat shock cognate 70 (Hsc70), that is activated once a CCV is pinched from the membrane [DeLuca-Flaherty *et al.*, 1990].

In spite of these roles in clathrin-coat assembly, tuning, and uncoating, the knockdown of LCs impact on clathrin-mediated endocytosis only in few reported cases. Ferreira and colleagues reported that knockdown of either LCa or LCb inhibit endocytosis of some G-protein coupled receptors, and that for the same process the phosphorylation of LCb residue S204 is also necessary [Ferreira *et al.*, 2012]. LCs are also critical for the endocytosis of less-canonical cargoes such as *Listeria monocytogenes* [Bonazzi *et al.*, 2011]. In this process, LCs re-localize Hip1R at the site of internalization and this event, stimulates the polymerization of actin and the subsequent membrane curvature of the clathrin-coated pits. Interestingly, actin engagement is necessary to complete membrane deformation into a coated pit on apical surfaces of polarized cells and, more generally, on the surface of any cell in which the plasma membrane is under tension from osmotic swelling or mechanical stretching [Boulant *et al.*, 2011]. In this context where membrane tension seems to determine the actin dependence of clathrin-coat assembly both LC and its interactor Hip1R are necessary to complete the invagination process [Boulant *et al.*, 2011].

2. MATERIALS AND METHODS

2.1 Solutions

2.1.1 10X SDS-PAGE running buffer

Glycine	192 mM
Tris HCl, pH 8.3	250 mM
SDS	1%

2.1.2 10X Western transfer buffer

Glycine	192 mM
Tris HCl, pH 8.3	250 mM

For 1X western transfer buffer, the 10X stock was diluted 1:10 with ddH2O and 20% v/v methanol or ethanol.

2.1.3 50X TAE (Tris-Acetate-EDTA)

Tris base	2 M
Acetic acid	1 M
EDTA, pH 8	10 mM

The pH was adjusted to 8.5 with HCl and distilled H2O was added to bring the volume up to 1 liter.

2.2 Protein buffers

2.2.1 1X JS buffer

HEPES, pH 7.4	50 mM
NaCl	50 mM

Glycerol	10%
Triton X-100	1%
$MgCl_2$	1.5 mM
EGTA	5 mM

200X Protease inhibitor cocktail from Calbiochem, sodium pyrophosphate pH 7.5 20mM, sodium fluoride 250 mM, PMSF 2 mM, and sodium orthovanadate 10 mM were added to the buffer just before use.

2.2.2 1X Laemmli buffer

SDS	2 %
Tris HCl, pH 6.8	62.5 mM
Glycerol	10%
Bromophenol blue	0.1%
β-Mercaptoethanol	5 % (v/v)

2.3 Reagents

2.3.1 Antibodies

Antibodies and their suppliers were: anti-FLAG (F3165, Sigma), anti-His (16B12, Babco), anti-myosin VI (MUD-19, Sigma), anti-myosin VI (1295, generated by EUROGENTEC S.A.), anti-Clathrin Heavy Chain antibody (MA1-065, Pierce), anti-Clathrin Heavy Chain (clone 23, 610499, BD bioscience), anti-CLINT1 (NBP1-05991, Novus biological), anti-COPB2 (sc13332, Santa Cruz), anti PI3KC2α (611046 BD Biosciences), Anti-Dab2 (610465, BD Biosciences), Anti-GFP (G1544, Sigma), Anti GFP agarose/GFP-Trap (gta-20, Chromotek).

2.3.2 RNAi oligos

Myosin VI Oligo#2:

5'-CAAGGAGTTATGCTGACATAATTCT-3´

Myosin VI Oligo#3:

5'-GAGGCTGCACTAGATACTTTGCTAA-3´

HeLa stably knocked down for Myosin VI were generated using a pSUPER vector carrying the following shRNA, targeting a sequence in the motor domain:

For:

5'-TGGAATATTGTGCTGAATTATTCAAGAGATAATTCAGCACAATATTCCTTTTTTC-3´

Rev:

5'-GAGAAAAAAGGAATATTGTGCTGAATTATCTCTTGAATAATTCAGCACAATATTCC-3´

2.4 Cloning techniques

2.4.1 Agarose gel electrophoresis

DNA samples were loaded on 0.8%-2% agarose gels along with DNA markers (1kb or 100bp DNA Ladder, NEB). Gels were made in TAE buffer containing ethidium bromide (Sigma), according to manufacturer's instructions, and run at 80 V until desired separation was achieved. DNA bands were visualized under a UV lamp.

2.4.2 Minipreps

Individual colonies were used to inoculate 2 ml LB (containing the appropriate antibiotic) and grown overnight at 37°C. Bacteria were transferred to Eppendorf tubes and centrifuged for 5 minutes at 16,000xg using a 5415 R centrifuge. Minipreps

were performed with the Wizard Plus SV Minipreps Kit (Promega) following manufacturer's instructions. The plasmids were eluted in 50 µl nuclease free H2O.

2.4.3 Large scale plasmid preparation

Cells containing transfected DNA were expanded into 250 ml cultures overnight. Plasmid DNA was isolated from these cells using the Qiagen Maxi-prep kit according to manufacturer's instructions.

2.4.4 Transformation of competent cells

An aliquot of competent cells TOP10 (Invitrogen) were thawed on ice for approximately 10 minutes prior to the addition of plasmid DNA. Cells were incubated with DNA on ice for 30 minutes and then subjected to a heat shock for 45 seconds at 42°C. Cells were returned to ice for an additional 5 minutes. Then, 300 µl of SOC was added and the cells were left at 37°C for further 60 minutes before plating them onto agar plates with the appropriate antibiotic. Two plates for each reaction were used, one plated with 100 µl of the transformed bacterial cells and the other one with the rest. Plates were incubated overnight at 37°C.

2.5 Constructs and plasmids

GFP-PI3KC2a was kindly provided by Dr. Emilio Hirsch, SFB-DDB1 by Dr. Maddika Subba Reddy, GFP-optineurin by Dr. Alain Israel, FLAG-T6BP by Dr. Folma Buss, His-GIPC by Dr. Guido Serini, FLAG-NDP52 by Dr. Felix Randow.

Human myosin VI cDNA KIAA0389 (isoform 1) was obtained from Kazusa DNA Research Institute (Kisarazu, Japan); PCR amplified and cloned into pGEX 6P1 (Amersham Pharmacia Biotech), pEGFP-C2 (Clontech). Myosin VI isoform 2 and

isoform 3 were generated by mutagenesis (deletion and insertion, respectively) using isoform 1 as template and the following primers:

iso2 for: 5'-GGTACTAAGAAATATGATCTTAGTAAATGG-3´

iso2 rev: 5'-TCTCCGCAGCGCCAGGTCGGC-3´

iso3 for: 5'-CCGGTGACAAGCAAAAATGATGGAACAAGACCCAAAATGA-3´

iso3 rev: 5'-ATAGCTATCCAGGCTCCGCAGCGCCAGGTCGGCC-3´

All other constructs described were engineered by site-directed mutagenesis or recombinant PCR and sequence verified.

2.5 Cell culture

2.5.1 Cell lines

HEK293T (ILC) and HEY (CELLution biosystems) cells were maintained in monolayer cultures in Dulbecco's Modified Eagle's Medium (DMEM, Lonza) supplemented with 10% fetal calf serum and 2 mM L-glutamine. MCF10A cells (ATCC) were cultured in DMEM/F12 medium (Gibco) supplemented with 5% horse serum, hydrocortisone (0.5 µg/ml), insulin (10 µg/ml), cholera toxin (50 ng/ml) and EGF (20 ng/ml). OVCAR-3, OVCAR-4, OVCAR-5, OVCAR-8, MDA-MB-231 (NCI-60) and COLO-704 (DSMZ) cells were maintained in RPMI-1640 (Lonza) containing 10% fetal calf serum and 2 mM L-glutamine. SKOV 3 cells were grown in McCoy's 5A (Gibco) medium supplemented with 10% fetal calf serum. HeLa cells (ATCC) were maintained in Minimum Essential Medium (MEM, Gibco) supplemented with 10% fetal calf serum, 1% non-essential amino acids, 2 mM L-glutamine and 1 mM Na-Pyruvate. All cell lines were authenticated at each batch freezing by STR profiling (StemElite ID System, Promega). All cell lines were tested for mycoplasma at each batch freezing with both PCR and a biochemical test (MycoAlert, Lonza).

2.5.2 Isolation, culture and processing of primary epithelial ovarian cancer cells

Patient-derived tissue samples were collected with the approval of the Ethical Committee of the European Institute of Oncology. Fresh biopsies of ovarian cancer were obtained from patients with high-grade epithelial ovarian serous carcinoma who underwent surgical tumour debulking. Fresh biopsies of normal ovaries were obtained upon informed consent from patients undergoing adnexectomy for non-ovarian gynaecological pathologies.

All tumours were digested in DMEM/F12 medium (Gibco) containing 2 mM glutamine, 1% Penicillin/Streptomycin, 200 U/ml collagenase IA and 100 U/ml hyaluronidase. Normal ovaries were digested in 5U/ml Dispase for 30 minutes at 37°C and then the organ surfaces were scraped to isolate the epithelial cells. The derived primary epithelial cells were maintained in monolayer adherent cultures in collagen I Cellware coated flask (Corning) in DMEM/F12 medium (Gibco) containing 1% fetal bovine serum, 2 mM glutamine, 1% Penicillin/Streptomycin, 0.2% gentamicin, 0.2% amphotericin, 10 mg/ml transferrin, 1 mg/ml insulin, 1 mg/ml hydrocortisone, 10 mM HEPES pH 7.5, 50 mM ascorbic acid, 15 nM sodium selenite, 50 ng/ml cholera toxin, 10 nM EGF, 35 mg/ml bovine pituary extract, 10 nM T3, 10 nM β-estradiol. For RNA extraction, $5x10^6$ primary cells were washed in PBS and the cell pellets were snap frozen in dry ice.

2.5.3 Transfections

RNAi transfections

RNAi transfections were performed using LipofectAMINE RNAi MAX reagent from Invitrogen, according to manufacturer's instructions. Cells were subjected to a single reverse transfection, treated with 8 nM RNAi oligo and analyzed 4 days after

DNA transfections

For biochemical purposes (i.e., GST-protein pull-down assay), DNA transfections were performed using Lipofectamine 2000 reagent from Roche, according to manufacturer's instructions. Briefly, cells were plated at 80% confluency on 10 cm cell culture dishes. The day after cells were transfected with 5 µg DNA and 20 µl Lipofectamine. 24 hours after transfection cells were lysed and subjected to pull-down assay.

For immunofluorescence studies, DNA transfections were performed using FuGENE 6 reagent from Roche, according to manufacturer's instructions. Briefly, cells were plated at 50% confluency in 10 cm cell culture dishes. The day after cells were transfected with 5 µg DNA and 30 µl of FUGENE 6. The following day cells were plated on 28 mm coverslips and 48 hours after transfection cells were analyzed by live imaging.

2.5.4 Isoform detection by PCR

Expression of myosin VI isoforms in various cell lines was assessed by PCR. Messenger RNA was isolated from cells grown on plastic dishes using TRIzol reagent (Invitrogen) and RNeasy Mini Kit (Qiagen) according to the manufacturer's protocols. Genomic DNA and RNA retro-transcription was performed with QuantiTect Reverse Transcription Kit (Qiagen). cDNA obtained was used in PCR reactions with primers flanking the spliced region:

For: 5´-CCGAGCTCATCAGTGATGAGGC-3´

Rev: 5´-CCAAGCATGATACACTTTTAGTCTCC-3´

2.6 Protein procedures

2.6.1 Cell lysis

After washing with PBS 1X, cells were lysed in JS directly in the cell culture plates using a cell-scraper and clarified by centrifugation at 16,000 xg for 20 min at 4ºC using a 5415 R centrifuge. Protein concentration was measured by the Bradford assay (Biorad) following manufacturer's instructions.

2.6.2 SDS-Polyacrylamide gel electrophoresis (SDS-PAGE)

Gels for resolution of proteins were made from a 30%, 37,5:1 mix of acrylamide: bisacrylamide (Sigma). As polymerization catalysts, 10% ammonium persulphate (APS) and TEMED were used.

Separating gel mix

	Gel %			
	6	**8**	**10**	**15**
Acrylamide mix (ml)	2	2.7	3.3	5
1.5M Tris HCl pH 8.8 (ml)	2.5	2.5	2.5	2.5
ddH2O (ml)	5.3	4.6	4	2.3
10% SDS (ml)	0.1	0.1	0.1	0.1
10% APS (ml)	0.1	0.1	0.1	0.1
TEMED (ml)	0.01	0.01	0.01	0.01
TOTAL (ml)	10	10	10	10

Separating gel mix

Acrylamide mix (ml)	1.68
1M Tris HCl pH 6.8 (ml)	1.36
ddH2O (ml)	6.8
10% SDS (ml)	0.1
10% APS (ml)	0.1
TEMED (ml)	0.01
TOTAL (ml)	10

2.6.3 Immunoblot (IB)

Desired amounts of proteins were loaded onto 1-1.5 mm thick SDS-PAGE gels for electrophoresis (Biorad). Proteins were transferred in western transfer tanks (Biorad) to nitrocellulose (Schleicher and Schnell) in 1X Western transfer buffer (supplemented with 20% methanol or ethanol) at 30 V overnight or 100 V for 1 hour for small gels and at 30 V overnight or 0.8 A for 2 hours for large gels. Ponceau staining was used to determine the efficiency protein transfer onto the filters. Filters were blocked for 1 hour (or overnight) in 5% milk in TBS supplemented with 0.1% Tween (TBS-T). After blocking, filters were incubated with the primary antibody, diluted in TBS-T 5% milk, for 1 hour at room temperature, followed by three washes of five minutes each in TBS-T. Filters were then incubated with the appropriate horseradish peroxidase-conjugated secondary antibody diluted in TBS-T for 30 min. After the incubation with the secondary antibody, the filter was washed 3 times in TBS-T (5 minutes each) and the bound secondary antibody was revealed using the ECL method (Amersham).

2.6.4 Immunoprecipitation

For co-immunoprecipitation experiments, HeLa cells stably knocked-down for myosin VI were transfected using Lipofectamine (Life Technologies) according to manufacturer's instruction and IP was performed using 500 µg of lysate and GFP-Trap (Chromotek) in JS buffer.

2.7 Protein production and purification

2.7.1 GST-fusion protein production

GST-fusion proteins were expressed in *E. coli* strain BL21 (DE3) Rosetta at 18°C for 16 hr after induction with 1 mM IPTG at an OD_{600} of 0.5. Cells were then pelleted at 4000 rpm for 10 minutes at 4°C and resuspended in GST-lysis buffer (20 ml/liter of bacteria). Samples were sonicated 5 times for 20 seconds each on ice and lysates were cleared by centrifugation at 20000 rpm for 30 minutes at 4°C. 1 ml of glutathione-sepharose beads (GE healthcare), previously washed 3 times with GST-lysis buffer, was added to the supernatants and samples were incubated for 2 hour at 4°C with rocking. Beads were washed with PBS/0.1% Triton and equilibrated in storage buffer.

GST lysis buffer

Hepes, pH 7.5	50 mM
NaCl	150 mM
EDTA	1 mM
Glycerol	5 %
NP40	0.1%
Protease Inhibitors	1:500

GST maintenance buffer

Hepes, pH 7.5	50 mM
NaCl	100 mM
EDTA	1 mM
Glycerol	10 %
DTT	1 mM

2.7.2 Cleavage of GST-fusion proteins

GST-fusion proteins were cleaved with PreScission Protease. 1 unit of enzyme for 100 µg of fusion protein was added to the beads in the presence of GST-maintenance solution and either incubated overnight at 4°C or for 4 hours at room temperature. After cleavage the supernatant containing the cleaved protein was collected and beads were washed twice to allow the complete recovery of the cleaved protein.

2.7.3 Fast protein liquid chromatography

After cleavage from the GST tag, proteins were purified using size exclusion chromatography. Prior to run on a Superdex 75 column, connected to an ÄKTAFPLC system (GE-Healthcare), samples were concentrated using Vivaspin concentrators (GE-Healthcare) and centrifuged at 6000 x g at 4°C. The concentrated sample was run onto a Superdex 75 column in the following gel filtration buffer:

Gel filtration buffer

20	mM	Tris pH 7
100	mM	NaCl

1	mM	EDTA
1	mM	DTT
5%		glycerol

Purity of the peak was assayed by SDS-PAGE gel. The desired fractions were collected, pooled, and concentrated using Vivaspin tubes. The final concentration of the samples was obtained as the ratio between the measured absorbance at 280 nm and the theoretical molar extinction coefficient at 280 nm, according to Lambert–Beer's law.

2.7.4 GST pull-down

GST-fusion proteins immobilized onto GSH beads were incubated for 2 h at 4°C in JS buffer (50 mM Hepes pH 7.5, 50 mM NaCl, 1.5mM $MgCl_2$, 5mM EGTA, 5% glycerol and 1% Triton X-100) with either 1 mg of HEK293T cellular lysate or 200 µg of transfected HEK293T cellular lysate. Detection was performed by immunoblotting using specific antibody. Ponceau-stained membrane was used to show loading of GST-fusion proteins.

2.8 Mass spectrometry

2.8.1 Liquid chromatography-tandem MS (LC-MS/MS) analysis

Proteins were resolved by SDS-PAGE on a gradient gel (4-12 % TGX Precast Gel, Biorad) and stained with Colloidal Blue (Colloidal Blue Staining Kit, Invitrogen). Each lane was divided into 5 slices and digested with trypsin. Briefly, samples were subjected to reduction in 10 mM DTT for 1 hour at 56ºC. Digestion was carried out saturating the gel with 12.5 ng/µL sequencing grade modified trypsin (Promega) in 50 mM ammonium bicarbonate, overnight. Peptide mixtures were acidified with tri-

fluoro acetic acid (TFA, final concentration 3%), extracted from gel slices with 30% acetonitrile (ACN)/ 3% TFA, dried in a Speed-Vac and resuspended in 20 µL of 0.1% FA. Three technical replicates of 5 µL injected for each sample were analysed on a Fourier transformed-LTQ mass spectrometer (Thermo Electron, San Jose, CA). Peptides separation was achieved by a linear LC gradient from 100% solvent A (5 % ACN, 0.1% formic acid) to 20% solvent B (ACN, 0.1% formic acid) over 33 min and from 20% to 80% solvent B in 4 min at a constant flow rate of 0.3µL/min on Agilent chromatographic separation system 1100 (Agilent Technologies, Waldbronn, Germany) equipped with a 15 cm fused-silica emitter of 75 µm inner diameter (New Objective, Inc. Woburn, MA USA), packed in-house with ReproSil-Pur C18-AQ 3 µm beads (Dr. Maisch GmbH, Ammerbuch, Germany) using a high-pressure bomb loader (Proxeon, Odense, Denmark). Survey MS scans were acquired in the FT from m/z 350-1650 with 100,000 resolution. The five most intense doubly and triply charged ions were automatically selected for fragmentation. Target ions already selected for the MS/MS were dynamically excluded for 60s.

2.8.2 Data processing and protein quantification analysis

Raw MS files were converted into peaklist (.msm files); all MS/MS samples were analysed using Mascot (Matrix Science, London, UK; version 2.3.02) set up with the following parameters: UniProt_CP_Human_20140416 database (88708 entries), Taxonomy Homo sapiens, enzyme Trypsin, maximum missed cleavages 2, fixed modification carbamidomethyl cysteine, variable modifications methionine oxidation and acetyl (protein N-terminus), peptide tolerance 10 ppm, MS/MS tolerance 0.5 Da, instrument ESI-TRAP.

Interactomics results were generated with Scaffold_4.3.4 (Proteome Software Inc., Portland, OR) and protein quantitation was displayed as Total Spectral Count. Peptide

identifications were accepted if they could be established at greater than 95.0% probability by the Peptide Prophet algorithm with Scaffold delta-mass correction [Keller *et al.*, 2002]. Protein identifications were accepted if they could be established at greater than 99.0% probability and contained at least 2 identified peptides. Protein probabilities were assigned by the Protein Prophet algorithm [Nesvizhskii *et al.*, 2003]. Proteins that contained similar peptides and could not be differentiated based on MS/MS analysis alone were grouped to satisfy the principles of parsimony. Proteins sharing significant peptide evidence were grouped into clusters.

Label-free quantification was obtained using MaxQuant software (1.4.0.5). MS/MS peak lists were searched against the Uniprot_cp_human_2013_07 in which trypsin specificity was used with up to two missed cleavages allowed. Searches were performed selecting alkylation of cysteine by carbamidomethylation as fixed modification, and oxidation of methionine and N-terminal acetylation as variable modifications. Mass tolerance was set to 20 ppm and 0.5 Da for parent and fragment ions, respectively. The false discovery rate for both peptides and proteins was set at 0.01. Additionally, we required at least two peptide identifications per protein, of which at least one unique. "LFQ intensities", which are the intensity values normalized across the entire dataset, were used for quantification based on unique plus razor peptides. Statistical analysis was performed using Perseus. Proteins were filtered applying Benjamini Hochberg and t-test. The proteomic data as raw files, total proteins and peptides identified with relative intensities and search parameters have been deposited on Peptide Atlas repository (accession number PASS00591).

2.9 NMR spectroscopy

The NMR experiments were acquired at 10 °C on Bruker 700, 800, and 850 MHz spectrometers equipped with gradient cryoprobes. 15N-, 13C- or 13C,15N-labeled

samples used for titration experiments ranged from 0.1 to 0.2 mM, whereas experiments acquired for structure determination were performed with 0.5 to 0.8 mM samples; all experiments were conducted in 20 mM sodium phosphate buffer (pH 6.5), 50 mM sodium chloride, 2 mM DTT, 0.01 % NaN3, and 10 % 2H2O / 90 % 1H2O. 2D [1H, 15N]-HSQC and 3D HNCO, HN(CA)CO, HNCA, HN(CO)CA, HNCACB, and CBCA(CO)NH spectra were used for backbone 1H, 15N, and 13C assignments. Side chain 1H and 13C assignments were obtained by 2D [1H, 13C]-HSQC and 3D HBHA(CO)NH, H(CCCO)NH, (H)CC(CO)NH, HCCH-COSY, HCCH-TOCSY, and (H)CCH-TOCSY spectra . Assignments were checked for consistency with 3D 15N/13C – NOESY-HSQC spectra recorded with mixing times of 120 or 100 ms.

2.9.1 Structure determination

The regions for Ramachandran plot statistics and RMSD calculations include T1054-R1068 and Y1084-S1126. NMR spectra were processed with NMRPipe and analysed with KUJIRA [Kobayashi *et al.*, 2007] and SPARKY. CYANA2.1 [Guntert, 2004] was used for automated NOE assignment and to calculate the structures by torsion angle dynamics; each NOE assignment was manually inspected and confirmed or corrected. Dihedral angle restraints were derived by TALOS [Cornilescu *et al.*, 1999]. A total of 100 structures were independently calculated and the twenty conformers with the lowest target-function values were selected for refinement with Xplor-NIH. Structures were evaluated with PROCHECK-NMR [Laskowski *et al.*, 1996], visualized with MOLMOL, and figures generated by PYMOL (The PyMOL Molecular Graphics System, http://www.pymol.org/).

2.10 Immunofluorescence

To remove soluble cellular proteins, cells were extracted with 0.03% saponin in cytosolic buffer (25 mM Hepes-KOH, pH 7.4, 25 mM KCl, 2.5 mM magnesium acetate, 5 mM EGTA, 150 mM K-glutamate) for 1 min prior to fixation. Cells were fixed with 4% paraformaldehyde for 15 minutes, and permeabilised at room temperature with 0.1% Triton-X100. Cells were incubated with primary antibodies for 1 hour followed by secondary antibodies (Cy3, LifeTechnologies) for 30 minutes, at room temperature. Coverslips were mounted in a glycerol solution (20% glycerol, 50 mM Tris pH=8.4) to avoid mechanical deformation of the sample. Images were captured using a Leica inverted SP2 microscope with a laser scanning confocal system. Analysis was performed with ImageJ (http://imagej.nih.gov/ij/). For co-localization analysis ROIs were drawn around individual cells and the Pearson's coefficients obtained using JACoP plugin and processed for statistical analysis with Prism (GraphPad software).

2.11 Wound-healing assay

$3x10^4$ cells were plated into each chamber of a Culture–Insert for wound healing (Ibidi) 48-72 hours before the beginning of the experiment. After insert removal, cells pictures were acquired every 5 minutes for 24 hours. Live-imaging was performed using an ORCA-ER camera (Hamamatsu) on an Olympus IX81 automatic microscope equipped with closed heating and CO_2 perfusion devices. Data analysis was performed automatically using ImageJ (http://rsb.info.nih.gov/ij/), and a script designed in order to distinguish and measure the wound area from the area covered by cells. Wound closure rate values correspond to normalized slopes of linear equations derived from regression analyses of the area over time plots.

2.12 RNAseq analysis

RNA-Seq Analysis RNA-Seq exons quantification data were downloaded from 'The Cancer Genome Atlas' Data Portal (https://tcga-data.nci.nih.gov/tcga/dataAccessMatrix.htm). Downloaded files included experiments which were analysed with the pipeline named RNAseq and conducted on neoplastic cells belonging to ten different tissues: bladder urothelial carcinoma (BLCA), breast invasive carcinoma (BRCA), esophageal carcinoma (ESCA), head and neck squamous cell carcinoma (HNSC), kidney renal clear cell carcinoma (KIRC), liver hepatocellular carcinoma (LIHC), lung adenocarcinoma (LUAD), lung squamous cell carcinoma (LUSC), stomach adenocarcinoma (STAD), and uterine corpus endometrial carcinoma (UCEC). Control experiments were also downloaded for each neoplastic counterpart. Additionally, experiment files relative to four additional neoplasic tissues were considered: colon adenocarcinoma (COAD), kidney renal papillary cell carcinoma (KIRP), serous cystadenocarcinoma (OV), and rectum adenocarcinoma (READ). For these last four sets, control counterparts were not available. Despite the availability of RNA-Seq data from acute myeloid leukemia (LAML), such files were discarded, due to peculiar non-comparable exon notation. The resulting dataset consisted of 293 control and 1646 tumour samples, belonging to 14 different tumour types. For each experiment, the exon quantification file was considered. The 'raw counts' (RC) and 'Reads Per Kilobase of Exon Model per Million Mapped Reads' (RPKM) were extracted for the genomic positions corresponding to exons 27 to 33 of the MYO VI gene, which follow

E27: chr6:76600945-76601023:+

E28: chr6:76602247-76602407:+

E31: chr6:76608090-76608128:+

E32: chr6:76617322-76617425:+

E33: chr6:76618213-76618344:+

All the positions are relative to the hg19 genome assembly. Exons E29 and E30 were not individually annotated due to the presence of a confounding overlapping first exon (chr6:76603648-76604977:+). Exon expression changes between cancer and normal samples were estimated using RPKM, a measure of expression that reflects the molar concentration of a transcript in the sample by normalizing read counts for mRNA length and for the total read number in the sample. Exon E31 relative abundances (E31RA) were then obtained for each sample as the ratio of their RPKM and the average RPKM values of the four flanking constitutive exons (namely E27, E28, E32 and E33). E31 Normalized Relative Abundances (E31NRA) were obtained for each cancer type as the ratio between each sample E31RA and the median E31RA value of the corresponding control samples. These normalized values can be compared among different cancer types. For cancer types with no matched control set, we obtained E31NRA as the ratio between each sample E31RA and the median E31RA value of all the control samples. Wilcoxon test has been performed by using the R-package (http://www.R-project.org/.) to verify the hypothesis that the logRatio between tumours and control samples E31NRA values is negative (i.e. the median E31NRA is less in tumours than in controls).

3. RESULTS

3.1 Different myosin VI isoforms show different interaction partners

3.1.1 Myosin VI undergoes alternative splicing

As stated in the introduction, myosin VI can exist in a number of different isoforms, which represent splice variants with inserts in the tail [Dance *et al.*, 2004]. The number of isoforms differs between different organisms, and they are expressed in a tissue-specific manner. Despite certain knowledge about their diverse functions, a complete understanding of the mechanism of alternative splicing regulation is still missing. Similarly, we lack studies on the molecular mechanism that determines the differences observed between the various myosin VI isoforms [Buss *et al.*, 2001; Dance *et al.*, 2004].

We attempt to answer these questions analyzing the human myosin VI transcripts in detail. The protein is encoded by 36 exons and two major splicing events were described close to- or included in- the CBD of the tail. Depending on their length they are named large-insert (LI) and short-insert (SI), respectively (see **Figure 5** for the position of the two sites).

We focused our study on the LI. Three exons codify for it (exon 29, 30, and 31), and their combination give rise to 3 different isoforms named isoform 2 (the shortest, lacking all the three exons), and isoforms 1 and 3 (which differ in the absence or presence of exon 29, respectively). We examined the level of conservation among different species, of the myosin VI sequence close to the LI. We also looked at the presence of known protein domains and the predicted secondary structure. The sequences showed a high conservation level around the LI (colour coded in **Figure 13**), the presence of a previously described Ubiquitin-Interacting-Motif [Penengo *et*

al., 2006], and the proximity of the well-known ^{1116}RRL^{1118} motif that accounts for several protein-protein interactions [Sahlender *et al.*, 2005]; [Spudich *et al.*, 2007]. Furthermore, the secondary structure prediction highlighted the possible presence of several alpha helices.

a)

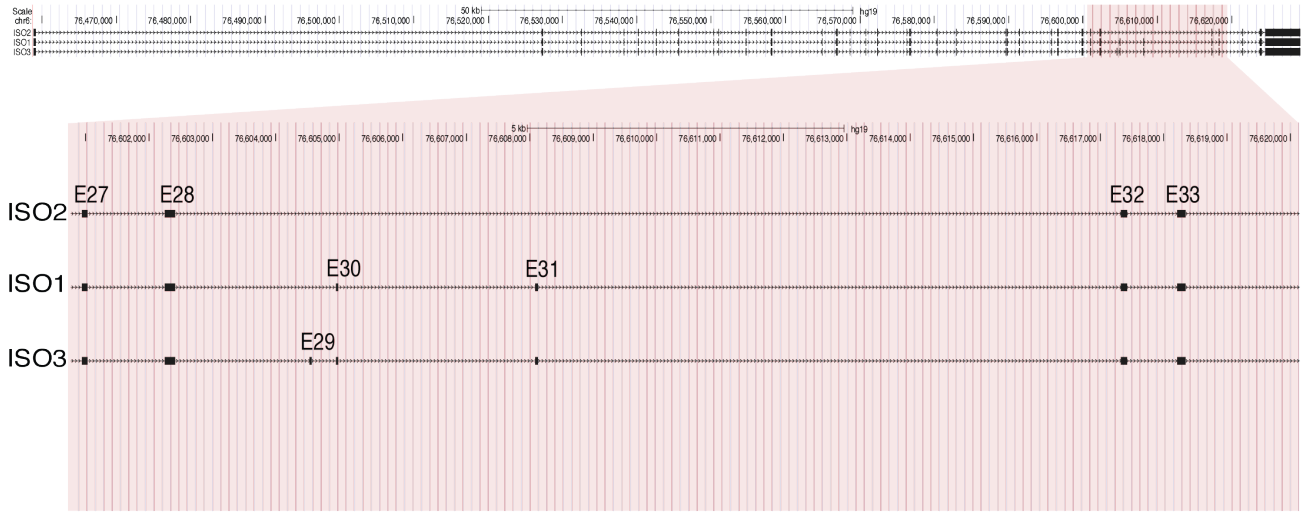
ISO2
ISO1
ISO3
E27
E28
E29
E30
E31
E32
E33

b)

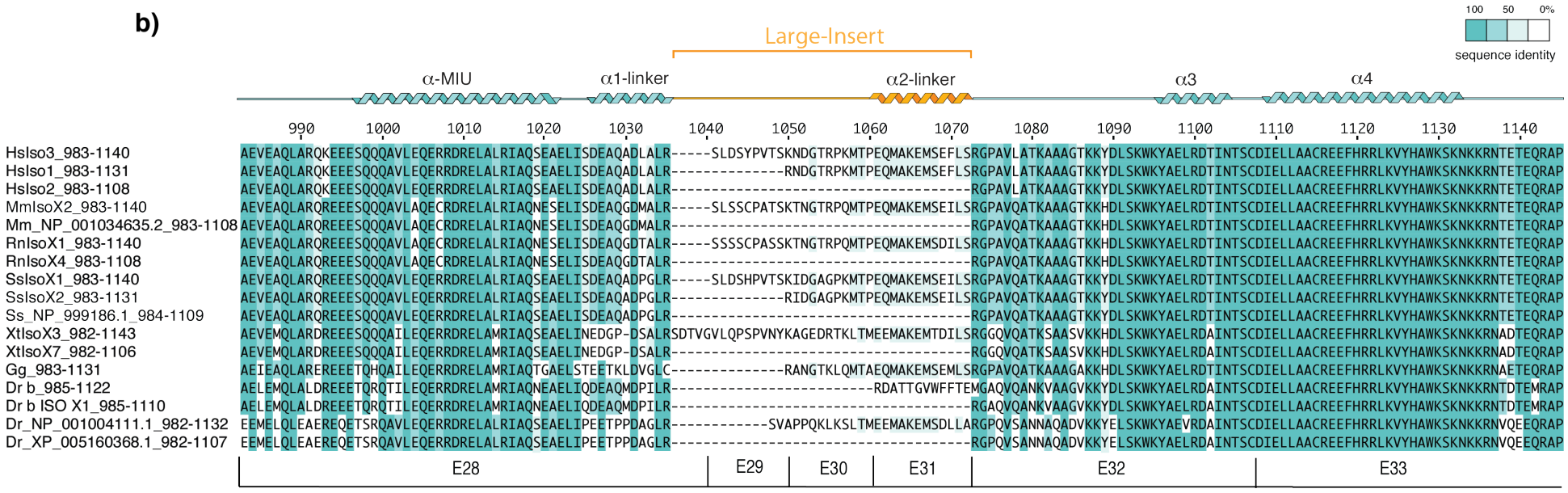
Large-Insert
α-MIU
α1-linker
α2-linker
α3
α4
100
50
0%
sequence identity
990 1000 1010 1020 1030 1040 1050 1060 1070 1080 1090 1100 1110 1120 1130 1140
Hsiso3_983-1140
Hsiso1_983-1131
Hsiso2_983-1108
MmisoX2_983-1140
Mm_NP_001034635.2_983-1108
RnIsoX1_983-1140
RnIsoX4_983-1108
SsIsoX1_983-1140
SsIsoX2_983-1131
Ss_NP_999186.1_984-1109
XtIsoX3_982-1143
XtIsoX7_982-1106
Gg_983-1131
Dr b_985-1122
Dr b ISO X1_985-1110
Dr_NP_001004111.1_982-1132
Dr_XP_005160368.1_982-1107
E28
E29
E30
E31
E32
E33

Figure 13: Myosin VI undergoes alternative splicing. a) position of the alternatively spliced exons of the large insert on the human myosin VI gene. **b)** Amino acids sequence alignment covering the region used for the following experiments, color-coded according to sequence conservation. The sequences of all the myosin VI isoforms from different species (Hs: *Homo sapiens*; Mm: *Mus musculus*; Rn: *Rattus norvegicus*; Ss: *Sus scrofa*; Xt: *Xenopus tropicalis*; Gg: *Gallus gallus*; Dr: *Danio rerio*) were retrieved from the NCBI database and analysed using ClustalOmega. Secondary structure elements, predicted using http://www.predictprotein.org and later confirmed by structural data are depicted above the sequence. The large insert corresponds to the linker region that varies between the short (iso 2) and the long (iso 1, 3) isoforms, and is depicted in orange. Numbering on top of the sequence alignment refers to human isoform 3.

3.1.2 Alternative splicing of myosin VI regulates its interactome

To verify if alternative splicing could modify the interactome of myosin VI, and thus its functions, we performed a mass spectrometry-based proteomic screen aimed at comparing the interaction profiles of the different isoforms. Myosin VI spanning amino acid 998-1131 of the three isoforms were cloned into pGEX vector. The corresponding purified myosin VI proteins were used in pull-down assays with HEK293T cellular lysates. Bound proteins were washes and resolved on SDS-PAGE gel. Notably, isoform 1 and 3 show similar binding pattern where isoform 2 behaves differently (**Figure 14a**). Bands were then in-gel digested and analysed by mass-spectrometry. A label-free quantitative experiment was performed in order to score differences between the constructs. Data resulting from this approach were analysed by MaxQuant software and are presented in **Table 1**, reported as total-peptide counts (TPC). Data confirmed the initial observations. Isoforms 1 and 3 have almost identical binding partners. Most of them are implicated in endocytosis and vesicular trafficking and are not shared by isoform 2. In particular, we identified clathrin heavy chain, a set of adaptor proteins that form the AP2 complex, well-known endocytic adaptors of the ep15/epsin family (CLINT1 and EPS15), and a COPII component (SEC16A), that may connect myosin VI to the anterograde transport from ER to Golgi. Few

interactors common to all three isoforms were identified, among them COPB2 an essential component of the Golgi vesicles. Surprisingly, isoform 2-specific interactors were mostly protein linked to the DNA damage response.

As isoforms 1 and 3 showed no difference in their interactome, we decided to refer to them collectively as myosin VI_{long}, while using myosin VI_{short} to indicate isoform 2.

Gene name		Iso1 (TPC)	Iso2 (TPC)	Iso3 (TPC)
CLTC	clathrin, heavy chain (CLTC)	1050	*153	1068
SEC16A	SEC16 homolog A (S. cerevisiae)	175	0	145
AP2B1	adaptor-related protein complex 2, beta 1 subunit	91	0	107
AP2A2	adaptor-related protein complex 2, alpha 2 subunit	87	0	89
AP2A1	adaptor-related protein complex 2, alpha 1 subunit	85	0	90
AP1G1	adaptor-related protein complex 1, gamma 1 subunit	28	0	32
AP2M1	AP-2 complex subunit mu	35	0	51
CLINT1	clathrin interactor 1 (EPSIN4)	138	0	146
PIK3C2A	Class 2 phosphatidylinositol-4-phosphate 3-kinase	73	0	90
PICALM	Phosphatidylinositol-binding clathrin assembly protein	15	0	19
EPS15	Epidermal growth factor receptor substrate 15	6	0	5
REPS	RalBP1-associated Eps domain-containing protein 1	10	0	5
COPB2	Coatomer subunit beta'	45	50	57
DDB1	DNA damage-binding protein 1	137	251	123
EPRS	Bifunctional glutamate/proline--tRNA ligase	206	686	183

VPRBP	Vpr (HIV-1) binding protein (DCAF)	0	140	0
DCTN1	dynactin 1	0	105	0
GTPBP4	Nucleolar GTP-binding protein 1 (NOG1)	5	44	0
ARHGEF12	Rho guanine nucleotide exchange factor 12	6	64	0
YTHDC2	Probable ATP-dependent RNA helicase	4	37	2
DCTN2	Dynactin subunit 2	2	37	0
DOCK7	Dedicator of cytokinesis protein 7	2	32	4

Table 1 List of the top hits of interactors identified by label-free quantitative mass spectrometry. Gene name, description and total peptide count (TPC) is reported for each protein. The * indicates that the same total peptide count was reported for the control (GST alone). The experiment was repeated once in the label-free quantitative setup, but same interactors were found in three different non-quantitative experiments.

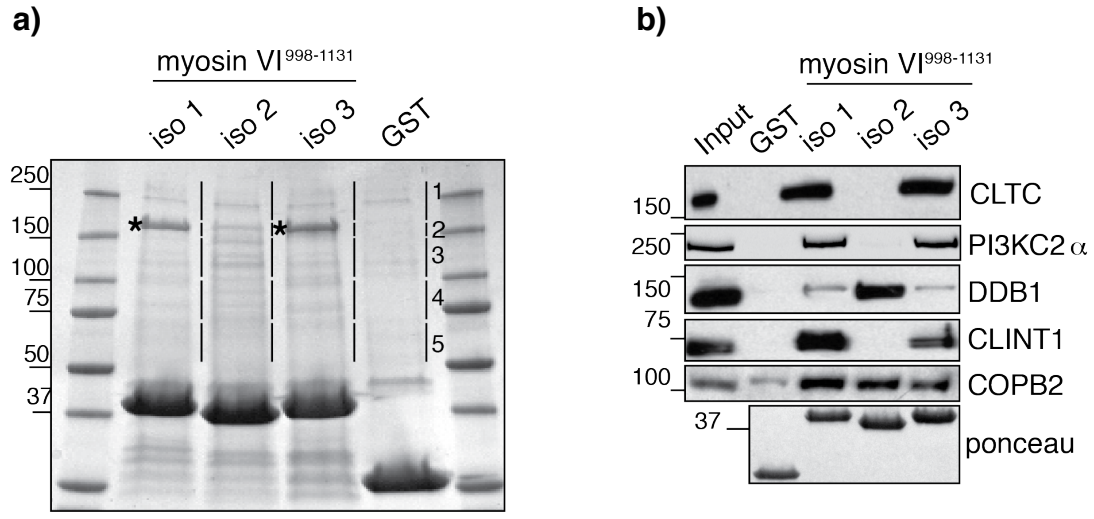

Figure 14: Proteomic analysis of myosin VI isoforms reveals different interactomes. a) GST-myosin VI$^{998-1131}$ fusion proteins representing the three different isoform variants were used to pulldown 1mg of HEK293T total cell lysate. Bound proteins were washed, resolved in SDS-PAGE, and Coomassie-stained. Numbering and lines refer to the slices cut for the mass spectrometry identification. Asterisks indicate clathrin heavy chain bands, being one of the most abundant interactor. **b)** Validation analysis. GST fusion proteins were incubated with HEK293T cellular lysate. Bound proteins were resolved by SDS-PAGE and analysed by immunoblotting (IB) as indicated. In case

of DDB1 and PI3KC2α, tagged constructs were transiently transfected in HEK293T cells and IB were performed with anti-tag antibody. Comparable loading of GST-tagged proteins is shown by Ponceau staining (bottom panel).

Experimental validation confirmed the most abundant identified interactors (5 out of 5 tested) and their specificity (**Figure 14b**). Validation was performed through the same experimental setting used for the mass-spectrometry. GST-myosin VI$^{998\text{-}1131}$ were used to pulldown HEK293T total cell lysate and immunoblot analysis revealed a selective interaction of myosin VI$_{long}$ with endogenous CLTC, CLINT1, and overexpressed PI3KC2α. At the same time we verified the specific binding of DDB1 with myosin VI$_{short}$, while COPB2 was found to interact with both isoforms (**Figure 14b**).

3.1.3 Dab2 is not necessary for myosin VI$^{998\text{-}1131}$ interaction with clathrin heavy chain

Inspection of the gel shown in **Figure 14a**, revealed sharp bands visible in the isoform 1 and 3 lanes, with an apparent molecular weight of around 180 kDa (labelled with an asterisk in the figure). These bands represent clathrin heavy chain (CLTC), an exclusive and abundant binding partner of myosin VI$_{long}$ (**Figure 14b**).

It has been previously reported that Disabled-2 (Dab2) is the critical player that mediates the interaction between myosin VI and clathrin [Morris *et al.*, 2002]. Notably, the ^{1191}WWY^{1193} motif of myosin VI responsible for this interactor binding [Spudich *et al.*, 2007] was not present in the constructs used for pulldown experiments. Furthermore Dab2, which is a 96kDa protein (a region of the gel that we analysed by mass-spectrometry), was not identified in the mass-spectrometry analysis. We reasoned that this might be due to the low level of expression of this

protein in HEK293T cells (**Figure 15a**). To better understand the role of Dab2 in our experimental settings, HeLa cells were chosen as a second cellular system since they are positive for Dab2 expression (**Figure 15a**). Also in this case, we easily scored specific binding of myosin VI_{long} constructs to clathrin heavy chain while no interaction with Dab2 was detected (**Figure 15b**). We repeated the experiment transfecting GFP-Dab2 in HEK293T cells with identical results (**Figure 15c**). Thus, we identified a novel surface of interaction between myosin VI and clathrin. Whether the binding is direct or mediated by the presence of a third molecule remains to be investigated.

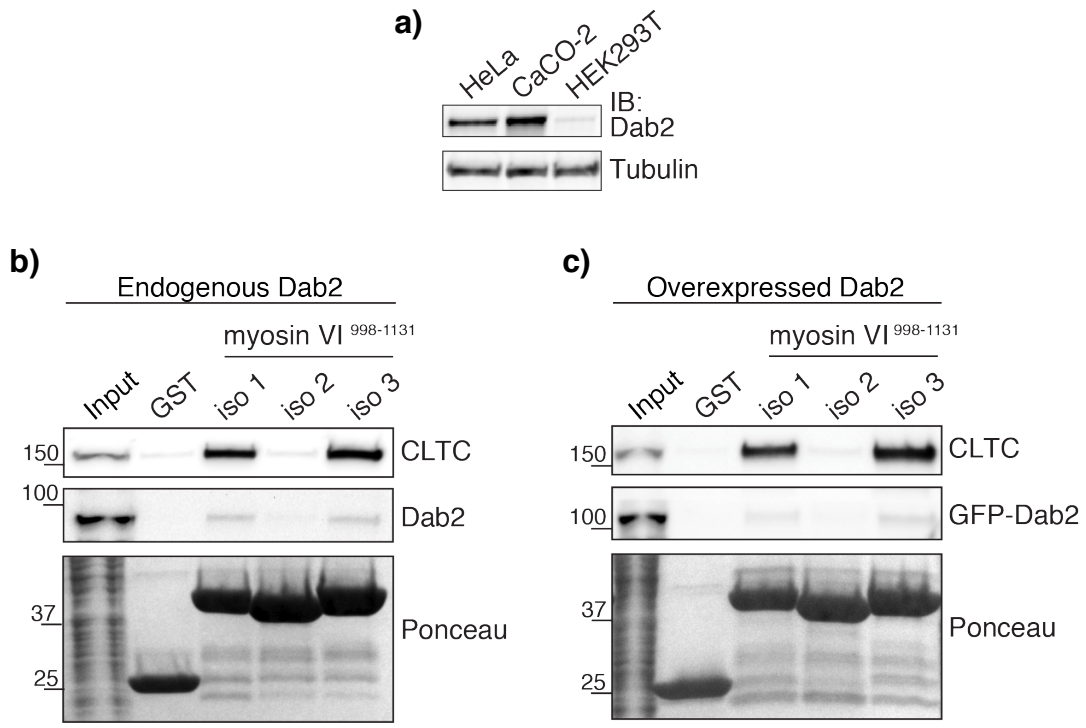

Figure 15: Dab2 does not interact with myosin $VI^{998-1131}$. a) Immunoblot analysis aimed at comparing the level of expression of Dab2 in different cell lines. 25µg of HeLa, CaCO-2, and HEK293T total cell lysate were resolved in SDS-PAGE and analysed by immunoblot with a monoclonal anti-Dab2 antibody. Anti-Tubulin was used as loading control. **b)** GST-myosin $VI^{998-1131}$ fusion proteins were incubated with HeLa cellular lysate (endogenous Dab2). Bound protein were resolved in SDS-PAGE and analysed by immunoblot (IB) as indicated. Comparable loading of GST-tagged proteins is shown by

Ponceau staining (bottom panel). **c)** same as in **b)** but GFP-Dab2 was transfected in HEK293T and IB was performed with anti-GFP antibody.

3.1.4 Clathrin heavy chain C-terminus is necessary for the interaction with myosin VI

In order to unravel the nature of this novel interaction we searched the binding surface on CLTC. We exploited three GFP-tagged clathrin constructs bearing different truncations at the C-terminus of the molecule (aa 1-479, aa 1-1074 and aa 1-1675, respectively, see **Figure 16a**, and the Material and Methods section). Transfected HEK293T cellular lysates were used in pulldown experiments, using GST-myosin $VI^{998\text{-}1131}$ fusion proteins as bait representing the three isoforms. Bound protein were analysed in immunoblot using an antibody raised against the N-terminus of clathrin heavy chain. This antibody was able to recognize simultaneously GFP-tagged and endogenous CLTCs, allowing a direct comparison between the overexpressed and the endogenous proteins. As shown in **Figure 16b** only the full-length GFP-CLTC construct was able to bind specifically GST-myosin VI_{long} but not GST-myosin VI_{short},. None of the other fragments, even if expressed at the same level, were able to do the same.

These results indicate that the critical determinant for myosin VI binding resides in the 1074-1675 region of CLTC, at its C-terminus.

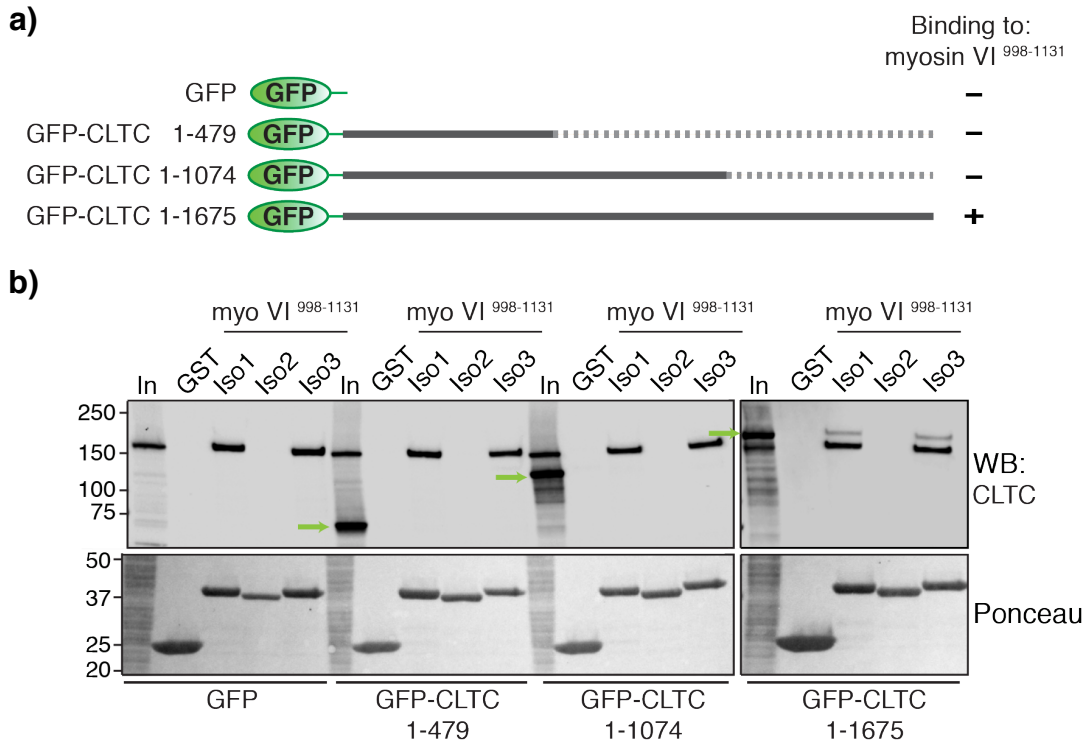

Figure 16: Full-length clathrin heavy chain is needed for the interaction with myosin VI$^{998\text{-}1131}$. **a)** Scheme of the different GFP-tagged clathrin heavy chain constructs used in the experiment together with their ability to interact with myosin VI^{long}. **b)** GST-myosin VI$^{998\text{-}1131}$ fusion proteins were incubated with total cell lysates (TCL) from HEK293T transfected either with GFP alone, GFP-CLTC 1-479, GFP-CLTC 1-1074 or GFP-CLTC 1-1675 (full-length). Bound proteins were resolved in SDS-PAGE and analysed by immunoblot using anti-CLTC antibody. Pale-green arrows highlight bands accounting for GFP-CLTC fusion proteins. Comparable loading of GST-tagged proteins is shown by Ponceau staining (bottom panel).

3.1.5 Myosin VI$^{998\text{-}1131}$ does not interact directly with clathrin heavy chain

To verify a possible direct interaction between clathrin heavy chain and myosinVI$^{998\text{-}1131}$, we decided to purify GST-clathrin fusion proteins from bacteria. The full-length protein spans 1675 amino acids, making difficult to express it in a good amount. Therefore, we choose to purify different regions of the protein separately. The full-length clathrin is composed of several domains, which differ functionally and structurally [Brodsky, 2012] and can appropriately fold on their own. We selected three GST-tagged constructs, a first encompassing aa 1-479, a second spanning aa 1-1074, and a third which contained aa 1075-1675 (see **Figure 17a**). The three together cover the entire length of the protein. The fusion proteins were used in an *in*

vitro pulldown against increasing amount of a GST-cleaved and purified myosin VI$^{998-1131}$ polypeptide. As visible from **Figure 17b,** no specific binding was scored between the clathrin constructs and the myosin fragment even at the highest concentration (1 µM bait vs. 12 µM prey).

These results led us to investigate the possibility that an additional protein could mediate the interaction.

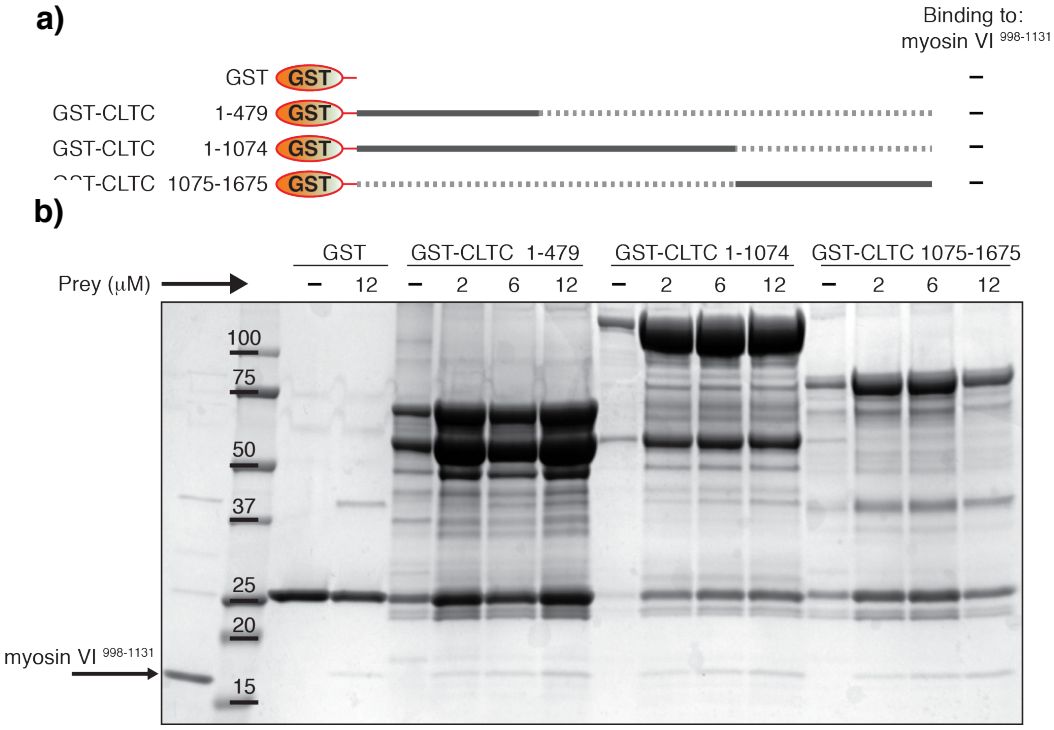

Figure 17: Purified clathrin heavy chain and myosin VI$^{998-1131}$ do not interact *in vitro*. a) Schematic representation of the different GST-tagged clathrin heavy chain fusion protein used in the experiment together with their ability to bind myosin VI $^{998-1131}$. **b)** 1 µM of bacterially purified GST-tagged proteins (bait) were incubated with the indicated amount of purified myosin VI $^{998-1131}$ (prey). Bound proteins were resolved in SDS-PAGE and Coomassie stained.

3.1.6 Myosin VI$^{998-1131}$ interacts with clathrin light chain

To date clathrin light chains (LCs) are the only protein known to bind CLTC C-Terminus [Brodsky, 2012]. Thus, we hypothesized clathrin light chain to be the molecule bridging myosin VI and clathrin heavy chain. To assess this hypothesis, we

produced and purified from bacteria GST-tagged LC that was used as bait against purified myosin VI$^{998\text{-}1131}$ polypeptides, representing the long and short isoforms. As shown in **Figure 18**, we found that myosin VI$_{long}$ but not myosin VI$_{short}$ interacts with clathrin light chain.

These results validate the isoform specific binding of myosin VI$_{long}$ to clathrin that we found in mass-spectrometry and led us to conclude that we identify a new direct binding partner of myosin VI**.**

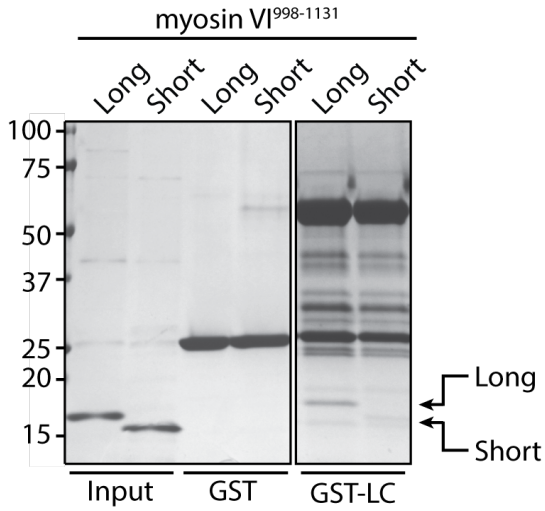

Figure 18: Purified clathrin light chain and myosin VI$^{998\text{-}1131}$ interact *in vitro*. 1 µM GST-tagged LC were incubated with 3 µM cleaved and purified myosin VI $^{998\text{-}1131}$. Bound proteins were resolved in SDS-PAGE and Coomassie stained.

3.1.7 Mapping the clathrin light chain interaction surface

Once we defined clathrin light chain as a new interactor of myosin VI, we performed a structure/function analysis aimed at elucidating the region of LC involved in the binding. Clathrin light chains are translated from 2 different genes (LCa and LCb), and even though no functional differences are known between LCa and LCb proteins, their primary sequences show some differences (see **Figure 19**) [Brodsky, 2012].

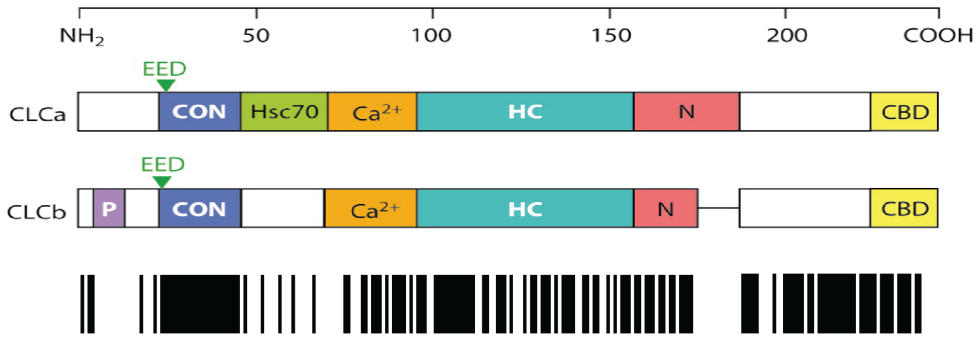

Figure 19: Alignment of LCa and LCb. Scheme of the domain organization of LCs as in **Figure 12a**, numbering of the amino acids on top. The black vertical lines on the bottom represent site of identity between the two primary sequences. Alignment was performed using ClustalOmega and modified with JalView.

We exploited the two genes coding for similar proteins to gather a first set of information about the possible site of interaction. Thus, we cloned also LCb into a pGEX vector and we used purified GST-LCs fusion proteins to pulldown cleaved and purified myosin VI$^{998\text{-}1131}$ fragment. As reported in **Figure 20,** we detected specific binding of GST-LCa with myosin VI, while no interaction was found with the LCb counterpart.

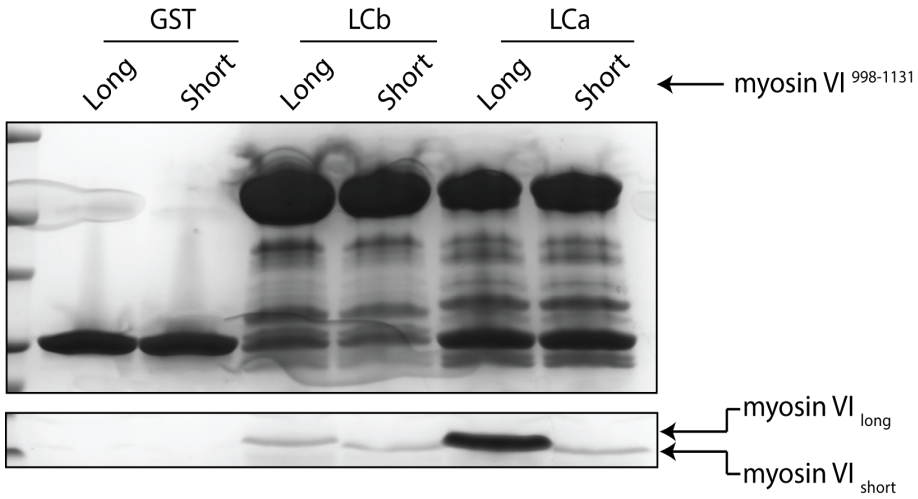

Figure 20: LCa and LCb differ in their ability to interact with myosin VI$^{998\text{-}1131}$. 1 µM of GST and GST-tagged LCs were used to pulldown 3 µM myosin VI$^{998\text{-}1131}$ representing long and short isoforms. Bound proteins were resolved in SDS-PAGE and Coomassie stained.

Next, we performed structure/function analysis by cloning different truncation constructs of LCa (refer to **Figure 19a** for a scheme). In order to avoid possible misfolding, we considered the boundaries of known functional domains of the protein. Various fragments were successfully expressed in bacteria, purified and used to pulldown cleaved and purified myosin VI$^{998\text{-}1131}$ polypeptides of long and short myosin VI isoforms. This analysis allowed us to identify the region of LCa spanning between aa 47 and aa 97 as the minimal surface required for the interaction (**Figure 21**). Not surprisingly, this region shows the poorest sequence similarity with LCb, explaining the differences scored in the myosin VI binding. Through the same region, LCa was shown to bind Hsc70, an interaction that is not conserved in LCb [DeLuca-Flaherty *et al.*, 1990].

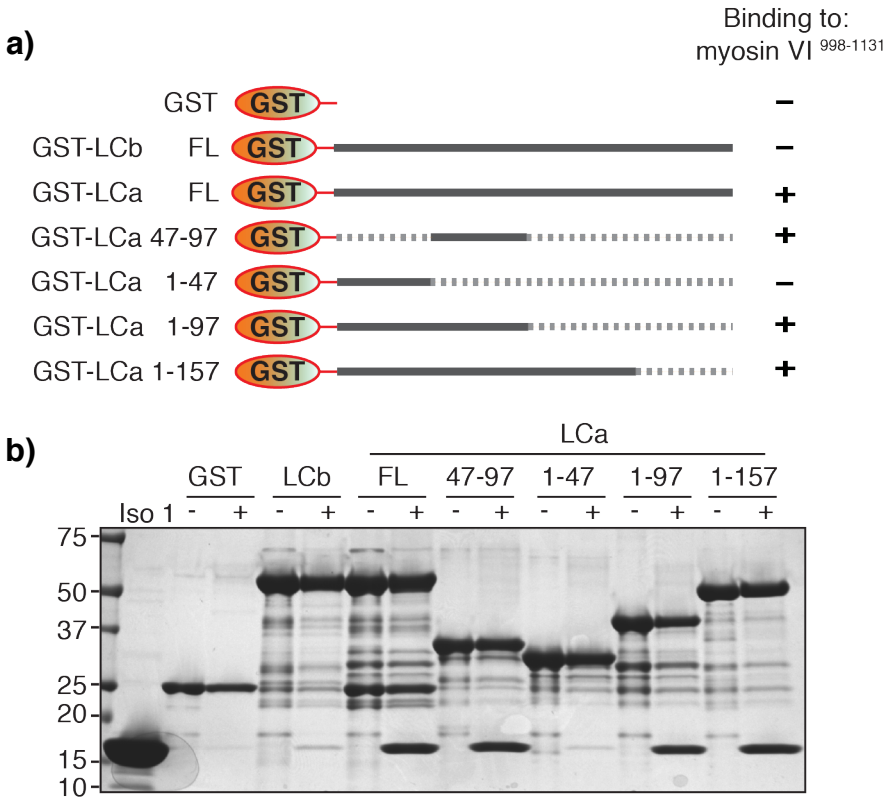

Figure 21: Myosin VI$^{998\text{-}1131}$ directly interact *in vitro* with LCa$^{47\text{-}97}$. a) Scheme of the different fusion proteins together with their ability to bind myosin VI$^{998\text{-}1131}$. **b)** 1 µM GST alone, GST-LCa, GST-LCb, as

well as different GST-LCa truncations were used as bait to pulldown 6 μM purified myosin VI$^{998-1131}$ isoform 1 in an *in vitro* pulldown. Bound proteins were resolved in SDS-PAGE and Coomassie stained.

To better understand this interaction, we investigated whether the two proteins were able to form a stable complex in solution. To this purpose, we used analytical size exclusion chromatography (SEC). Myosin VI$^{998-1131}$ fragment from isoform 1 was cleaved and purified through ion exchange chromatography (data not shown). The purified protein eluted in a S75 column as a single, narrow peak (red line in **Figure 22**) between the 14kDa and the 29kDa molecular weight (MW) markers. The same behaviour was observed for the LCa$^{47-97}$ (green line in **Figure 22**) that is actually run aberrantly, possibly due to its elongated and unfolded structure [Wilbur *et al.*, 2010]. The two proteins were then mixed at 1:1 molar ratio and allowed to interact for 15 min at 4 °C. After injection, the pre-formed complex eluted in a single peak in correspondence of the 29 kDa marker (blue line in **Figure 22**), confirming the formation of a stable complex in solution.

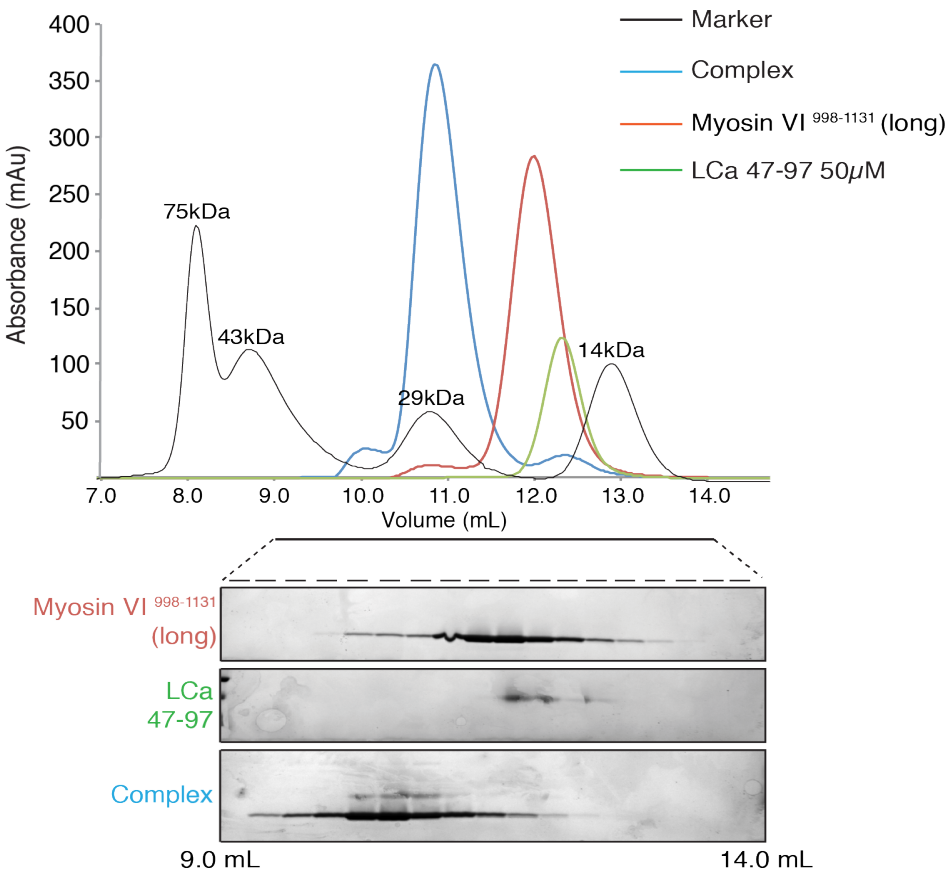

Figure 22: LCa$^{47-97}$ and myosin VI$^{998-1131}$ form a stable complex in solution. Analytical size exclusion chromatography of 50 µM purified LCa 47-97 fragment (green line), 50 µM myosin VI$^{998-1131}$ (red line) and the complex of the two polypeptides (blue line). The two fragments were incubated together for 15 min at 4 °C to allow interaction. Fractions from 9-14 ml were separated by gradient (4-20%) SDS-PAGE and stained with Coomassie.

Based on the these results, we attempted to solve the crystal structure of myosin VI:LCa using the protein complex purified as in **Figure 22** (LCa$^{47-97}$ and myosin VI$^{998-1131}$). First, we used static light scattering (SLS) to determine the effective molecular weight of the two proteins singularly and in complex. The proteins (16kDa for myosin and 5 kDa for LCa) and their complex (21kDa) weighted exactly as predicted (data not shown). Proteins resulted monodisperse and therefore suitable for crystallization attempts. We exploited several crystallization trays at 4 °C and 20 °C (i.e. PACT and JCSG-Plus), with the complex at a final concentration of 20 mg/mL and 40 mg/mL. Unfortunately, most of the drops were clear, testifying a high

solubility of the complex. Difficulties in the crystallization of clathrin light chain were already reported in the past and ascribed to the lack of a proper secondary structure [Wilbur *et al.*, 2010].

To define the minimal interaction surface on LCa, we prepared a new set of GST-tagged constructs, shortening either the C- or the N-terminus of the LCa$^{47-97}$ fragment. Four different constructs were assessed for their ability to bind myosin VI$_{long}$ *in vitro* and none of them resulted impaired in this ability (**Figure 23**). Thus, we concluded that the interaction with myosin VI is restricted to the thirty amino acids of the LCa$^{51-80}$ fusion protein.

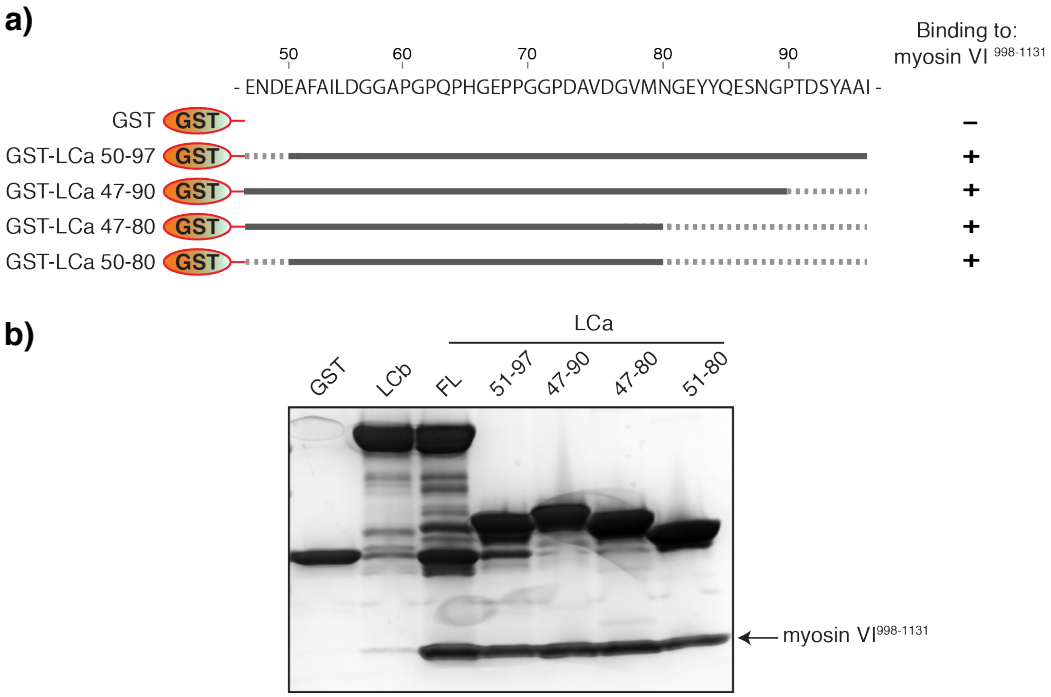

Figure 23: LC a$^{51-80}$ and myosin VI$^{998-1131}$ interact *in vitro*. a) Scheme of the GST-LCa fragments used in the experiment. **b)** 1 µM GST alone, GST-LCa, GST-LCb, as well as the GST-LCa truncation were used as bait against 6 µM purified myosin VI$^{998-1131}$ isoform 1 in an *in vitro* pulldown. Bound proteins were resolved in SDS-PAGE and Coomassie stained.

To further reduce the surface of interaction on LCa at its minimal boundaries, we then generated premature stop codons in GST-LCa$^{51-80}$ at position 61 or 71. The

two constructs, namely GST-LCa$^{51-60}$ and GST-LCa$^{51-70}$ (**Figure 24a**), were used again in a *in vitro* pulldown with purified myosin VI$_{long}$. GST-LCa full-length (FL), GST-LCa$^{47-97}$ and GST-LCa$^{51-80}$ were used as positive controls. As reported in **Figure 24b**, trimming of LCa down to a stretch of ten amino acids didn't show any impairment in myosin VI binding.

We also designed GST-LCa full-length constructs with deletion of the 51-60 and 51-70 regions, namely GST-LCa$^{\Delta 51-60}$ and GST-LCa$^{\Delta 51-70}$ (**Figure 24a**). Corroborating our previous findings, using LCa$^{\Delta 51-60}$ and LCa$^{\Delta 51-70}$ fusion proteins the interaction with myosin VI was reduced to background level (**Figure 24c**). We concluded that the region spanning aa 51 to aa 60 of LCa is both necessary and sufficient for the interaction with myosin VI$_{long}$.

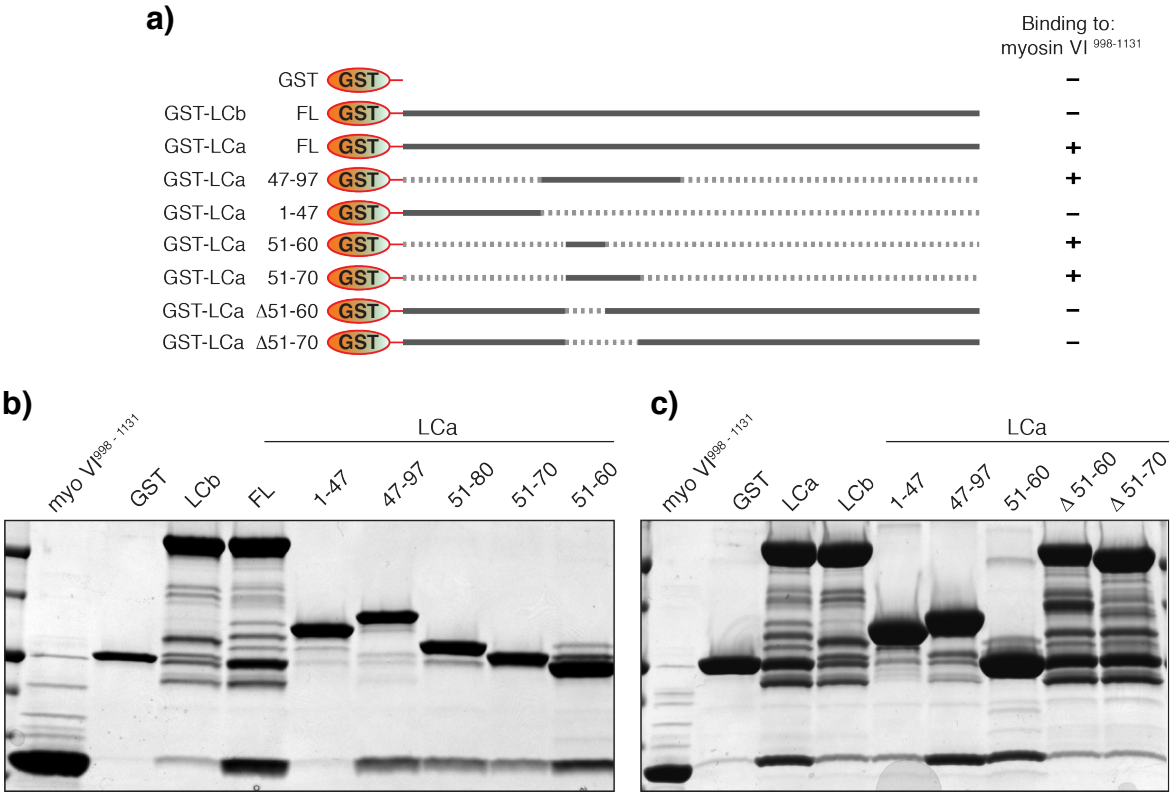

Figure 24: LCa$^{51-60}$ fragment binds myosin VI$^{998-1131}$ *in vitro*. a) Scheme of the GST-LCa fragments used in the experiment together with their ability to bind myosin VI$_{long}$. **b)** 1 µM GST alone, GST-LCa, GST-LCb, as well as the GST-LCa truncations were used as bait to pulldown 6 µM purified myosin VI$^{998-1131}$ isoform 1 in an *in vitro* pulldown. Bound proteins were resolved in SDS-PAGE and Coomassie stained. **c)** Same as **b)** with the addition of GST-LCa deletion constructs.

Before embarking in new crystallization trails a more precise quantitation of the affinity between LCa and myosin VI would be of help. To this end, we recently obtained fluorescently labelled LCa fragments encompassing the region between aa 51 and aa 60 that will be used to perform fluorescent polarization assay.

3.1.8 Structure/function analysis of the myosin VI_{long} binding region for clathrin

We also attempted to define the minimal clathrin interaction surface on myosin VI molecule. To this purpose, we designed and generated a panel of GST-tagged myosin VI constructs, trimming either the C- or the N-terminus of the isoform 3 myosin $VI^{998-1131}$ construct, which was used for the proteomic screen. As these experiments were performed before the identification of the clathrin light chain as the direct interactor, the read out of these experiments was clathrin heavy chain binding detected by immunoblot. This can be considered as a proxy of the LCa binding ability of myosin VI. A schematic representation of the different constructs used is reported on top of each panel of **Figure 25**.

Regions deleted from the C-terminal end did not show any clathrin interaction (**Figure 25b**), thus proving the requirement of this region for the binding. As expected, by itself, the region following the alternative splicing was not sufficient for the interaction. The construct bearing only myosin VI aa 1080-1131 failed to pulldown clathrin while the binding was retained by other fusion proteins carrying a longer N-terminus that includes at least part of the LI (**Figure 25c**).

To conclusively define the determinants of myosin VI:clathrin interaction, we designed deletion constructs that remove part of the LI region of myosin VI (myosin $VI^{\Delta 1045-1069}$ and myosin $VI^{\Delta 1055-1069}$). As shown in **Figure 25d**, these constructs loose the ability to pulldown clathrin.

Taken together these results allowed us to narrow down the region between aa 1055 and aa 1131 of myosin VI_{long} as the minimal interaction surface and define the LI region as critical determinant for clathrin binding.

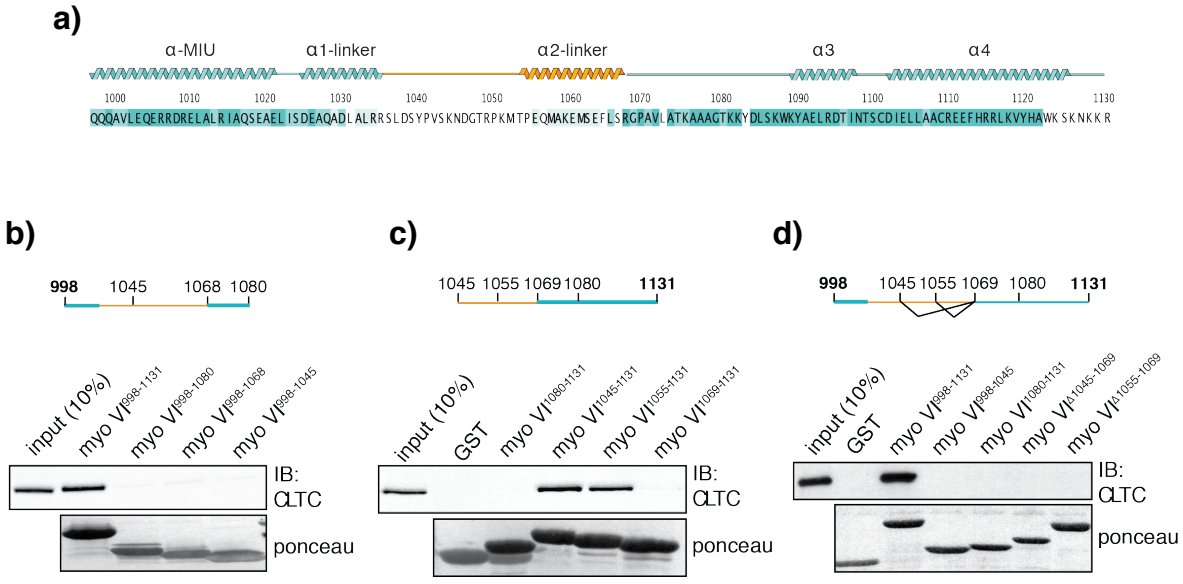

Figure 25: Myosin $VI^{1055-1131}$ is the minimal region required for clathrin binding. a) scheme of the myosin VI region used in the following experiments. In **b)**, **c)**, and **d)** 500 µg of HEK293T TCL were incubated with the GST-tagged myosin VI schematized on top of every single panel to allow interaction. Bound proteins were then resolved in SDS-PAGE and assessed for CLTC presence by immunoblot using monoclonal anti-CLTC antibody. Comparable loading of GST-tagged proteins is shown by Ponceau staining (bottom panel).

3.2 "RRL-interactors" and clathrin are mutually exclusive binding partners of myosin VI

3.2.1 The ^{1116}RRL^{1118} motif of myosin VI is crucial for clathrin binding

Several binding partners of myosin VI were shown to interact with a three-amino acids stretch on the myosin VI molecule, known as the "RRL motif", which resides in the CBD region of the motor protein (reviewed in [Tumbarello *et al.*, 2013]). We noticed that the ^{1116}RRL^{1118} motif was embedded in the myosin $VI^{1055-1131}$ construct.

We therefore tested if the motif was directly involved in clathrin binding. To this purpose, we generated single point mutations of the ^{1116}RRL^{1118} motif as well as a triple AAA mutation previously described in literature to validate interactions with known myosin VI binders. As shown in **Figure 26**, GST-tagged myosin VI$_{long}$ fusion proteins carrying R1117A (RAL), L1118A (RRA) and the triple AAA mutation are impaired in clathrin binding from cell lysates. In the same experiment the R1116A (ARL) mutant behaved as the wild type.

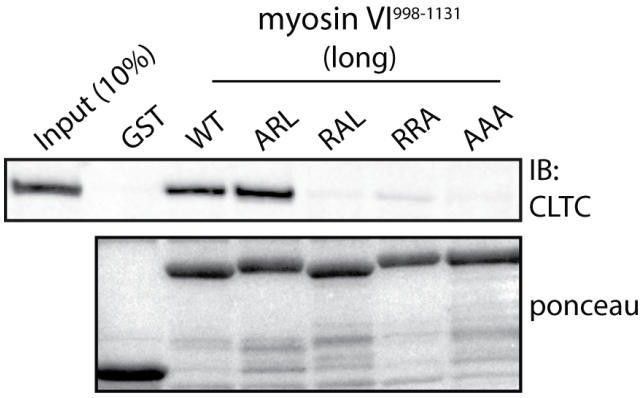

Figure 26: The ^{1116}RRL^{1118} motif is crucial for clathrin binding. GST-tagged myosin VI$_{long}$ (aa 998-1131) wild-type or ^{1116}RRL^{1118} mutants were used against 500 µg of HEK293T TCL. Bound proteins were then resolved in SDS-PAGE and assessed for CLTC presence by immunoblot using monoclonal anti-CLTC antibody. Comparable loading of GST-tagged proteins is shown by Ponceau staining (bottom panel).

During our subsequent structural analysis we found that the residue R1117 makes important contact, required for the structural integrity of this myosin VI region (data not shown). Indeed, the R1117A mutant protein is unfolded, as demonstrated by circular-dichroism data (**Figure 27**). Thus, for the following functional studies we focused on the L1118A mutant that retains a correct fold.

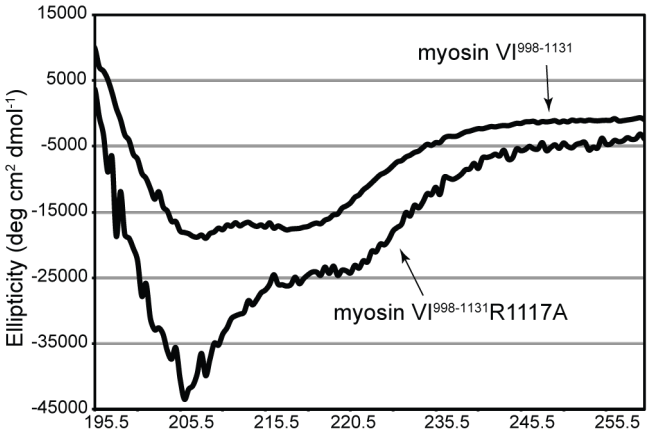

Figure 27 Myosin VI R1117A mutation causes unfolding of the protein. Circular dichroism data of the myosin VI$^{998\text{-}1131}$ R117A fragment, ellipticity of the fragment is perturbed in the R1117A mutant.

To corroborate our biochemical results regarding the interaction between myosin VI$_{long}$ and clathrin, we generated GFP-tagged versions of the tail of myosin VI (Δ1-834 constructs). Truncated myosin VI constructs (lacking the motor-domain) have been extensively used in previous studies as they retain the ability to interact with the known partners and they are easier to express in cell lines. We cloned wild-type (Tail$_{long}$) and L1118A mutant (Tail$_{long}$RRA) as well as Tail$_{short}$. As our results showed that Dab2 might be dispensable for myosin VI$^{998\text{-}1131}$ and clathrin to interact in our setup, we decided to clone a GFP-fusion construct bearing the Tail$_{long}$WLY mutant since the W1192L mutation was reported to abrogate Dab2 binding [Spudich *et al.*, 2007]. To avoid any influence due to the possible dimerization of the GFP-tails constructs with the endogenous myosin VI, we transfected them into HeLa cells where endogenous myosin VI had been stably knocked-down. First, we looked at the co-localization of the different myosin VI tails with clathrin heavy chain in immunofluorescence studies. As previously reported, Tail$_{long}$ strongly co-localized with clathrin, whereas Tail$_{short}$ exhibited no significant co-localization (**Figure 28a,b**) in confocal slices. Notably, both the RRA- and WLY- Tail$_{long}$ mutants failed to co-localize with clathrin, similarly to Tail$_{short}$ (**Figure 28a,b**).

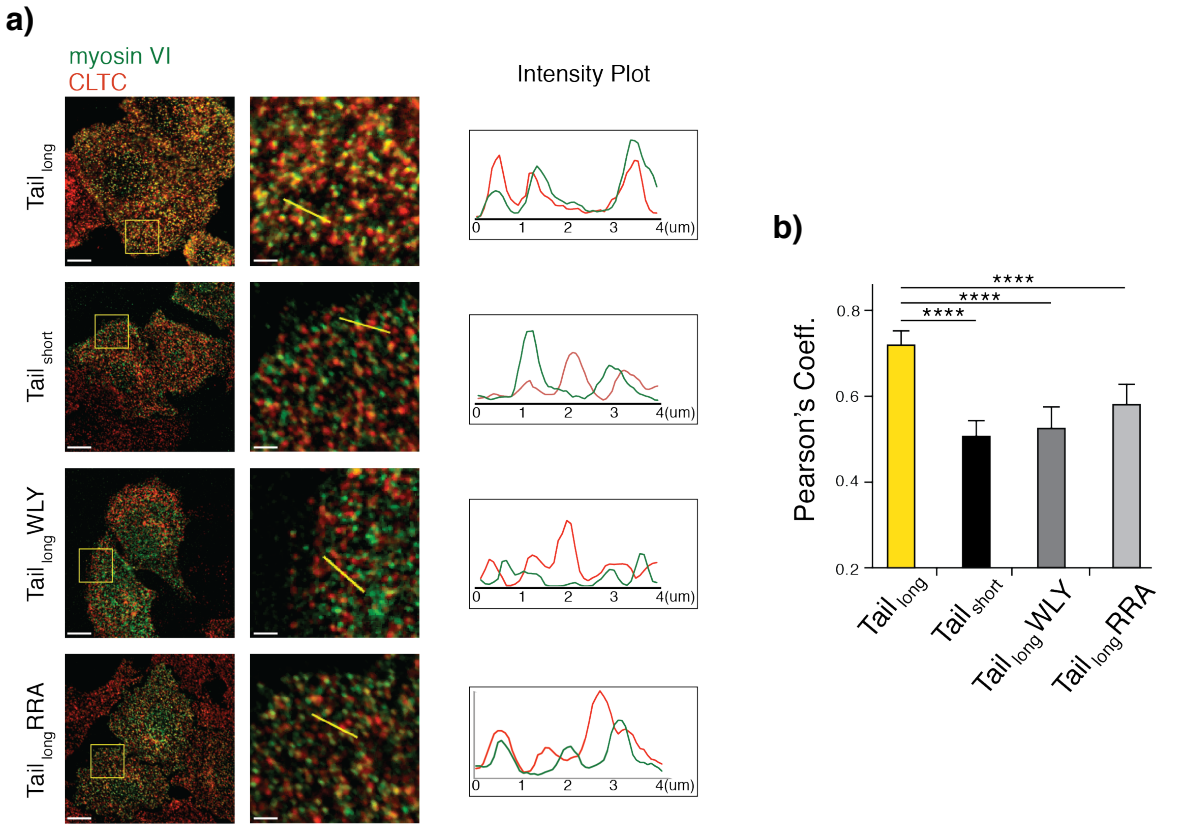

Figure 28: Myosin VI L1118A mutant fails to colocalize with clathrin heavy chain. a) Co-localization of GFP-tagged myosin VI tail constructs transfected into HeLa and endogenous clathrin heavy chain. On the right of each sample slice we enlarged a region of the cell and reported the normalized intensity-plot of the red and green pixels along the yellow line. **b)** Diagram reporting the average ±SE of Pearson's coefficient calculated from at least 15 cells for each transfected constructs from three independent experiments.

We confirmed these results through co-immunoprecipitation experiments. GFP-myosin VI tails were transiently transfected into HeLa cells lacking endogenous myosin VI and immunoprecipitated using an anti-GFP nanobody. As reported in **Figure 29a** we found that the L1118A point mutation was sufficient to abrogate the interaction with clathrin while binding to Dab2 was retained. Notably, when we immunoprecipitated the $Tail_{long}$ fusion protein bearing a mutation in the binding site (W1192L) we found that clathrin was co-immunoprecipitated similarly to the wild-type $Tail_{long}$ while Dab2 interaction was lost (**Figure 29a**). These results suggest that Dab-2 might be dispensable for the formation of a stable myosin VI:clathrin complex.

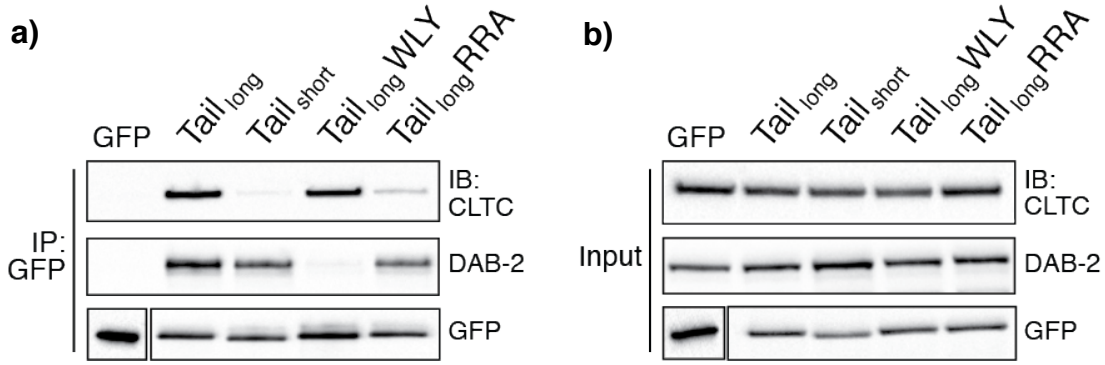

Figure 29: Myosin VI L1118A mutant fails to co-immunoprecipitate clathrin heavy chain from cell lysate. a) HeLa cells stably expressing shRNA against myosin VI (lacking endogenous protein) were transiently transfected with wild-type and mutants**,** shRNA-resistant, GFP-myosin VI tails. Anti–GFP nanobodies were used to immunoprecipite 1 mg of TCL. Bound proteins were resolved by SDS-PAGE and immunoblotted using anti-CLTC and anti-Dab2 monoclonal antibodies (the two proteins were expressed at endogenous level). A polyclonal anti-GFP antibody was used in immunoblot to check the equal amount of immunoprecipitated protein (panel **b**).

This observation led us to further analyse the effect of mutations of the ^{1116}RRL^{1118} motif towards known interactors of myosin VI, such as optineurin, T6BP, NDP52, and GIPC. As probed for clathrin (**Figure 26**), binding to partners was impaired by the structure-destabilizing R1117A mutation either alone or in the context of the triple AAA mutant (**Figure 30**). Analysis performed with the other single point mutants demonstrate that R1116 and L1118 are critical for GIPC and optineurin binding whereas T6BP and NDP52 associate with myosin VI in fashion which not only depends on ^{1116}RRL^{1118} (**Figure 30**). These two latter molecules might extend their interaction with myosin VI to a larger surface that encompass but is not limited to the RRL motif.

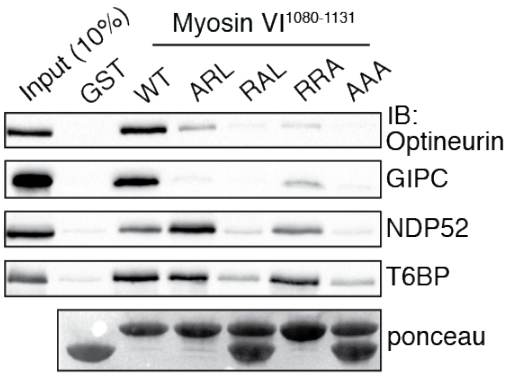

Figure 30: Effect of myosin VI L1118A mutation on the "RRL-interactors". GST-tagged myosin VI$^{1080-1131}$ wild-type and ^{1116}RRL^{1118} mutants were used against 500 µg of TCL from HEK293T transfected with GFP-optineurin, His-GIPC, Flag-NDP52, and Flag-T6BP. Bound proteins were then resolved by SDS-PAGE and assessed for the presence of the different interactors through immunoblot using anti-tag antibodies. Comparable loading of GST-tagged proteins is shown by Ponceau staining (bottom panel).

3.2.2 The presence/absence of the LI dictates myosin VI interactors

Our previous results demonstrated that for the clathrin heavy chain binding we need both the LI and ^{1116}RRL^{1118} motif. This prompted us to re-examine the interaction of Myosin VI with the previously characterized "RRL-interactors" respect to the alternative splicing of the LI. No direct and specific binding towards Myosin VI isoforms has been previously tested *in vitro*.

To get insights into this issue, GST-myosin VI$^{998-1131}$ constructs representing the three isoforms, together with the GST-myosin VI$^{1080-1131}$ constructs that contains the ^{1116}RRL^{1118} motif but not the LI were analysed against HEK293T cell lysate. Surprisingly, all four interactors, optineurin, GIPC, NDP52, and T6BP selectively bind to myosin VI$_{short}$, similar to myosin VI$^{1080-1131}$ construct (**Figure 31**). Thus, clathrin and "RRL-interactors" have different binding specificity and the presence/absence of the LI appears to dictate the myosin VI interactors. A possible explanation for the

above-described data implies that the different isoforms might assume different conformations and that, in the context of Myosin V_{long}, the ^{1116}RRL^{1118} motif necessary for interactor binding is not available.

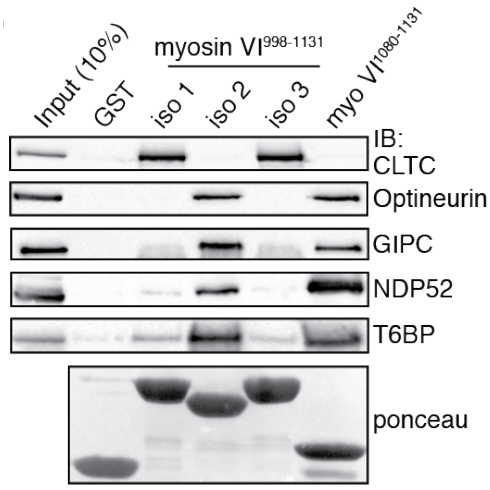

Figure 31: Mutually exclusive binding of myosin VI to clathrin and "RRL-interactors". GST-tagged myosin VI$^{998-1131}$ and myosin VI$^{1080-1131}$ constructs were used against 500 µg of TCL from HEK293T transfected with GFP-optineurin, His-GIPC, Flag-NDP52, and Flag-T6BP. Bound proteins were then resolved in SDS-PAGE and assessed for the presence of the different interactors through immunoblot using anti-tag antibodies, except for CLTC. Comparable loading of GST-tagged proteins is shown by Ponceau staining (bottom panel).

3.2.3 Structure of the myosin VI clathrin-binding domain

To shed light on the different behaviour of myosin VI we started a collaboration with the Kylie Walters group at NIH (Bethesda, USA). We used modern NMR techniques to solve the structure of the myosin VI_{long} fragment responsible for clathrin binding; this region spans R1050-R1131 and includes the isoform-specific LI region (in orange in **Figure 25**). Twenty calculated NMR structures with lowest energy converged well with a backbone root mean square deviation (RMSD) of 0.18 Å. The structure confirmed the predicted α2-linker helix (shown **Figure 25**). The LI region encompassing P1055 to R1068 residues forms an amphipathic α-helix that packs

against two other helices present in all isoforms (**Figure 32a**). A hydrophobic surface of α2-linker formed by M1058, M1062, and L1066 inserts into cleft at the α3/α4 interface for interaction with hydrophobic residues Y1091, F1114, L1118, and Y1121 (**Figure 3.20a**).

Notably the residue L1118, critical for clathrin binding (RRA mutant, **Figure 26**), is buried in the interface between α2-linker and α3/α4 (**Figure 32b**). Thus, leucine to alanine substitution in this position most likely acts changing the configuration of the domain rather than directly affecting the surface of interaction with clathrin. As visible in the structure, R1117 forms a salt bridge with S1087 of the α3 (**Figure 32b**) and this clarifies the importance of this residue to maintain the structural integrity of this region. These structural details proved that the ^{1116}RRL^{1118} motif remains inaccessible for interactors binding in the case of myosin VI$_{long}$. This validates our observation that all four "RRL-binders" have a clear preference for myosin VI$_{short}$ when tested in pull-down assay (**Figure 31**) and the idea of a conformational difference between the myosin VI isoforms induced by the presence of the LI.

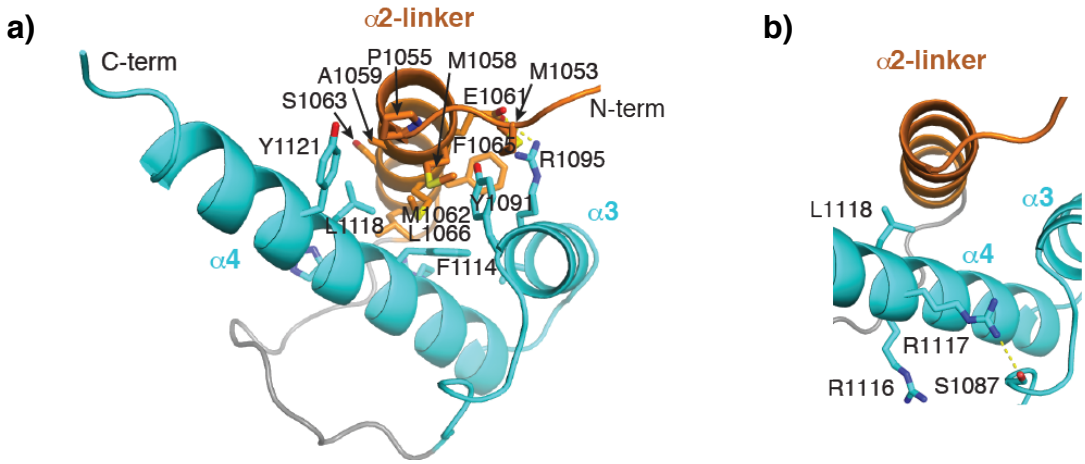

Figure 32: Structure of the myosin VI clathrin-binding domain. a) Ribbon representation of the myosin VI R1050-R1131 structure. The isoform specific α-2 linker is in orange, α-3 and α-4 helices in cyan. **b)** Expanded view of **a** that illustrates the position of the RRL motif residues.

Taken together, these data imply that packing of the α2-linker against the α3/α4 helices in myosin VI_{long} determines: i) its exquisite clathrin-binding ability and ii) its impairment in RRL-mediated binding (i.e. optineurin). Thus, myosin VI isoforms have mutually exclusive association with clathrin and RRL interactors (i.e. optineurin, as schematise in **Figure 33**).

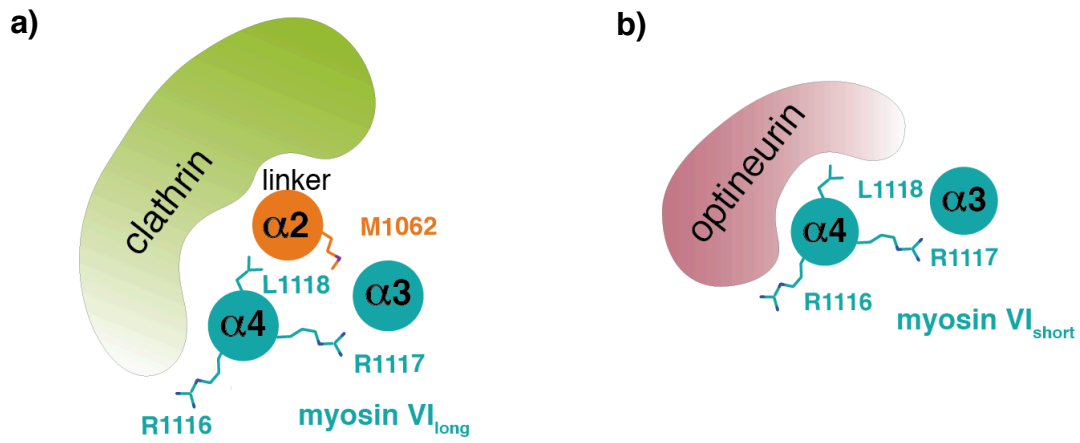

Figure 33: Model representation of the interaction of myosin VI_{long} and myosin VI_{short}. a) The α2-linker (orange) packs against the α3/α4 helices and mask the RRL motif in myosin VI_{long} contemporarily allowing clathrin to interact. **b)** Absence of the α2-linker unmasks the RRL motif, thus permitting the interaction of myosin VI_{short} with the "RRL-interactors".

We endeavoured to validate the functional impact of the myosin VI_{long} conformation testing point mutation/s capable of disrupting interaction between α3/α4 and the α2-linker (**Figure 34a**). M1062, which is sandwiched between α3 and α4, was replaced with glutamine, and this variant, as well as the previously characterized L1118A mutant (**Figure 26** and **Figure 30**), were evaluated for binding to RRL-specific interactors in pull-down assays. As shown in **Figure 34b**, M1062Q was impaired in clathrin binding, similarly to L1118A. GIPC and optineurin showed increased binding to M1062Q, but not to L1118A, consistent with the evidence that

L1118 belongs to their interaction surface. Finally, NDP52 and T6BP bind to both mutants at levels similar to myosin VI_{short}.

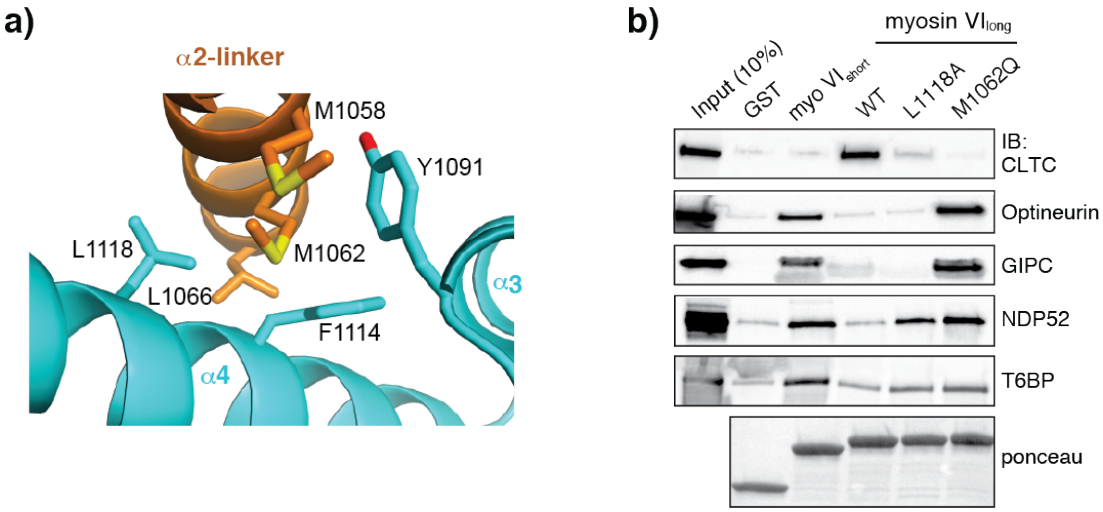

Figure 34: Structural-based mutagenesis of the α-2 linker of myosin VI_{long}. a) enlarged view of the ribbon representation of the myosin $VI^{1050-1131}$ structure that illustrate the position of the residues important for the tertiary structure. The isoform specific α-2 linker is in orange, α-3 and α-4 helices in cyan. **b)** GST-tagged myosin $VI^{998-1131}$ wild type and mutants constructs were used against 500µg of TCL from HEK293T transfected with GFP-optineurin, His-GIPC, Flag-NDP52, and Flag-T6BP. Bound proteins were then resolved in SDS-PAGE and assessed for the presence of the different interactors by immunoblot using anti-tag antibodies, except for CLTC. Comparable loading of GST-tagged proteins is shown by Ponceau staining (bottom panel).

These results confirmed the conformational differences between the myosin VI isoforms induced by the presence of the α2-linker, and established the molecular mechanism underlying their mutually exclusive association with clathrin and RRL interactors.

3.3 The exon 31 of myosin VI, which encodes for the α2-linker, is frequently skipped in cancer

3.3.1 Ovarian cancer predominantly express myosin VI_{short}

Overexpression of myosin VI has emerged in ovarian and prostate cancer and confidently linked to metastatic aggressiveness and worsening of prognosis [Dunn *et al.*, 2006; Yoshida *et al.*, 2004]. While this information was available, there are no evidences regarding the myosin VI isoform expressed in malignant tumours. In the last few years, the contribution of deregulated splicing in human disease, particularly in cancer, has been widely recognized [Singh *et al.*, 2012]. To gain insight into possible differential expression of myosin VI isoforms in tumours, we concentrated our efforts on ovarian cancer, analyzing the isoform expression in high-grade primary ovarian cancer cells cultured *in vitro* for two passages. We designed PCR-primers positioned on exons 28 and 33 (flanking the LI region, **Figure 35a**) in order to perform RT-PCR starting from cDNA of tumour and control samples. In this way we could discriminate between the different isoforms, as demonstrated in the control lanes of **Figure 35b**. Surprisingly, while normal ovarian samples (ovarian surface epithelium, OSE) express different myosin VI isoforms, all the tumours samples analysed (ten out of ten), showed almost exclusively expression of myosin VI_{short}.

This result suggests a possible positive selection for this isoform in tumour progression and metastasis.

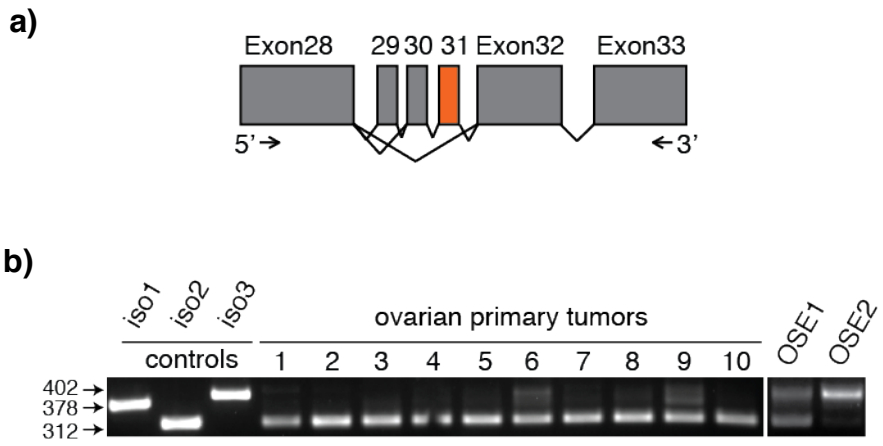

Figure 35: Myosin VI$_{short}$ is prevalently expressed in ovarian cancer cells. a) Schematic representation of the region amplified by RT-PCR. Grey boxes represent coding exons and alternative splicing events are depicted. Exon 31 that codifies for the α2-linker is represented in orange. Oligos used for the PCR mapped in Exon 28 and Exon 33 and are indicated by arrows. **b)** RT-PCR from cDNA prepared from the indicated primary cells. PCR controls are from plasmids carrying myosin VI of the different isoforms. Samples were loaded on a 2% agarose gel and stained with ethidium bromide. Cells from normal tissue (OSE-Ovarian Surface Epithelium), were used as control to compare cancer vs. normal myosin VI isoform expression.

3.3.2 Cells that express only myosin VI$_{short}$ are addicted to myosin VI for cell migration

We then searched for the biological meaning lying behind our structural findings. To this purpose we exploited ovarian-derived cell lines available for possible *in vitro* studies. First, we evaluated the myosin VI isoform prevalently expressed by these cell lines under normal cultured condition. As visible from **Figure 36,** 7 out of 8 cell lines tested showed the exclusive expression myosin VI$_{short}$ isoform.

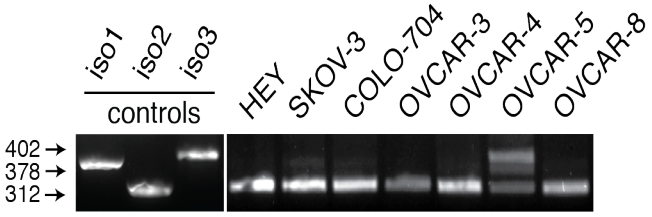

Figure 36: Most ovarian cell lines selectively express Myosin VI_{short} in cultured conditions. Myosin VI isoform expression was assessed by RT-PCR from cDNA prepared from the indicated cell line. PCR controls are from plasmids carrying myosin VI of the different isoforms. Samples were loaded on a 2% agarose gel and stained with ethidium bromide.

Next, we wondered whether there could be differences among cells that express only the short isoform o myosin VI and cells that express also the longer ones. To this purpose we challenged the cell to express myosin VI_{long} by growing them in confluent condition for 2 to 4 days. It was previously reported that during in vitro epithelial cell polarization a myosin VI isoform switch occurs toward longer isoforms [Buss *et al.*, 2001]. Of the selected cell lines, SKOV-3 and HEY did not show any switch in the expression of myosin VI isoform, as visible in **Figure 37**. On the other hand, we could score a different behaviour for OVCAR-5 cell line, which increased the expression of myosin VI_{long} upon confluency (**Figure 37**).

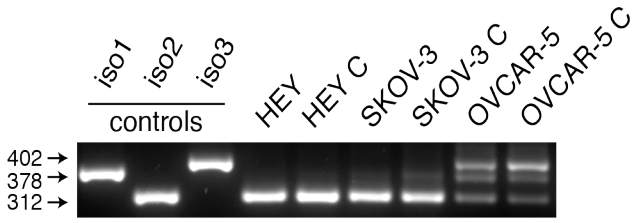

Figure 37: Isoform switch of ovarian cell lines upon polarization. Myosin VI isoform expression was assessed by RT-PCR from cDNA prepared from the indicated cell line grown in normal (no mark) and confluent condition (marked with C). PCR controls are from plasmids carrying myosin VI of the different isoforms. Samples were loaded on a 2% agarose gel and stained with ethidium bromide.

It was previously reported that knocking-down myosin VI substantially inhibits migration *in vitro* and reduces dissemination of ovarian tumour cells propagated in nude mice [Yoshida *et al.*, 2004]. Wound-healing assay *in vitro* can be considered as a proxy for cancer metastasis. Thus, we analysed the effect of myosin VI depletion in a wound-healing assay, comparing the behaviour of the ovarian cancer

cell lines that showed different myosin VI expression. Depletion of myosin VI, achieved through transient siRNA transfection, was comparable in all cell lines tested and was close to 100% (immunoblots on the right of **Figure 38 a-e**). Knockdown of myosin VI with two different siRNA oligos in SKOV-3 and HEY cells resulted to impair wound closure speed (**Figure 38 a-d**). Surprisingly the same treatment did not impact on the migration efficiency of OVCAR-5 (**Figure 38 e**). Possibly, myosin VI_{short} could give a selective advantage that would explain the high percentage of ovarian cancer that prevalently express this isoform.

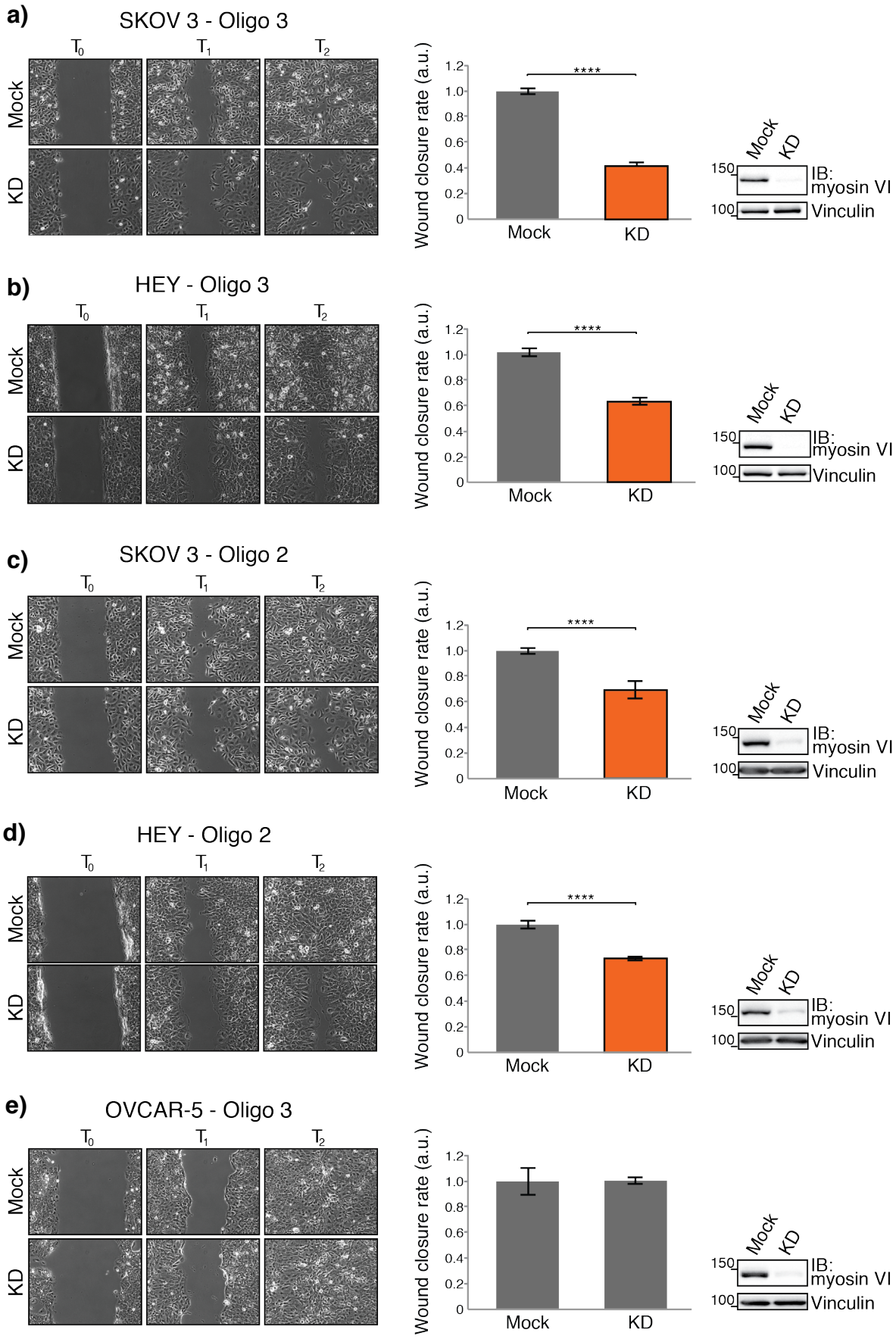
a)
SKOV 3 - Oligo 3
b)
HEY - Oligo 3
c)
SKOV 3 - Oligo 2
d)
HEY - Oligo 2
e)
OVCAR-5 - Oligo 3
T0
T1
T2
Mock
KD
Wound closure rate (a.u.)
****
IB:
myosin VI
Vinculin
150
100

Figure 38: Ovarian cell lines that express only myosin VI_{short} need myosin VI for proper cell migration. Same for **a) - e)**: Wound-healing assay. The indicated cell lines were transiently transfected with different siRNA targeting myosin VI to achieve knockdown of the protein (marked as KD) or mock treated (marked as Mock). Left panel, sample images: T_0 first frame, T_1 and T_2 arbitrary time-points identical for Mock and KD of the same cell lines. Central panel: quantification of the wound closure speed relative to control that represents the average of 6 different measures from three independent experiments +/- SD. Right panel: anti-myosin VI IB and anti-Vinculin IB performed at T_0 to allow quantification of the efficiency of the knockdown.

3.3.3 Exon 31 skipping is a common event in many cancer types

Previous results prompted us to extend our analyses of myosin VI isoform expression to other cancer types using an *in silico* approach, in collaboration with Uberto Pozzoli (IRCCS E.MEDEA, Italy). As a source of data, we used The Cancer Genome Atlas (TCGA) database and included all of the experiments performed using RNAseq technology. The resulting dataset consisted of 293 control and 1646 tumour samples, belonging to 14 different tumour types.

Exon 31 encodes for the α2-linker that we proved being the necessary for the isoform-specific conformation. For this reason, as discriminating marker of myosin VI_{long} isoforms the relative expression of exon 31 was evaluated. The relative abundance of exon 31 (E31RA) was obtained as the ratio of its RPKM (Reads Per Kilobase of Exon Model per Million Mapped Reads, see Materials and Methods for details) and the average RPKM values of the four flanking constitutive exons (namely E27, E28, E32 and E33). The box plot relative to the analysis (**Figure 39**) indicates that exon 31 skipping is a common event occurring with significantly increased frequency in tumour compared to normal samples. Thus, myosin VI_{short} is selectively expressed in many tumour types. The analysis conducted at the single cancer type level showed that exon skipping is highly frequent among certain tumours, but not others, and suggested that myosin VI_{short} functions may be critical and positively

selected only in specific types of cancers. Of note, in the case of ovarian cancer, no "normal" controls were present in the database, but compared to the average of normal samples, exon E31RA is barely measurable (**Figure 40**), further confirming the data obtained in primary tumours.

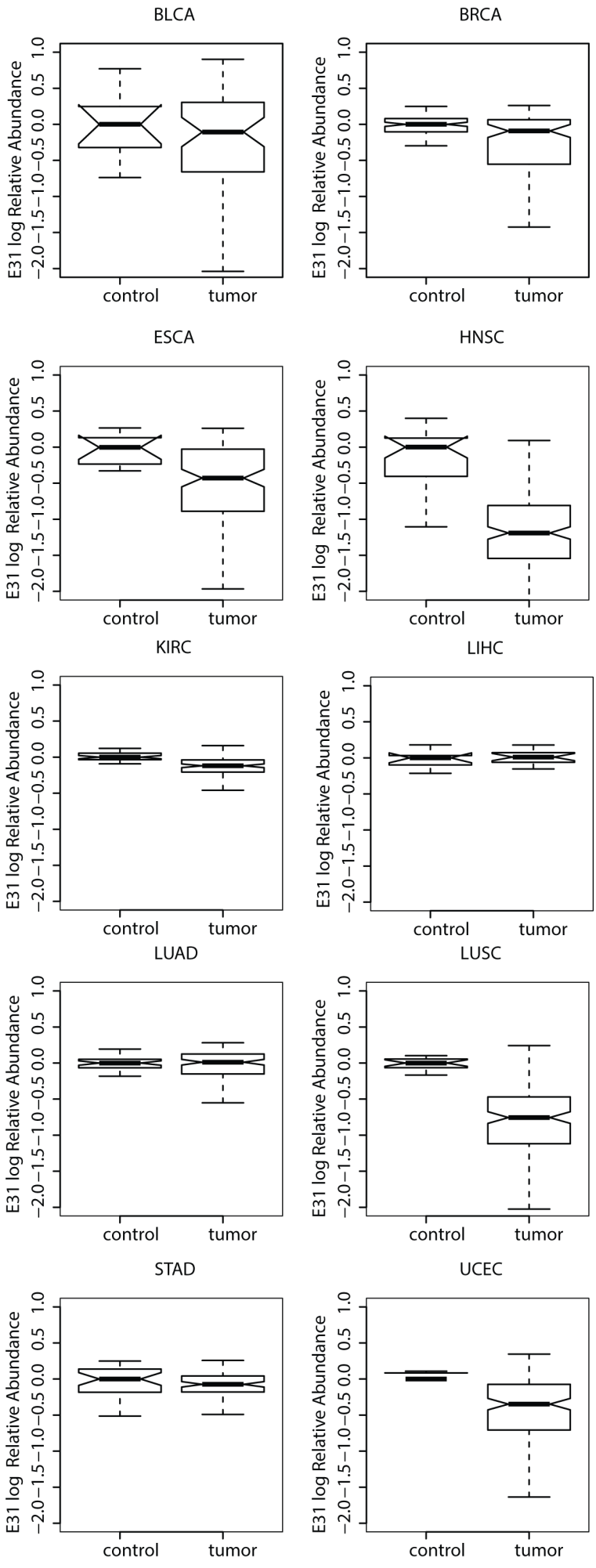
BLCA
BRCA
ESCA
HNSC
KIRC
LIHC
LUAD
LUSC
STAD
UCEC
E31 log Relative Abundance
−2.0 −1.5 −1.0 −0.5 0.0 0.5 1.0
control
tumor

Figure 39: Exon E31 relative abundance in different cancer types. Exon E31 relative abundance at the single tumour level compared with their normal counterparts. E31RA has been calculated for each sample dividing E31 RPKMS by the average of the flanking constitutive exons (i.e. E27, E28, E32, E33). All values have been normalized by their median in the tumour matched control samples. Bladder urothelial carcinoma (BLCA), breast invasive carcinoma (BRCA), esophageal carcinoma (ESCA), head and neck squamous cell carcinoma (HNSC), kidney renal clear cell carcinoma (KIRC), liver hepatocellular carcinoma (LIHC), lung adenocarcinoma (LUAD), lung squamous cell carcinoma (LUSC), stomach adenocarcinoma (STAD), and uterine corpus endometrial carcinoma (UCEC).

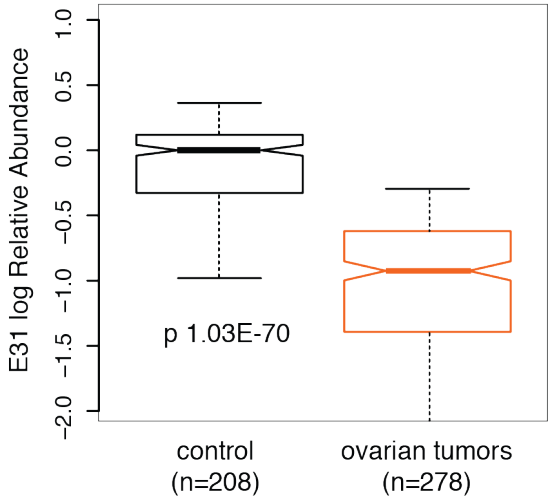

Figure 40: Exon 31 expression is barely detectable in ovarian cancer. Exon E31 relative abundance in ovarian cancer compared to the average of normal samples from all available cancer types. P-value is reported.

As proof of principle, we selected two breast cell lines, MCF10A (normal cells) and MDA-MB-231. This latter cancer cell line showed high levels of myosin VI_{short}-only, in both sparse and confluent conditions, while MCF10A could switch the expression to all the three isoforms (**Figure 41a**). Upon myosin VI depletion, MDA-MB-231 cells displayed a clear impairment in wound closure (**Figure 41b**) while

MCF10A cells were unaffected (**Figure 41c**). Thus, also breast cancer cells that selectively express myosin VI_{short}-only are addicted to myosin VI for cell migration.

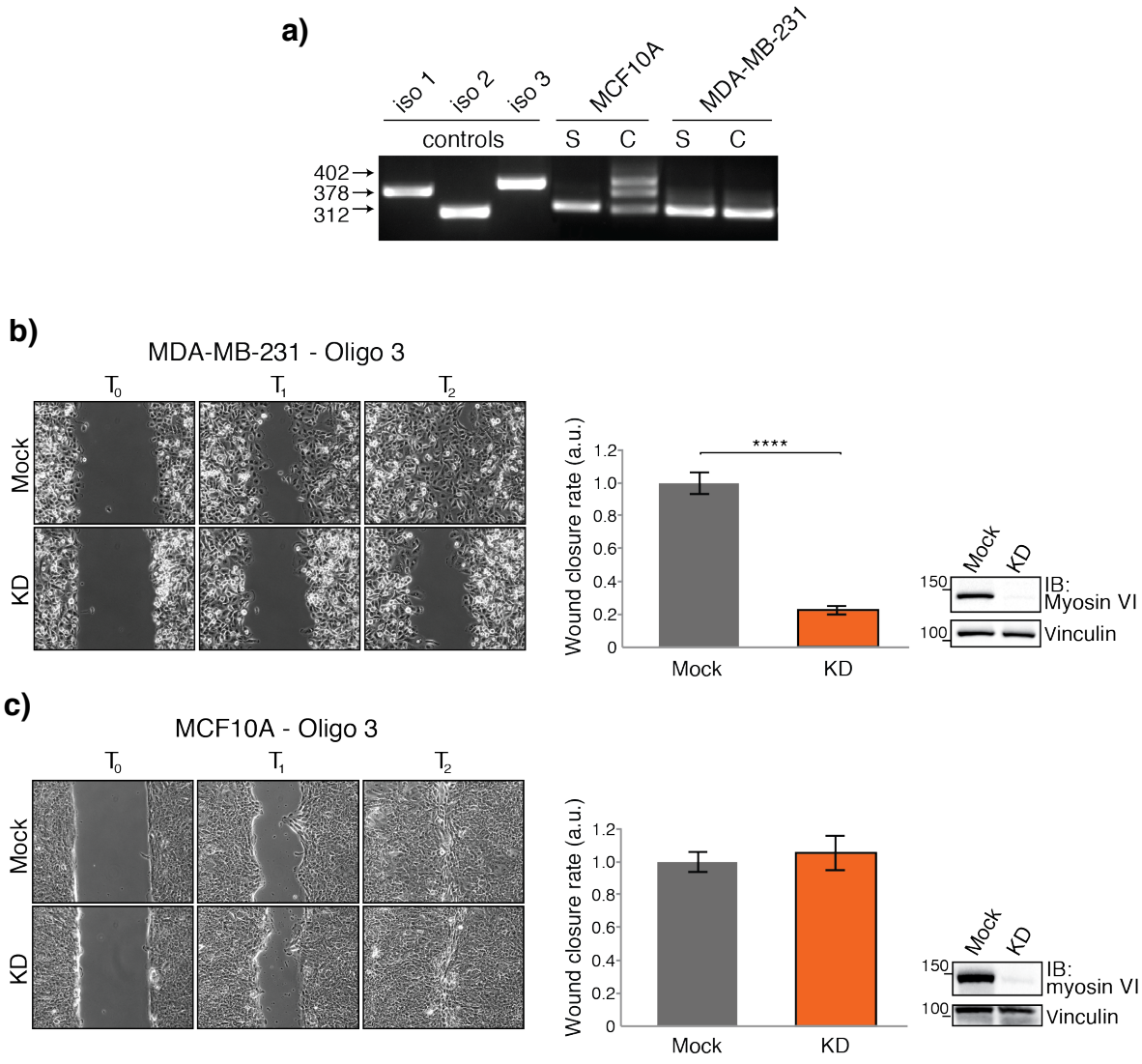

Figure 41: Breast cancer-derived cell lines recapitulate the behaviour of ovarian cancer. a) myosin VI isoform expression was assessed by RT-PCR from cDNA prepared from the indicated cell line grown in sparse (marked with S) or confluent condition (marked with C). PCR controls are from plasmids carrying myosin VI of the different isoforms. Samples were loaded on a 2% agarose gel and stained with ethidium bromide. **b),** and **c)**: Wound healing assay. The indicated cell lines were transiently transfected with siRNA targeting myosin VI to achieve knockdown of the protein (marked as KD) or mock treated (marked as Mock). Left panel, sample images: T_0 first frame, T_1 and T_2 arbitrary time-points identical for Mock and KD of the same cell lines. Central panel: quantification of the wound closure speed relative to control that represents the average of 6 different measures from three independent experiments +/- SD. Right panel: anti-myosin VI IB and anti-Vinculin IB performed at T_0 to allow quantification of the efficiency of the knockdown.

4. DISCUSSION

Phosphorylation, dimerization, and alternative splicing have been suggested to be crucial for myosin VI activity [Buss *et al.*, 2008]. In this thesis, we focused on myosin VI isoforms and in particular on the large insert, codified by exons 29,30,31. In literature it is known that the alternatively spliced isoforms of myosin VI are targeted to different intracellular locations through a yet undefined mechanism [Tumbarello *et al.*, 2013]. Here, by studying the interactomes and the conformational structure of myosin VI isoforms, we provide mechanistic insights into how myosin VI function becomes pathological in human cancers, and demonstrate the importance of an isoform-specific helix in assigning myosin VI to distinct functional roles.

4.1 Myosin VI isoforms (long and short) have different interactomes, among which clathrin is selective for the long

The subcellular localization of any given protein correlates with its function. In this framework, myosin VI has been seen at the apical membrane of highly polarized cells exerting a role in endocytosis [Ameen *et al.*, 2007], shaping the microvilli [Buss *et al.*, 2001], colocalizing with intracellular coated and uncoated vesicles [Dance *et al.*, 2004], or at the leading edge of migrating cells [Chibalina *et al.*, 2010]. Although myosin VI is widely expressed in most tissues, isoforms containing the LI are specifically found in polarized epithelial cells. Up to now, isoforms lacking the LI were shown to localize in Rab5/APPL1-positive endosomes [Tumbarello *et al.*, 2012], are required for polarized transport of tyrosine motif containing basolateral membrane proteins [Au *et al.*, 2007], and for the maintaining an active pool of secretory granules near the plasma membrane of neurosecretory cells [Tomatis *et al.*, 2013]. How the

presence of LI in the tail influences the functions and intracellular targeting of myosin VI is not known.

In our studies we specifically investigated how alternative splicing of the large insert of myosin VI regulates the structural and functional properties of the molecule. Many of the binding partners of myosin VI were found in yeast-two hybrid screens where chicken myosin VI tail+LI was the bait [Morris *et al.*, 2002; Morriswood *et al.*, 2007; Sahlender *et al.*, 2005]. To identify specific interactors of the various isoforms, we undertook a different approach coupling GST-pulldown of a HEK293T total cell lysate to a quantitative mass-spectrometry analysis.

The results presented in **Table 1** demonstrate that the presence or the absence of the large insert dictates specific myosin VI interactors. Lack of the LI (see **Figure 13b**), generates the isoform 2 that we named myosin VI_{short}, that appears to bind a set of previously undescribed interactors. Isoform 1 and 3 that differs for the presence or the absence of exon 29, show basically no difference in terms of interactors. This led us to name them collectively as myosin VI_{long}.

Interestingly, myosin VI_{short} interact with many nuclear-resident proteins related to the DNA damage response pathway. In our immunofluorescence studies we failed to see a nuclear localization of myosin VI_{short}, but additional studies are required to evaluate possible re-localization of the protein upon DNA damage. Nonetheless, our data corroborate previous reports on the role of myosin VI in RNA polymerase-II dependent transcription and p53-mediated DNA damage response [Cho *et al.*, 2010; Jung *et al.*, 2006; Vreugde *et al.*, 2006]. On the other hand, the identification of myosin VI_{long} interactors such as clathrin heavy chain and clathrin adaptors (APs) are in accordance with the role of myosin VI in clathrin-mediated endocytosis [Ameen *et al.*, 2007; Buss *et al.*, 2001; Kravtsov *et al.*, 2012].

Previous studies have considered Dab-2 as the adaptor that links myosin VI to clathrin-mediated function [Inoue *et al.*, 2002; Morris *et al.*, 2002; Spudich *et al.*, 2007]. The Dab-2:myosin VI interaction, however, fails to explain the myosin VI_{long}-specific interaction with clathrin, as the Dab-2 binding region is remote from the LI [Morris *et al.*, 2002; Yu *et al.*, 2009]. Our pulldown assays (**Figure 15**) suggested either a direct binding with clathrin heavy chain or an indirect binding mediated by an alternative adaptor.

Clathrin heavy chain truncation constructs have been exploited for both biochemical and cell-biological studies. The molecule's tertiary structure allow to divide it into a terminal, leg, and trimerization domains that can exert their functions even when isolated from the rest of the molecule. We used GST- and GFP-tagged clathrin heavy chain truncations, kindly given from SJ Royle (Division of Biomedical Cell Biology, Warwick Medical School, Gibbet Hill Road, Coventry), to determine the possible site of interaction of myosin VI on the CLTC molecule. As only the full-length was able to bind to myosin VI_{long} (**Figure 16**), we concluded that the critical determinant for the interaction with myosin VI is at the C-terminus of clathrin heavy chain. Intriguingly, even though expressed at the same level of the endogenous, transfected GFP-CLTC full-length did not show the same stoichiometry of interaction of endogenous CLTC to myosin VI_{long}, arguing against the complete functionality of the overexpressed protein (**Figure 16**). When we tested the direct binding with bacterially purified proteins, none of the GST-CLTC fusion proteins was able to interact with a myosin $VI^{998-1131}$ (**Figure 17b**). As the isolated clathrin hubs that we used in experiment are reported to self-assemble into trimeric units [Liu *et al.*, 1995] we can exclude a requirement of triskelion for myosin VI interaction.

4.2 Myosin VI_{long} binds directly to clathrin light chain A

The evidences described above prompted us to hypothesize a direct binding of myosin $VI^{998-1131}$ with the only known protein capable of binding the C-terminus of CLTC, namely clathrin light chains. The direct binding of purified LC and myosin $VI^{998-1131}$ protein (**Figure 18**) definitely confirmed our idea. Thus, we can add a new player in the myosin VI activity towards clathrin-mediated endocytosis. The elevated affinity of clathrin light chains towards their heavy counterpart ($K_D \approx 10^{-11}$ M [Winkler *et al.*, 1983]) can account for high amount of CLTC we scored in our initial pulldown using GST-myosin $VI^{998-1131}$ against cell lysates. We did not score LC in the mass spec data as proteins with a molecular mass lower than 50 kDa were automatically excluded from the analysis (we cut slices higher than immunoglobulins heavy chain).

Although clathrin light chain and myosin VI have never been directly linked to each other in clathrin-mediated endocytosis, they were both demonstrated to have critical role in this process. CME of the most studied cargoes, such as transferrin-receptor (TfnR) or epidermal growth-factor receptor (EGFR) is not influenced by depletion clathrin light chain [Huang *et al.*, 2004], nor by depletion of myosin VI (previous unpublished results of our lab). Nevertheless, recent evidences have shown that LCs are involved in the trafficking of mannose-6-phosphate receptor [Poupon *et al.*, 2008] and G-protein-coupled receptor [Ferreira *et al.*, 2012]. The finding of a Hip1 and Hip1R binding site on LCs [Chen *et al.*, 2005] laid the foundations for a novel link between clathrin-mediated endocytosis and the actin cytoskeleton. Altogether these evidences drive to hypothesize a broader list of functions of LCs, yet to be studied. In the very same way, a critical role of myosin VI in CME has been suggested, but few direct evidences have been reported. Alterations of myosin VI activity were shown to inhibit CFTR internalization in several cellular systems [Swiatecka-Urban *et al.*, 2004]; [Ameen *et al.*, 2007]; [Collaco *et al.*, 2010]. Interestingly, CFTR endocytosis

occurs via CME [Bradbury *et al.*, 1999]. The regulation of surface sodium type-IIa cotransporter (NaPi2a) at the apical membrane of renal proximal tubular cells also appears to depend on myosin VI and clathrin-mediated endocytosis [Blaine *et al.*, 2009]; [Chen *et al.*, 2014]. In such kind of highly polarized cells, endogenous myosin VI_{long} is enriched at the apical membrane, together with clathrin-rich structures [Buss *et al.*, 2001]. Notably, clathrin light chains and their binding partner Hip1/Hip1R are also needed at the apical membrane of polarized cells to achieve efficient clathrin-coated vesicle fission [Boulant *et al.*, 2011]. It is therefore tempting to speculate a coordinate function of myosin VI and LCs in such location, where tensile strength might rigidify the membrane, making it less prone to invagination.

Our study also offers a new perspective on the molecular mechanism that regulates the monomer-dimer conversion of this anchor-motor protein [Lu *et al.*, 2014b; Sweeney *et al.*, 2010]. It is tempting to speculate that the existence of distinct interaction surfaces for clathrin and Dab-2, both required for co-localization with clathrin-coated pits (**Figure 28**) may provide critical synergy that regulates the myosin VI motor ability. Clathrin binding may recruit and concentrate myosin VI at clathrin-coated pits where Dab2 could tether it into a stable and active dimer, crucial to convert myosin VI in a processive cellular transporter [Yu *et al.*, 2009].

Our hypothesis might introduce a new layer of complexity in the endocytic processes, required in specific situation where the plasma membrane is under tension or in the case of endocytosis of larger cargoes such as *Listeria monocytogenes* [Bonazzi *et al.*, 2011], which resemble adherens junctions rearrangements [Bonazzi *et al.*, 2012], a process where myosin VI was demonstrated to play a role [Maddugoda *et al.*, 2007].

Committed to the idea that a complete mechanistic and structural understanding of the myosin VI:clathrin light chain interaction is of paramount

importance for further studies, we exploited several GST-pulldown, using purified proteins. A first identification of the specific interaction of myosin VI_{long} with LCa, compared to the unbound LCb (**Figure 20**), led us to investigate the binding surface using truncated LCa fusion proteins. This analysis allowed us to identify LCa^{47-97} as the minimal region (**Figure 21**). LCs show a tendency to be unstructured while in solution but can fold upon the establishment of partner interaction [Wilbur *et al.*, 2010]. Size exclusion chromatography analysis proved that the two proteins could form a stable complex in solution, even at low concentration (10 μM each, data not shown). Unfortunately, we were not able to obtain crystals. Further trimming of the molecule led us to conclude that the LCa^{51-60} is the minimal surface needed for the interaction (**Figure 23** and **Figure 24**). A LCa protein deleted of this latter region (GST-$LCa^{\Delta 51-60}$), resulted to be impaired in myosin VI_{long} binding **(Figure 24**), univocally proving that LCa^{51-60} fragment is both necessary and sufficient to contact the motor protein. We calculated the isoelectric points of the two proteins: LCa^{51-60} pI ≈ 4; myosin $VI^{998-1131}$ pI ≈ 8. Thus, we hypothesize an interaction mediate by electrostatic interaction and we intend to perform mutant analysis to prove/disprove this hypothesis.

4.3 Due to the disparate conformations adopted by myosin VI isoforms, clathrin and "RRL" interactors are mutually exclusive partners.

Using point mutants of myosin VI we investigated the effect of the ^{1116}RRL^{1118} motif in regulating the interaction with clathrin, since this has been prove to be one of the major hub for myosin VI interactors [Tumbarello *et al.*, 2013]. The triple ^{1116}AAA^{1118} mutant, as well as the R1117A and the L1118A single mutants, showed a complete impairment of the binding to the coat protein (**Figure 26**). R1117A mutation disrupts

the salt bridge that this amino acid establishes with the S1087 side chain (**Figure 32b**). Circular dichroism analysis confirmed unfolding of the myosin VI$^{998\text{-}1131}$ bearing the R1117A mutation (**Figure 27**). Thus, the previously characterized ^{1116}AAA^{1118} triple mutant has to be unfolded as well and the mapping of the binding site for T6BP and NDP52 [Morriswood *et al.*, 2007] is questionable. Indeed, binding of both proteins to myosin VI were unaffected by R1116A or L1118A mutation (**Figure 30**)

We selected the L1118A mutant to further study the myosin VI:clathrin interaction. This mutation negatively affect myosin VI binding to clathrin in co-immunoprecipitation and co-localization experiments, as shown in **Figure 28** and **Figure 29**. In these experiments, myosin VI$_{short}$ and myosin VI$_{long}$ W1192L mutant were used to check isoform specificity of the clathrin binding as well as Dab2 interaction. While myosin VI$_{short}$ failed to localize and coimmunoprecipitate with clathrin, it still retained the ability to bind Dab2 (**Figure 28** and **Figure 29)**. W1192L mutant did not colocalize with clathrin but could still bind the coat protein by coimmunoprecipitation. We ascribed these behaviors to a transient nature of the interactions between these three proteins at the level of clathrin coated pits and vesicles and to a redundant actions of Dab2 and clathrin light chain in recruiting myosin VI at the CME sites.

To better investigate this possibility dynamics studies are needed. Recent advantages in high-resolution time-lapse imaging techniques [Kural *et al.*, 2015; Li *et al.*, 2015] may allow to resolve in time and space the appearance of Dab2, clathrin, and myosin VI at the site of endocytosis. Possibly, this approach will be combined with gene substitution techniques (CRISPR/Cas9 knock-in), in order to avoid overexpression of fluorescent proteins, which have already been shown to influence their behavior [Dance *et al.*, 2004].

By NMR we structurally characterized the novel myosin VI_{long}-specific clathrin-binding domain that we identified. From the structure we learned that the α2-linker marks the specific conformation of myosin $VI_{long.}$ and prevents interaction with other functional adaptors that utilize the previously identified 'RRL' motif. This motif, embedded in the clathrin-binding domain, is masked in the structural configuration adopted by the myosin VI_{long}. Consequently, the previously identified interactors (optineurin, GIPC, NDP52, and T6BP) show selective binding to myosin VI_{short} (**Figure 31**). Thus, the different isoform structural architectures establish mutual exclusivity of myosin VI binding partners, clathrin versus RRL interactors, and in turn, function. The tertiary structure is maintained through a series of hydrophobic interaction (highlighted in **Figure 34a**) that we abolished introducing mutation of L1118 to alanine and M1062 to glutamine. With these mutations we obtained a myosin VI_{long} protein that behaves like myosin VI_{short} in terms of interactors selectivity (**Figure 34b**).

Taken together our data showed a clear preference of RRL interactors towards myosin VI_{short}. Structural data provide a detailed rationale for optineurin and GIPC as R1116 and L1118, which belong to their interaction surface, are masked in the myosin VI_{long} conformation. A similar explanation could also apply for NDP52 and T6BP, although their precise interaction surface remains to be established. Whatever the case, our data suggest that myosin VI_{short} is the myosin VI isoform specifically involved in the functional interaction with these adaptor proteins while myosin VI_{long} is specifically involved in CME. These findings opens interesting scenario in which myosin VI isoforms exerts their specific cellular functions through their cargo adaptor proteins [Tumbarello *et al.*, 2013]. Whether myosin VI_{short} is the isoform specifically involved in autophagy and Golgi morphology and secretion requires further investigations.

4.4 Myosin VI_{short} is critically involved in cancer cells migration

Several studies reported overexpression of myosin VI in prostate and ovarian cancers, which positively correlates with their grade and metastatic potential [Dunn *et al.*, 2006; Yoshida *et al.*, 2004]. Though, no information was available concerning the specificity of isoform expression. We examined expression of myosin VI isoforms in primary tumours from ovarian cancer patients to find that myosin VI_{short} was the only isoform upregulated (**Figure 35**).

With an unbiased approach, we evaluated the relative abundance of the myosin VI exons. This analysis revealed that selective skipping of the exon 31, encoding the long isoform-specific helix, frequently occurs in specific tumours but not in others or in normal samples (**Figure 39**). Importantly, cancer cell lines selectively expressing the myosin VI_{short} isoform exhibit severe migration defects when myosin VI is knocked down (**Figure 38** and **Figure 41**).

In essence, we found that the isoform switch, a physiological event occurring during epithelial polarization [Buss *et al.*, 2001; Dance *et al.*, 2004], is deregulated in a large proportion of cancers. Exon skipping determines the expression of myosin VI_{short} only in these cancer cells that become addicted to myosin VI_{short} for tumour cell migration.

Myosin VI has been previously implicated in cell migration in Drosophila and mammals (reviewed in [Chibalina *et al.*, 2009]). However, published data led to an intriguing conundrum. On the one hand, myosin VI depletion from epithelial cells leads to loss of vinculin from adhesion sites, and weakens E-cadherin complexes [Maddugoda *et al.*, 2007]. Such rearrangement results in loss of cohesive forces in epithelial layers, a well-known prerequisite for invasive cancer cell migration. On the

other hand, myosin VI is significantly upregulated in prostate and ovarian cancer cells, where its overexpression correlates with clinically aggressive behaviour [Dunn *et al.*, 2006; Yoshida *et al.*, 2004]. In this context, silencing of myosin VI expression in ovarian and prostate cancer cell lines decreases the migratory potential of these cells *in vitro,* and ovarian tumour dissemination *in vivo* [Dunn *et al.*, 2006; Yoshida *et al.*, 2004].

Our results provide a molecular explanation for this conundrum, ascribing the cohesive and migratory defects to the two different myosin VI isoforms. We found that myosin VI_{short} is overexpressed in ovarian and other invasive cancers, whereas myosin VI_{long} is expressed in polarized epithelial cells, in which it likely promotes E-cadherin stabilization at cell-cell junctions and, possibly, their rearrangements through clathrin-mediated endocytosis.

The border cell migration occurring during oogenesis in Drosophila is reminiscent of tumour cell invasion [Yoshida *et al.*, 2004]. Initially, the border cells are polarized epithelial cells with strong cell-cell contacts. To start migration, cell polarity changes from apico-basal to front-rear, and proteins found at cell-cell junctions reorganize at the invasive edge of the cell to facilitate motility and invasion [Pinheiro *et al.*, 2004]. During these events, myosin VI changes localization, from the baso-lateral membrane to membrane ruffles at the front of moving cells [Pinheiro *et al.*, 2004]. An interesting possibility is that at the onset of border cell migration, an isoform switch towards the shorter myosin VI isoform occurs. Nothing is known of the differential expression and functions of myosin VI isoforms in Drosophila. However, we noticed that different splicing variants also exist in the fly gene. Secondary structure prediction analysis suggested that, even if the primary sequence is not conserved, the exon that is skipped in the shortest isoforms encodes an alpha helix with length and position similar to the α2-linker in mammals.

In the last few years, the contribution of alternative splicing in human disease, particularly in cancer, has been widely recognized [Singh *et al.*, 2012]. Unbalanced expression of splicing variants or failure to properly express the correct isoform is clearly part of the biology of cancer cells [Biamonti *et al.*, 2014]. Cancer-associated alternative splicing variants are now considered new tools for the diagnosis and classification of cancers and could become targets for innovative therapeutic interventions based on highly selective splicing correction approaches. The selective expression of myosin VI_{short} in several types of cancer, which we reported in **Figure 39** and **40**, may very well fit in this context. Our data suggest that cancer cells positively select myosin VI_{short} because it confers them with a migratory advantage. Although more work is required to understand how exon skipping of myosin VI is occurring in cancer cells, our findings reveal an unappreciated function for the regulation of alternative splicing of myosin VI in cancer biology. The identification of myosin VI_{short} as a regulator of cancer cell migration provides an exciting starting point to understand and therapeutically exploit novel key events in pathological cell migration.

REFERENCES

Alajlouni, R.*, et al.* (2011). Lipid-mediated membrane binding properties of Disabled-2. Biochimica et biophysica acta *1808*, 2734.

Ameen, N.*, et al.* (2007). Defective CFTR apical endocytosis and enterocyte brush border in myosin VI-deficient mice. Traffic *8*, 998.

Au, J.S.*, et al.* (2007). Myosin VI is required for sorting of AP-1B-dependent cargo to the basolateral domain in polarized MDCK cells. The Journal of cell biology *177*, 103.

Avraham, K.B.*, et al.* (1997). Characterization of unconventional MYO6 , the human homologue of the gene responsible for deafness in Snell's waltzer mice. Human molecular genetics *6*, 1225.

Avraham., K.B.*, et al.* (1995). The mouse Snell's waltzer deafness gene encodes an unconventional myosin required for structural integrity of the inner ear hair. Nature Genetics *11*, 369.

Baker, J.P.*, et al.* (1997). A Family of Unconventional Myosins from the Nematode Caenorhabditis elegans. Journal of Molecular Biology *272*, 523.

Biamonti, G.*, et al.* (2014). The alternative splicing side of cancer. Seminars in cell & developmental biology *32*, 30.

Birgisdottir, A.B.*, et al.* (2013). The LIR motif - crucial for selective autophagy. Journal of cell science *126*, 3237.

Blaine, J.*, et al.* (2009). PTH-induced internalization of apical membrane NaPi2a: role of actin and myosin VI. American journal of physiology Cell physiology *297*, C1339.

Bonazzi, M.*, et al.* (2012). A common clathrin-mediated machinery co-ordinates cell-cell adhesion and bacterial internalization. Traffic *13*, 1653.

Bonazzi, M.*, et al.* (2011). Clathrin phosphorylation is required for actin recruitment at sites of bacterial adhesion and internalization. The Journal of cell biology *195*, 525.

Bond, L.M.*, et al.* (2011). Myosin VI and its binding partner optineurin are involved in secretory vesicle fusion at the plasma membrane. Molecular biology of the cell *22*, 54.

Boulant, S.*, et al.* (2011). Actin dynamics counteract membrane tension during clathrin-mediated endocytosis. Nature cell biology *13*, 1124.

Bradbury, N.A.*, et al.* (1999). Characterization of the internalization pathways for the cystic fibrosis transmembrane conductance regulator. am J Physiol *276*, 659.

Brodsky, F.*, et al.* (1991). Clathrin light chains: arrays of protein motifs that regulate coated-vesicle dynamics. trends in Biochemical Science *16*, 208.

Brodsky, F.M. (2012). Diversity of clathrin function: new tricks for an old protein. Annual review of cell and developmental biology *28*, 309.

Bryant, Z.*, et al.* (2007). The power stroke of myosin VI and the basis of reverse directionality. Proceedings of the National Academy of Sciences of the United States of America *104*, 772.

Bunn, R.C.*, et al.* (1999). Protein Interactions with the Glucose Transporter Binding Protein GLUT1CBP That Provide a Link between GLUT1 and the Cytoskeleton. Molecular Biology of the Cell *10*.

Buss, F.*, et al.* (2001). Myosin VI isoform localized to clathrin-coated vesicles with a role in clathrin-mediated endocytosis. The EMBO Journal *14*, 3676.

Buss, F., *et al.* (2008). How are the cellular functions of myosin VI regulated within the cell? Biochemical and biophysical research communications *369*, 165.

Buss, F., *et al.* (1998). The Localization of Myosin VI at the Golgi Complex and Leading Edge of Fibroblasts and Its Phosphorylation and Recruitment into Membrane Ruffles of A431 Cells after Growth Factor Stimulation. The Journal of cell biology *143*, 1535.

Carlier, M.F., *et al.* (2015). Control of polarized assembly of actin filaments in cell motility. Cellular and molecular life sciences : CMLS *72*, 3051.

Chandrasekar, I., *et al.* (2014). Nonmuscle myosin II is a critical regulator of clathrin-mediated endocytosis. Traffic *15*, 418.

Chen, C.Y., *et al.* (2005). Huntingtin-interacting protein 1 (Hip1) and Hip1-related protein (Hip1R) bind the conserved sequence of clathrin light chains and thereby influence clathrin assembly in vitro and actin distribution in vivo. The Journal of biological chemistry *280*, 6109.

Chen, T., *et al.* (2014). Myosin VI mediates the movement of NHE3 down the microvillus in intestinal epithelial cells. Journal of cell science *127*, 3535.

Chibalina, M.V., *et al.* (2010). Myosin VI and optineurin are required for polarized EGFR delivery and directed migration. Traffic *11*, 1290.

Chibalina, M.V., *et al.* (2009). Potential roles of myosin VI in cell motility. Biochemical Society transactions *37*, 966.

Cho, S.J., *et al.* (2010). Myosin VI is differentially regulated by DNA damage in p53- and cell type-dependent manners. The Journal of biological chemistry *285*, 27159.

Collaco, A., *et al.* (2010). Alpha-AP-2 directs myosin VI-dependent endocytosis of cystic fibrosis transmembrane conductance regulator chloride channels in the intestine. The Journal of biological chemistry *285*, 17177.

Cornilescu, G., *et al.* (1999). Protein backbone angle restraints from searching a database for chemical shift and sequence homology. Journal of biomolecular NMR *13*, 289.

Dance, A.L., *et al.* (2004). Regulation of myosin-VI targeting to endocytic compartments. Traffic *5*, 798.

DeLuca-Flaherty, C., *et al.* (1990). Uncoating Protein (hsc70) Binds a Conformationally Labile Domain of Clathrin Light Chain LCa to Stimulate ATP Hydrolysis. Cell *62*, 875.

Deng, W.-M., *et al.* (1999). A targeted gene silencing technique shows that Drosophila myosin VI is required for egg chamber and imaginal disc morphogenesis. Journal of cell science *112*, 3677.

Dunn, T.A., *et al.* (2006). A novel role of myosin VI in human prostate cancer. The American journal of pathology *169*, 1843.

Enari, M., *et al.* (2006). Requirement of clathrin heavy chain for p53-mediated transcription. Genes & development *20*, 1087.

Erben, V., *et al.* (2008). Asymmetric localization of the adaptor protein Miranda in neuroblasts is achieved by diffusion and sequential interaction of Myosin II and VI. Journal of cell science *121*, 1403.

Ferreira, F., *et al.* (2012). Endocytosis of G protein-coupled receptors is regulated by clathrin light chain phosphorylation. Current biology : CB *22*, 1361.

Foth, B.J., *et al.* (2006). New insights into myosin evolution and classification. Proceedings of the National Academy of Sciences of the United States of America *103*, 3681.

Geeves, M.A. (1991). Thedynamicsofactinandmyosin associationandthe crossbridge model of muscle contraction. Biochem J *274*, 1.

Geisbrecht, E.R.*, et al.* (2002). Myosin VI is required for E-cadherin-mediated border cell migration. Nature cell biology *4*, 616.

Gotoh, N.*, et al.* (2010). Altered renal proximal tubular endocytosis and histology in mice lacking myosin-VI. Cytoskeleton *67*, 178.

Graydon B. Gonsalvez*, et al.* (2005). RNA localization in yeast: moving towards a mechanism. Biol Cell *97*.

Guntert, P. (2004). Automated NMR structure calculation with CYANA. Methods in molecular biology *278*, 353.

Gurel, P.S.*, et al.* (2014). Connecting the cytoskeleton to the endoplasmic reticulum and Golgi. Current biology : CB *24*, R660.

Haar, E.t.*, et al.* (1998). Atomic Structure of Clathrin: A β Propeller Terminal Domain Joins an α Zigzag Linker. Cell *95*, 563.

Hanahan, D.*, et al.* (2011). Hallmarks of cancer: the next generation. Cell *144*, 646.

Harburger, D.S.*, et al.* (2009). Integrin signalling at a glance. Journal of cell science *122*, 159.

Hasson, T.*, et al.* (1997). Unconventional Myosins in Inner-Ear Sensory Epithelia. The Journal of Cell Biology, *137*, 1287.

Hasson, T.*, et al.* (1994). Porcine Myosin-VI- Characterization of a New Mammalian Unconventional Myosin. The Journal of cell biology *127*, 425.

Heo, J.M., *et al.* (2015). The PINK1-PARKIN Mitochondrial Ubiquitylation Pathway Drives a Program of OPTN/NDP52 Recruitment and TBK1 Activation to Promote Mitophagy. Molecular cell *60*, 7.

Hodge, T., *et al.* (2000). A myosin family tree. Journal of cell science.

Huang, F., *et al.* (2004). Analysis of clathrin-mediated endocytosis of epidermal growth factor receptor by RNA interference. The Journal of biological chemistry *279*, 16657.

Humphries, A.C., *et al.* (2013). The non-canonical roles of clathrin and actin in pathogen internalization, egress and spread. Nature Reviews Microbiology *11*, 551.

Inoue, A., *et al.* (2002). DOC-2/DAB2 is the binding partner of myosin VI. Biochemical and biophysical research communications *292*, 300.

Jung, E.J., *et al.* (2006). Myosin VI is a mediator of the p53-dependent cell survival pathway. Molecular and cellular biology *26*, 2175.

K.Mishra, S., *et al.* (2002). Disabled-2 exhibits the properties of a cargo-selective endocytic clathrin adaptor. The EMBO Journal *21*, 4915.

Kelleher, J.F., *et al.* (2000). Myosin VI is required for asymmetric segregation of cellular components during C. elegans spermatogenesis. Current biology : CB *10*, 1489.

Keller, A., *et al.* (2002). Empirical statistical model to estimate the accuracy of peptide identifications made by MS/MS and database search. Analytical chemistry *74*, 5383.

Kellerman, K.A., *et al.* (1992). An Unconventional Myosin Heavy Chain Gene from Drosophila melanogaster. The Journal of cell biology *119*, 823.

Kisiel, M., *et al.* (2014). Localization and Mobility of Synaptic Vesicles in Myosin VI Mutants of Drosophila. PloS one *9*.

Kobayashi, N., *et al.* (2007). KUJIRA, a package of integrated modules for systematic and interactive analysis of NMR data directed to high-throughput NMR structure studies. Journal of biomolecular NMR *39*, 31.

Kravtsov, D.V., *et al.* (2012). Myosin Ia is required for CFTR brush border membrane trafficking and ion transport in the mouse small intestine. Traffic *13*, 1072.

Krendel., M., *et al.* (2005). Myosins: Tails (and Heads) of Functional Diversity. Physiology Reviews *20*, 239.

Kural, C., *et al.* (2015). Asymmetric formation of coated pits on dorsal and ventral surfaces at the leading edges of motile cells and on protrusions of immobile cells. Mol Biol Cell *26*, 2044.

Laskowski, R.A., *et al.* (1996). AQUA and PROCHECK-NMR: programs for checking the quality of protein structures solved by NMR. Journal of biomolecular NMR *8*, 477.

Li, D., *et al.* (2015). ADVANCED IMAGING. Extended-resolution structured illumination imaging of endocytic and cytoskeletal dynamics. Science *349*, aab3500.

Liu, S.-H., *et al.* (2001). A novel clathrin homolog that co-distributes with cytoskeletal components functions in the trans-Golgi network. The EMBO Journal *20*, 272.

Liu, S.H., *et al.* (1995). Regulation of Clathrin Assembly and Trimerization Defined Using Recombinant Triskelion Hubs. Cell *83*, 257.

Loerke, D., *et al.* (2009). Cargo and Dynamin Regulate Clathrin-Coated Pit Maturation. Plos Biology *7*, 0628.

Loikkanen, I., *et al.* (2009). Myosin VI is a modulator of androgen-dependent gene expression. Oncology Reports *22*.

Lu, L., *et al.* (2014a). From endosomes to the trans-Golgi network. Seminars in cell & developmental biology *31*, 30.

Lu, Q., *et al.* (2014b). Cargo recognition and cargo-mediated regulation of unconventional myosins. Accounts of chemical research *47*, 3061.

Maddugoda, M.P., *et al.* (2007). Myosin VI and vinculin cooperate during the morphogenesis of cadherin cell cell contacts in mammalian epithelial cells. The Journal of cell biology *178*, 529.

Mangold, S., *et al.* (2012). The juxtamembrane domain of the E-cadherin cytoplasmic tail contributes to its interaction with Myosin VI. Bioarchitecture *2*, 185.

Mattila, P.K., *et al.* (2008). Filopodia: molecular architecture and cellular functions. Nature reviews Molecular cell biology *9*, 446.

McMahon, H.T., *et al.* (2011). Molecular mechanism and physiological functions of clathrin-mediated endocytosis. Nature reviews Molecular cell biology *12*, 517.

Melchionda, S., *et al.* (2001). MYO6, the human homologue of the gene responsible for deafness in Snell's waltzer mice, is mutated in autosomal dominant nonsyndromic hearing loss. American journal of human genetics *69*, 635.

Mermall, V., *et al.* (1995). The 95F Unconventional Myosin Is Required for Proper Organization of the Drosophila Syncytial Blastoderm. The Journal of cell biology *129*, 1575.

Mettlen, M., *et al.* (2009). Dissecting dynamin's role in clathrin-mediated endocytosis. Biochemical Society transactions *37*, 1022.

Mohiddin, S.A., *et al.* (2004). Novel association of hypertrophic cardiomyopathy, sensorineural deafness, and a mutation in unconventional myosin VI (MYO6). Journal of Medical Genetics *41*, 309.

Morris, S.M., *et al.* (2002). Myosin VI Binds to and Localises with Dab2, Potentially Linking Receptor-Mediated Endocytosis and the Actin Cytoskeleton. Traffic *2*, 331.

Morris, S.M., *et al.* (2001). Disabled-2 Colocalizes with the LDLR in Clathrin-Coated Pits and Interacts with AP-2. Traffic *2*, 111.

Morrison, J.K., *et al.* (2008). Genetic characterization of the Drosophila jaguar322 mutant reveals that complete myosin VI loss of function is not lethal. Genetics *179*, 711.

Morriswood, B., *et al.* (2007). T6BP and NDP52 are myosin VI binding partners with potential roles in cytokine signalling and cell adhesion. Journal of cell science *120*, 2574.

Mukherjea, M., *et al.* (2014). Myosin VI must dimerize and deploy its unusual lever arm in order to perform its cellular roles. Cell reports *8*, 1522.

Mukherjea, M., *et al.* (2009). Myosin VI dimerization triggers an unfolding of a three-helix bundle in order to extend its reach. Molecular cell *35*, 305.

Nesvizhskii, A.I., *et al.* (2003). A statistical model for identifying proteins by tandem mass spectrometry. Analytical chemistry *75*, 4646.

Nishikawa, S., *et al.* (2002). Class VI myosin moves processively along actin filaments backward with large steps. Biochemical and biophysical research communications *290*, 311.

Noguchi, T.*, et al.* (2009). Coiled-Coil–Mediated Dimerization Is Not Required for Myosin VI to Stabilize Actin during Spermatid Individualization in Drosophila melanogaster. Molecular Biology of the Cell *20*, 358.

Noguchi, T.*, et al.* (2006). Myosin VI Stabilizes an Actin Network during Drosophila Spermatid Individualization. Molecular Biology of the Cell *17*, 2559.

Nurnberg, A.*, et al.* (2011). Nucleating actin for invasion. Nature reviews Cancer *11*, 177.

Ouderkirk, J.L.*, et al.* (2014). Non-muscle myosins in tumor progression, cancer cell invasion, and metastasis. Cytoskeleton *71*, 447.

Park, H.*, et al.* (2007). The unique insert at the end of the myosin VI motor is the sole determinant of directionality. Proceedings of the National Academy of Sciences of the United States of America *104*, 778.

Pathak, D.*, et al.* (2010). Evidence that myosin activity opposes microtubule-based axonal transport of mitochondria. The Journal of neuroscience : the official journal of the Society for Neuroscience *30*, 8984.

Pearse, B.M.F. (1976). Clathrin:A unique protein associated with intracellular transfer of membrane by coated vesicles. Proceedings of the National Academy of Sciences of the United States of America *73*, 1255.

Penengo, L.*, et al.* (2006). Crystal structure of the ubiquitin binding domains of rabex-5 reveals two modes of interaction with ubiquitin. Cell *124*, 1183.

Pinheiro, E.M.*, et al.* (2004). Requirement for Par-6 and Bazooka in Drosophila border cell migration. Development *131*, 5243.

Pollard, T.D., *et al.* (1973). Acanthamoeba Myosin - Isolation from Acanthamoeba castellanii of an enzyme similar to muscle myosin. The Journal of biological chemistry *248*, 4682.

Porat-Shliom, N., *et al.* (2013). Multiple roles for the actin cytoskeleton during regulated exocytosis. Cellular and molecular life sciences : CMLS *70*, 2099.

Poupon, V., *et al.* (2008). Clathrin light chains function in mannose phosphate receptor trafficking via regulation of actin assembly. Proceedings of the National Academy of Sciences of the United States of America *105*, 168.

Puthalakath, H., *et al.* (2001). Bmf: A Proapoptotic BH3-Only Protein Regulated by Interaction with the Myosin V Actin Motor Complex, Activated by Anoikis. Science *293*, 1829.

Pylypenko, O., *et al.* (2011). Role of insert-1 of myosin VI in modulating nucleotide affinity. The Journal of biological chemistry *286*, 11716.

Quintero, O.A., *et al.* (2009). Human Myo19 is a novel myosin that associates with mitochondria. Current biology : CB *19*, 2008.

Richards, T.A., *et al.* (2005). Myosin domain evolution and the primary divergence of eukaryotes. Nature *436*, 1113.

Ridley, A.J. (2011). Life at the leading edge. Cell *145*, 1012.

Ridley, A.J., *et al.* (2003). Cell Migration: Integrating Signals from Front to Back. science *302*.

Rogat, A.D., *et al.* (2002). A role for myosin VI in actin dynamics at sites of membrane remodeling during Drosophila spermatogenesis. Journal of cell science *115*, 4855.

Royle, S.J., *et al.* (2005). Clathrin is required for the function of the mitotic spindle. Nature *434*, 1152.

Sahlender, D.A., *et al.* (2005). Optineurin links myosin VI to the Golgi complex and is involved in Golgi organization and exocytosis. The Journal of cell biology *169*, 285.

Schramek, D., *et al.* (2014). Direct in Vivo RNAi Screen Unveils Myosin IIa as a Tumor Suppressor of Squamous Cell Carcinomas. Science *343*, 309.

Seiler, C., *et al.* (2004). Myosin VI is required for structural integrity of the apical surface of sensory hair cells in zebrafish. Developmental biology *272*, 328.

Self, T., *et al.* (1999). Role of Myosin VI in the Differentiation of Cochlear Hair Cells. Developmental biology *214*, 331.

Sigismund, S., *et al.* (2012). Endocytosis and signaling: cell logistics shape the eukaryotic cell plan. Physiol Rev *92*, 273.

Singh, R.K., *et al.* (2012). Pre-mRNA splicing in disease and therapeutics. Trends in molecular medicine *18*, 472.

Sirotkin, V., *et al.* (2005). Interactions of WASp, myosin-I, and verprolin with Arp2/3 complex during actin patch assembly in fission yeast. The Journal of cell biology *170*, 637.

Smythe, E., *et al.* (2006). Actin regulation in endocytosis. Journal of cell science *119*, 4589.

Spink, B.J., *et al.* (2008). Long single alpha-helical tail domains bridge the gap between structure and function of myosin VI. Nature structural & molecular biology *15*, 591.

Spudich, G.*, et al.* (2007). Myosin VI targeting to clathrin-coated structures and dimerization is mediated by binding to Disabled-2 and PtdIns(4,5)P2. Nature cell biology *9*, 176.

Sweeney, H.L.*, et al.* (2010). Myosin VI rewrites the rules for myosin motors. Cell *141*, 573.

Swiatecka-Urban, A.*, et al.* (2004). Myosin VI regulates endocytosis of the cystic fibrosis transmembrane conductance regulator. The Journal of biological chemistry *279*, 38025.

Tomatis, V.M.*, et al.* (2013). Myosin VI small insert isoform maintains exocytosis by tethering secretory granules to the cortical actin. The Journal of cell biology *200*, 301.

Tumbarello, D.A.*, et al.* (2013). Myosin VI and its cargo adaptors - linking endocytosis and autophagy. Journal of cell science *126*, 2561.

Tumbarello, D.A.*, et al.* (2012). Autophagy receptors link myosin VI to autophagosomes to mediate Tom1-dependent autophagosome maturation and fusion with the lysosome. Nature cell biology *14*, 1024.

Tyska, M.J.*, et al.* (2002). The Myosin Power Stroke. Cell motility and the cytoskeleton *51*, 1.

Valdembri, D.*, et al.* (2009). Neuropilin-1/GIPC1 signaling regulates alpha5beta1 integrin traffic and function in endothelial cells. PLoS Biol *7*, e25.

Vassilopoulos, S.*, et al.* (2014). Actin scaffolding by clathrin heavy chain is required for skeletal muscle sarcomere organization. The Journal of cell biology *205*, 377.

Vassilopoulos, S.p.*, et al.* (2009). A Role for the CHC22 Clathrin Heavy-Chain Isoform in Human
Glucose Metabolism. science *324*, 1192.

Vreugde, S., *et al.* (2006). Nuclear myosin VI enhances RNA polymerase II-dependent transcription. Molecular cell *23*, 749.

Wakeham, D.E., *et al.* (2005). Clathrin heavy and light chain isoforms originated by independent mechanisms of gene duplication during chordate evolution. Proceedings of the National Academy of Sciences of the United States of America *102*, 7209.

Warner, C.L., *et al.* (2003). Loss of myosin VI reduces secretion and the size of the Golgi in fibroblasts from Snell's waltzer mice. The EMBO journal *22*, 569.

Wei, S., *et al.* (2008). GOLPH2 and MYO6: putative prostate cancer markers localized to the Golgi apparatus. The Prostate *68*, 1387.

Wilbur, J.D., *et al.* (2010). Conformation switching of clathrin light chain regulates clathrin lattice assembly. Developmental cell *18*, 841.

Winkler, F.K., *et al.* (1983). Clathrin heavy chain, light chain interactions. The EMBO Journal *2*, 1393.

Woolner, S., *et al.* (2009). Unconventional myosins acting unconventionally. Trends in cell biology *19*, 245.

Yamaguchi, H., *et al.* (2007). Regulation of the actin cytoskeleton in cancer cell migration and invasion. Biochimica et biophysica acta *1773*, 642.

Ybe, J.A., *et al.* (1999). Clathrin self-assembly is mediated by a tandemly repeated superhelix. Nature *399*, 371.

Ybe, J.A., *et al.* (2007a). Crystal structure at 2.8 A of the DLLRKN-containing coiled-coil domain of huntingtin-interacting protein 1 (HIP1) reveals a surface suitable for clathrin light chain binding. Journal of molecular biology *367*, 8.

Ybe, J.A., *et al.* (2007b). Light chain C-terminal region reinforces the stability of clathrin heavy chain trimers. Traffic *8*, 1101.

Yoshida, H., *et al.* (2004). Lessons from border cell migration in the Drosophila ovary: A role for myosin VI in dissemination of human ovarian cancer. Proceedings of the National Academy of Sciences of the United States of America *101*, 8144.

Yu, C., *et al.* (2009). Myosin VI undergoes cargo-mediated dimerization. Cell *138*, 537.

Zhang, H., *et al.* (2004). Myosin-X provides a motor-based link between integrins and the cytoskeleton. Nature cell biology *6*, 523.

ACKNOWLEDGMENT

I would like to thank all the people that made this thesis work possible.

Above all, I thank my Ph.D. supervisor Simona Polo, who gave me the opportunity to join her group and carry out this research project. She has been a great source of technical and theoretical scientific knowledge. The doors of her office were always opened for me to discuss about science, and sometimes to talk about life.

A special thank to Hans-Peter Wollscheid, who introduced me into the myosin VI world and guided me, hand in hand, through its troubles and joys.

I would also like to express my gratitude to Elena Maspero, a brilliant scientist, a great lab-manager, and a wonderful colleague. Whatever I was looking for, no matter is was a reagent or a suggestion, she had the answer.

I am grateful to all my colleagues and labmates who made all my days in the lab extremely pleased and fun.